WESTERN GULF OF ALASKA TIDES AND CIRCULATION

by

Paul Greisman

Dobrocky Seatech Ltd.
9865 West Saanich Road
P.O. Box 6506
Sidney, R C. V8L 4M7

Final Report
Outer Continental Shelf Environmental Assessment Program
Research **Unit** 657

July 1985

ACKNOWLEDGMENTS

I would like to express my gratitude to the many NOAA staff who participated in this study. The tide gauges and current meters were flawlessly prepared by T. Jackson, while the CTD system was set up by S. Macri. The officers and crew of the NOAA ship FAIRWEATHER provided enthusiastic support, Bosun Herb Padilla deserves special credit for his organization of the deck. Dr. M. Jawed Hameedi was the technical authority and provided useful advice to us despite his move (concurrent with the project) from Juneau to Anchorage.

Professor Tom Royer of the Institute of Marine Science at the University of Alaska lent his experience in the region to the project. He provided all the runoff and freshwater discharge data as well as numerous references which were used in this study.

The field work was performed by Randy Kashino and Dale McCullough of Dobrocky Seatech. The data recovery rate (100%) speaks for their expertise. The data processing and tidal analyses were performed by Allan Blaskovich of Dobrocky Seatech.

This study was funded by the Minerals Management Service, U.S. Department of the Interior, through interagency agreement with the National Oceanic and Atmospheric Administration, U.S. Department of Commerce, as part of the Outer Continental Shelf Environment Assessment Program.

TABLE OF CONTENTS

Page

LIST OF FIGURES

LIST OF FIGURES (continued)

LIST OF TABLES

1. INTRODUCTION

During June and August 1984, tidal height, current and CTD data were collected in the Western Gulf of Alaska principally as input to a numerical model of the continental shelf circulation. The model will be used to help assess the risks associated with a potential oilspill and will aid in the sale of leases by the Minerals Management Service.

The field program was carried out by Dobrocky Seatech technicians R. Kashino and D. McCullough from the NOAA vessel FAIRWEATHER. Current meters, tide gauges, acoustic releases and CTD were furnished and prepared by NOAA, while Seatech designed and fabricated the moorings. Seven tide gauges and four current meter moorings of two current meters each were deployed in June and all instruments were recovered in August. The data recovery was 100% attesting to the care taken in instrument set-up by NOAA's Pacific Marine Environmental Laboratory and the thoroughness of the field technicians. Details of the field program may be found in the field report (September 1984).

Current meters and tide gauge deployment sites are shown in Figure 1.1 along with the locations of the cross-shelf CTD transects. CTD measurements were also made at the current meter sites in order to permit computation of the internal tide modal structure. Specifics of the deployments of the tide gauges and current meters are given in Tables 1.1 and 1.2.

Aanderaa model RCM-4 current meters were used at all locations. The current meters recorded temperature, conductivity and pressure as well as speed and direction. A 15 minute sampling interval was used. Modified Savonius rotors were used on all instruments with the exception of the shallow meter at Sanak Island where an Alekseyev rotor was employed to reduce aliasing due to surface waves.

All tide gauges were Aanderaa model TG3A; a 7.5 minute sampling interval was used.

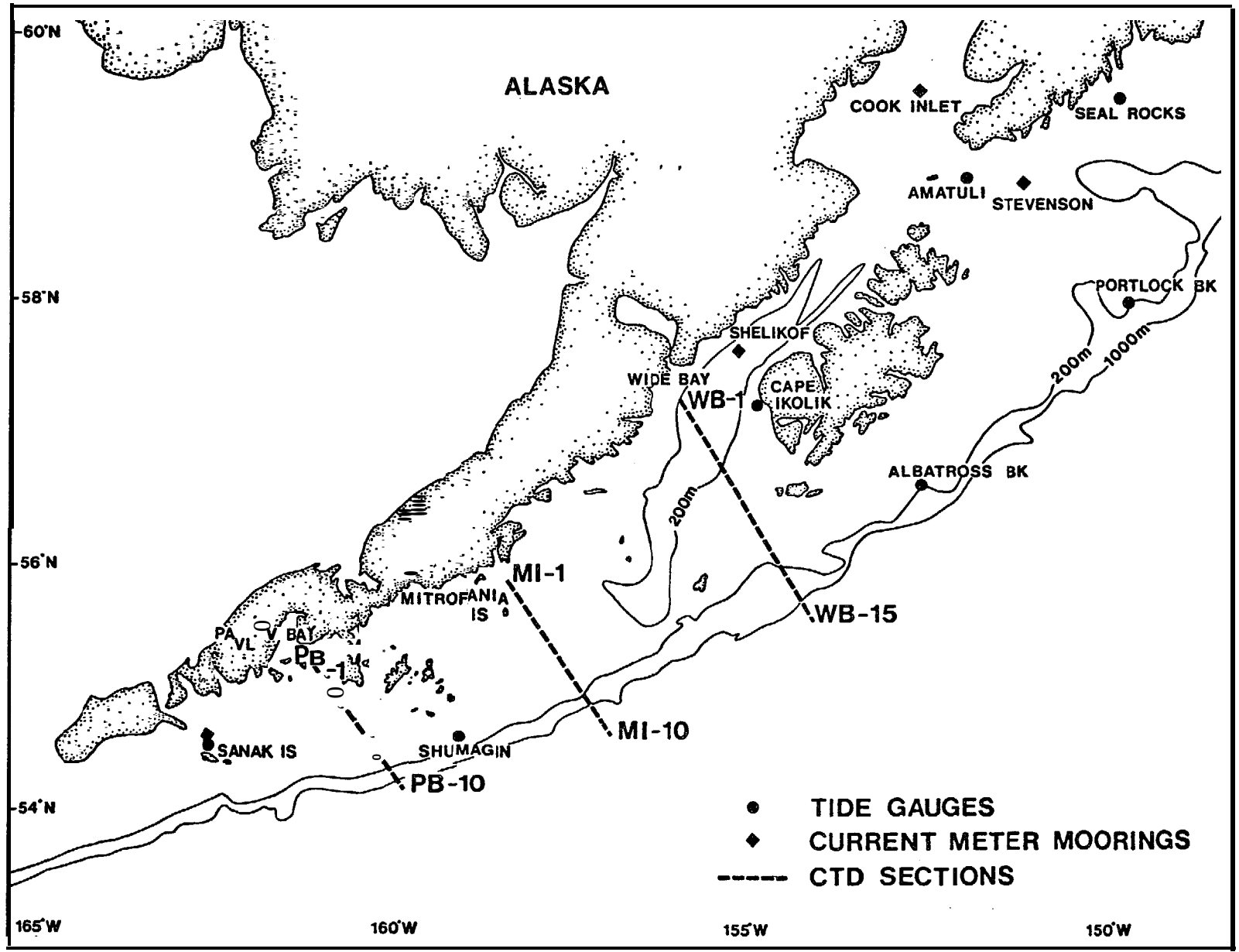

Figure 1.1 - Location of current meters, tide gauges, and CTD sections.

TABLE 1.1
CURRENT METER DEPLOYMENT SPECIFICS

Location		Water Depth (m)	C.M. No.	C.M. Depth (m)	First Good Record (GMT)		Last Good Record (GMT)	
Stevenson Entrance	58°53'73N	113	2493	45	1800	13 June 84	0945	9 Aug 84
North of Portlock Bk	150°57'23W		1807	75	1800	13 June 84	0945	9 Aug 84
Cook Inlet	59°35'02N	62	3710	36	0430	14 June 84	2015	9 Aug 84
	152°29'00W		3614	52	0430	14 June 84	2015	9 Aug 84
Shelikof Strait	57°39'00N	250	3127	40	2130	14 June 84	1400	10 Aug 84
	155°03'33W		1812	150	2130	14 June 84	1400	10 Aug 84
Sanak (Deer Island)	54°35'25N	49	3185*	18.5	1000	16 June 84	0445	13 Aug 84
	162°43'77W		1987	38.5	1000	16 June 84	0445	13 Aug 84

All current meters were equipped with temperature, conductivity and pressure sensors.

Sampling interval was 15 minutes on all current meters.

*This current meter was modified to utilize the Alekseyev rotor now available from Aanderaa.

TABLE 1.2
TIDE GAUGE DEPLOYMENT SPECIFICS

Location			Depth (m)	T.G. No.	First Good Record (GMT)	Last Good Record (GMT)
Albatross Bank	56°33'48N	152°26'95W	163	107	1200 12 June 84	0407.5 8 Aug 84
Portlock Bank	58°01'03N	149°29'58W	174	205	0100 13 June 84	1615 8 Aug 84
Seal Rocks	59°29'93N	149°29'57W	112	188	1000 13 June 83	0430 9 Aug 84
Amatuli Island	59°00'13N	151°50'03W	168	87	2230 13 June 84	1400 9 Aug 84
Cape Ikolik	57°15'00N	154°45'30W	62	120	0100 15 June 84	2315 10 Aug 84
Shumagin (Simeonof Is)	54°31'93N	158°58'08W	192	119	2000 15 June 84	1907.5 11 Aug 84
Sanak (Deer Is)	54°35'25N	162°43'77W	48	209	1000 16 June 84	0452.5 13 Aug 84

Sampling interval was 7.5 minutes for all tide gauges.

The current meters were deployed on taut line moorings of 1/4" 7 x 19 wire rope. Buoyancy was provided at the top of the mooring, above the lower current meter and above the acoustic release. Train wheels were used for anchors. Tide gauge moorings consisted of concrete blocks with recesses for the tide gauge. Sketches of each mooring type are presented in Figures 1.2 through 1.6. All moorings were suspended in the water column then gently lowered to the bottom with a device which releases upon loss of tension.

1.1 DATA REDUCTION

The Aanderaa data tapes were translated and converted to physical units using calibrations supplied by NOAA. Salinities were computed from temperature, conductivity and pressure with the UNESCO (1980) formula.

Time series plots were produced for each instrument and are available in our Data Report (Greisman 1984). Also produced were progressive vector diagrams, stick plots and histograms. These products aided in quality control as well as in forming a general impression of the data set.

Harmonic analyses of the tide gauge data and tidal stream analyses of the current meter data were performed using the methods of Foreman (1977 and 1978). The complete analyses are presented in Appendix 1.

Tables 1.3 and 1.4 show the tidal analyses for the largest constituents for the heights and currents respectively. Greenwich phase is used throughout. In the tidal stream analyses MAJ represents the amplitude of the semi-major axis of the tidal ellipse; MIN represents the semi-minor axis of the ellipse. The sign of MIN indicates the sense of rotation; positive implies anti-clockwise and negative clockwise. INC is the orientation of the northern semi-major axis of the ellipse anti-clockwise from east (mathematical rather than geographic convention). G is the Greenwich phase and represents the time at which the rotating velocity vector coincides with the northern semi-major axis of the ellipse.

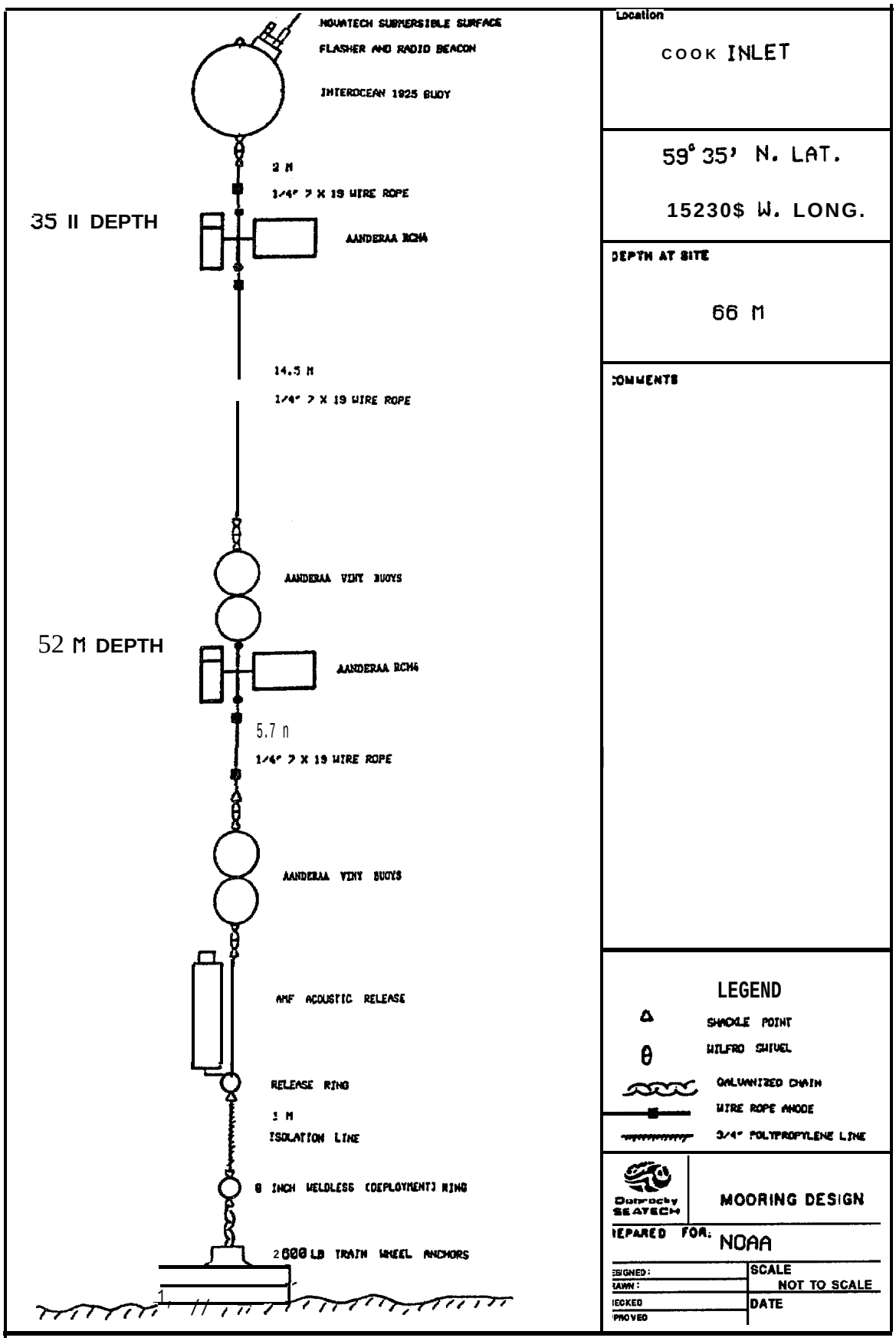

Figure 1.2 - Mooring configuration at Cook Inlet.

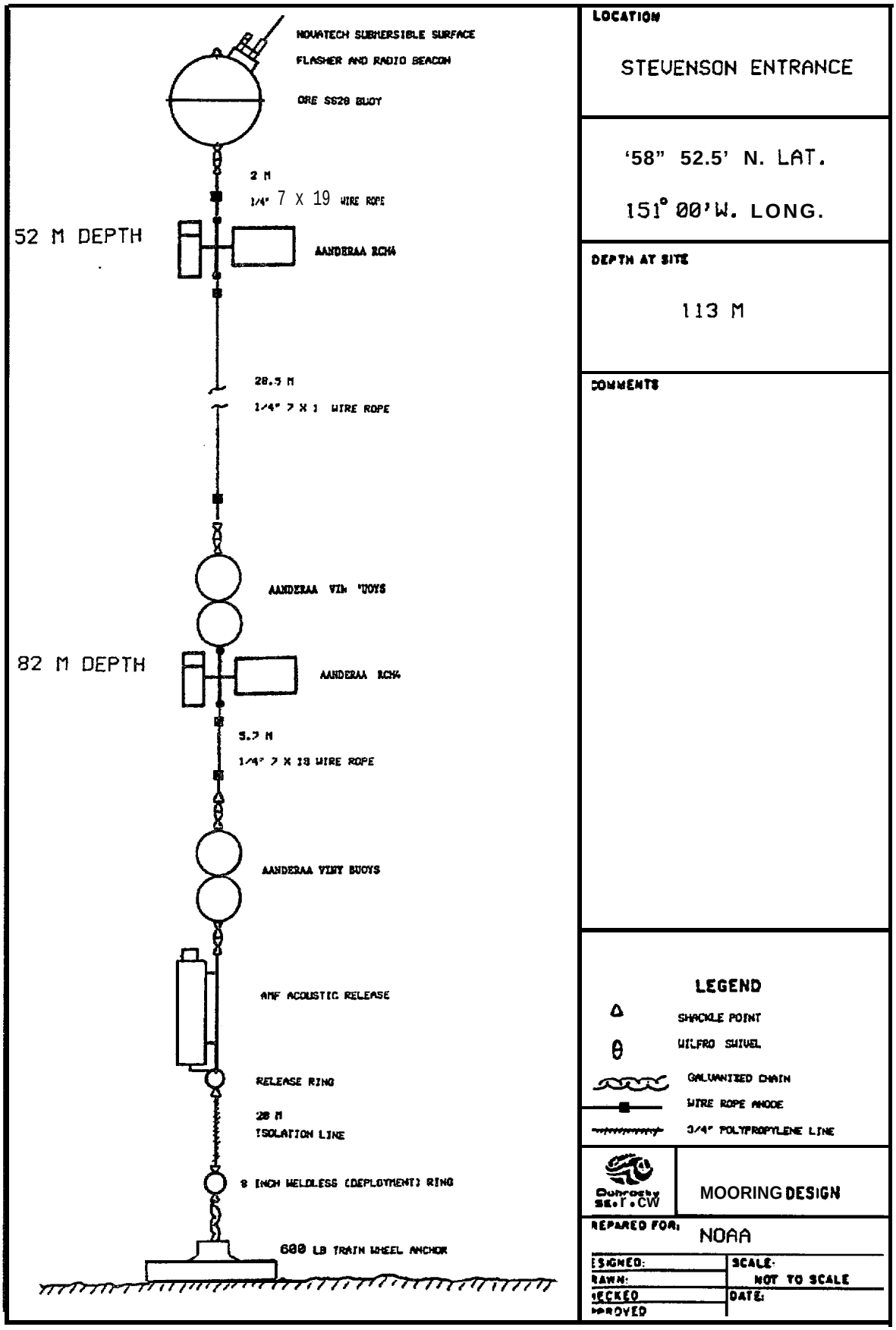

Figure 1.3 - Mooring configuration at Stevenson Entrance.

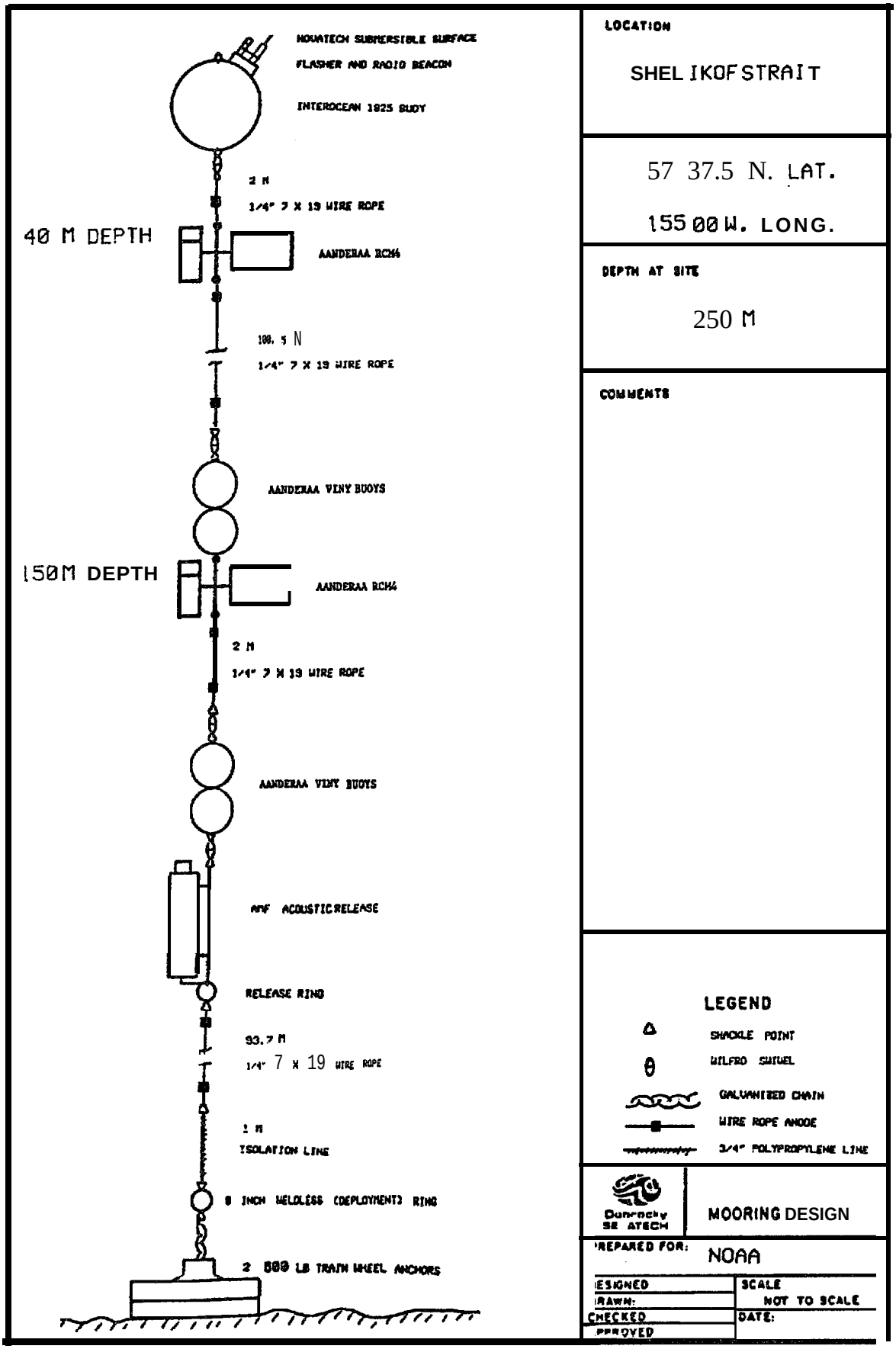

Figure 1.4 - Mooring configuration at Shelikof Strait.

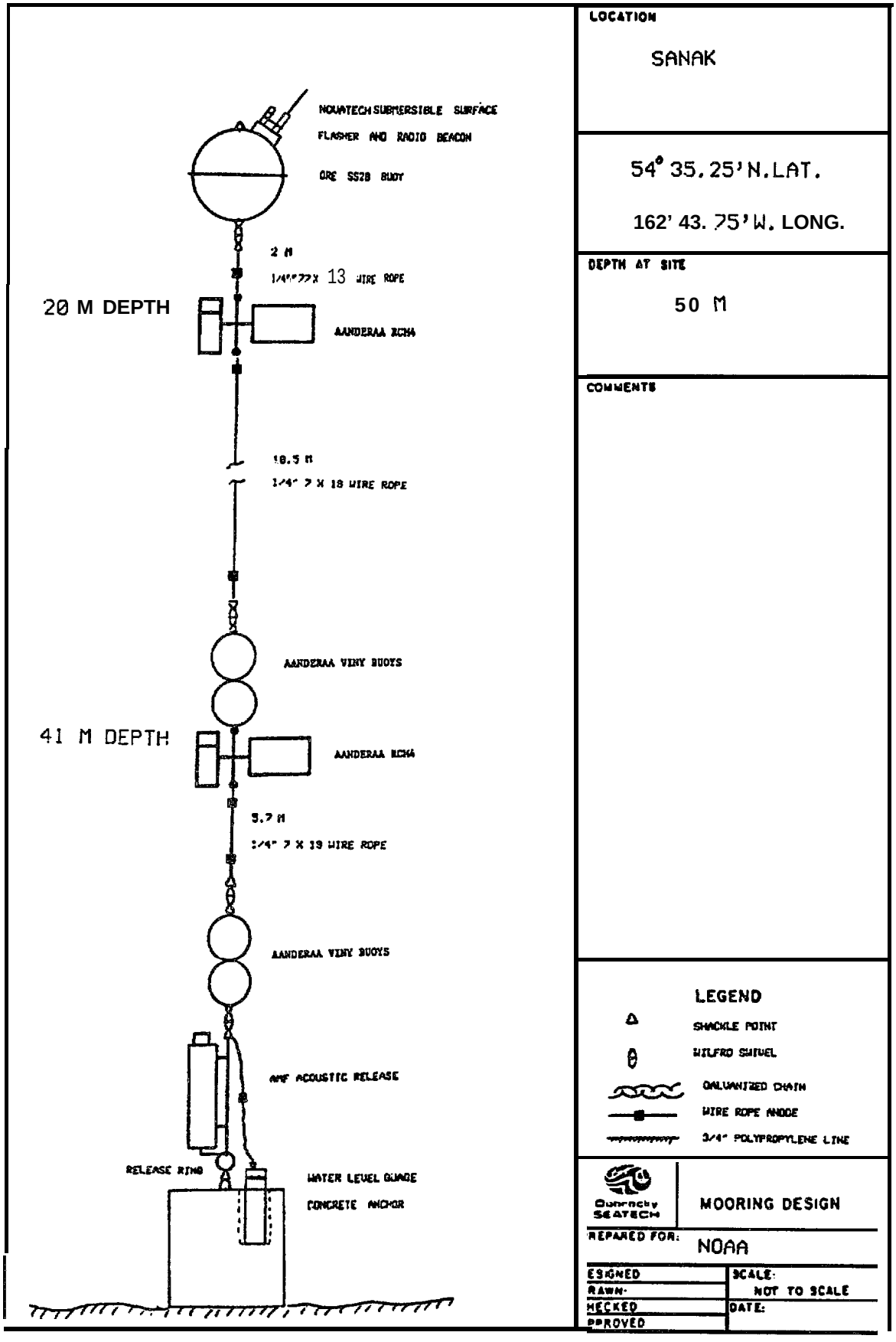

Figure 1.5 - Mooring configuration at Sanak.

PORTLOCK BANK SS 30'N. Mr. 149 30' u. LONG. 200 n
SEAL BANK 59 30'N. LAT.152 30' u. LONG.100 n
ALBATROSS BANK 56 30'N. LAT. 159 00' U. LONG. 200 M
SIMEONOFF ISLAND s4 30'N. LAT. 159 00' W. LONG. 20 M
AMATULI ISLAND 59 00'N. LAT. 1s2 00' u. LONG. 2s n
CAPE IKOLIK n 15'N. LAT. 154 45' W. LONG. 20 n

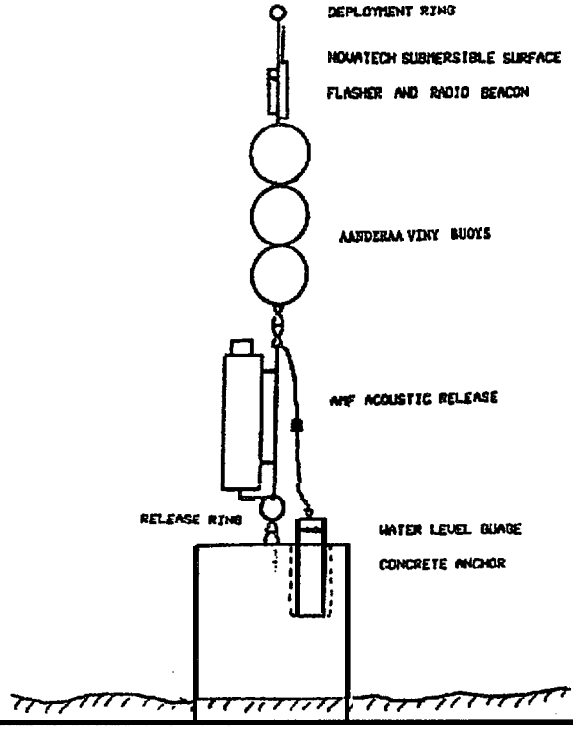

TIDE GAUGE MOORING

COMMENTS

LEGEND

Δ SHACKLE POINT

e WILFRO SWIVEL

GALVANIZED CHAIN

WIRE ROPE ANODE

3/4" POLYPROPYLENE LINE

Durnesby saa?acw

MOORING DESIGN

EPARED 'O" NOAA

SIGNED	SCALE: NOT TO SCALE
AWN:	
CHECKED	DATE:
APPROVED	

Figure 1.6 - Mooring configuration for the tide gauges.

TABLE 1.3
MAJOR TIDAL CONSTITUENTS
AMPLITUDES (METRES) AND GREENWICH PHASES

	Principal Lunar Diurnal		Soli-Lunar Declinational (Divisional)		Larger Lunar Elliptic (Semi-Diurnal)		Principal Lunar (semi-Diurnal)		Principal Solar (Semi-Diurnal)		
STATION	O_1 A	G	K_1 A	G	N_2 A	G	M_2 A	G	S_2 A	G	$F = \frac{K_1 + O_1}{M_2 + S_2}$
Sanak	.2691	269.93	.5041	293.03	.1331	314.13	.6306	330.12	.1579	003.55	0.981
Portlock Bk.	.2916	252.72	.5572	276.60	.1902	278.57	1.0140	293.48	.2499	334.36	0.672
Seal Rk.	.2846	256.09	.5431	279.69	.2216	274.53	1.1975	2S9.94	.3016	331.25	0.552
Cape Ikolik	.3070	265.70	.5928	289.37	.2770	303.52	1.3889	317.00	.3757	001.87	0.510
Shumagin	.2769	266.50	.5175	289.08	.1371	302.39	.6713	317.25	.1690	353.99	0.945
Albatross Bk.	.2905	255.04	.5520	278.29	.1698	279.03	.8940	294.57	.2171	334.37	0.759
Amatuli Is.	. 30S2	262.95	.5834	287.24	.3011	297.41	1.5548	312.60	.4184	357.54	0.452

TABLE 1.4
TIDAL STREAM ANALYSES
INCLUDING TIDAL HEIGHT ANALYSES FROM NEARBY TIDE GAUGES

		O_1						K_1					
STATION	DEPTH	MAJ	MIN	INC	G	A	G	MAJ	MIN	INC	G	A	G
Stevenson	54	3.7	-0.78	98	14			6.6	-2.2	101	41		
Stevenson	82	1.5	-1.7	91	22			6.4	-3.5	10s	36		
Amatuli I						.308	263					.5s3	287
Shelikof Str.	46	1.8	-0.13	39	227			3.4	0.08	41	244		
Shelikof Str.	1s7	1.5	-0.06	49	205			3.0	-0.15	48	226		
C. Ikolik						.307	266					.593	289
Sanak	20	2.3	-1.1	177	105			4.0	-2.0	167	14s		
Sanak	41	3.5	-0.90	1	274			7.1	-3.1	166	136		
Sanak						.269	270					.504	293
Cook In.	35	9.5	-0.70	79	224			19.0	-3.5	77	244		
Cook In.	52	8.0	-0.07	69	220			17.6	-3.4	78	239		

		N_2						M_2						S_2					
STATION	DEPTH	MAJ	MIN	INC	G	A	G	MAJ	MIN	INC	G	A	G	MAJ	MIN	INC	G	A	G
Stevenson	54	5.9	1.s	94	51			30.2	0.62	102	66			10.1	0.59	97	112		
Stevenson	82	6.0	-0.3	94	55			36.3	1.6S	91	76			11.6	1.10	84	126		
Amatuli I						.301	297					1.5.55	313					.41s	358
Shelikof Str.	46	2.5	0.7	39	230			13.8	-.02	40	251			4.5	-.03	41	297		
Shelikof Str.	157	3.1	1.0	46	233			14.9	.60	43	248			4.3	.14	47	296		
C. Ikolik						.277	304					1. 3s9	317					.376	002
Sanak	20	0.7	-0.3	90	269			3.1	.47	113	2ss			1.1	-.11	77	336		
Sanak	41	0.s	-0.5	64	239			4.1	1.0s	90	253			1.5	-.61	30	267		
Sanak						.133	314					.631	330					.158	004
Cook In.	35	14.4	-2.4	81	285			73.5	-s.9	7s	308			19.8	-2.5	s 4	352		
Cook In.	52	13.2	-3.6	83	279			59. s	-2.0	74	305			14. s	-1.8	$4	346		

NOTE: Semi-major and semi-minor ellipse axes in CMS^{-1}; INC is inclination of the northern semi-major axis anti-clockwise from east; G is the Greenwich phase A tidal height amplitude in metres.

The CTD data were translated, calibrated versus bottle casts, and vertical profiles plotted for each cast. The profiles are presented in the data report. Listings of roughly 1 m depth averaged values were produced for use in preparing cross sections.

More details on the data reduction are available in the data report.

1.2 OVERVIEW OF THE DATA

98.6% of the variance in the tide gauge records is due to tidal oscillations while 67% of the variance in the current meter records is tidal. In addition, the mean flows recorded at the current meters were about 4 cm s^{-1}, i.e. roughly an order of magnitude smaller than the tidal currents. Clearly the flow kinetic energy in the region is dominated by tides during the summer. However, from our data set we cannot address the winter period when easterly gales may have a great influence upon circulation on the shelf.

1.3 ANALYSES UNDERTAKEN

In Section 2 of this report conclusions based upon the distribution of properties (the CTD data) are presented and discussed. These include computations of dynamic height topographies and geostrophic current speeds and directions.

Section 3 comprises analyses of the tidal oscillations. Cotidal charts, tidal energy propagation and internal tides are discussed.

Section 4 deals with the non-tidal, specifically the subtidal, oscillations. We found ourselves somewhat limited in these analyses because of the relatively short period of measurement. The two month period between June and August 1984 is, of course, too short to address seasonal signals such as gross changes in the wind field and seasonal runoff variations. Nevertheless, aspects of the forcing of long period oscillations in the Western Gulf of Alaska, particularly Shelikof Strait are discussed.

2. PROPERTY FIELDS

(Salinity, Temperature, Density, Dynamic Topography)

The results of the June and August 1984 CTD surveys are discussed in this section. Field methods, calibration and quality control of the data were presented in the data report. It should be borne in mind that these data are of fair quality only probably due to the poor condition of the CTD winch slip rings.

2.1 moss SECTIONS

Cross sections of temperature, salinity and sigma-t were prepared for the Pavlov Bay, Mitrofania Island and Wide Bay sections for both June and August , The locations of these sections are shown in Figure 2.1. Salinity, temperature and sigma-t sections are presented in pairs for June, then August to enhance the reader's appreciation of temporal changes. It should be remembered that the data are non-synoptic, the occupation of stations along each section having consumed about one day.

2.1.1 Temperature

The most striking feature of the temperature sections (Figures 2.2, 2.3, 2.8, 2.9, 2.14, 2.15) is the pronounced warming of the surface layers to about 50 m depth between June and August. Surface temperature increased about 5° C during this period both over the continental shelf and slope. Since the measured mean flows are on the order of 5 cm s-', the temperature field would have been advected only about 200 km between June and August. The warming of the surface layers is, therefore almost certainly due to local insolation. The water column is everywhere temperature stratified below a few meters depth with the exception of the Trinity Islands Bank shown in the Wide Bay Section. Here the temperature is nearly constant with depth in both June and August likely due to strong

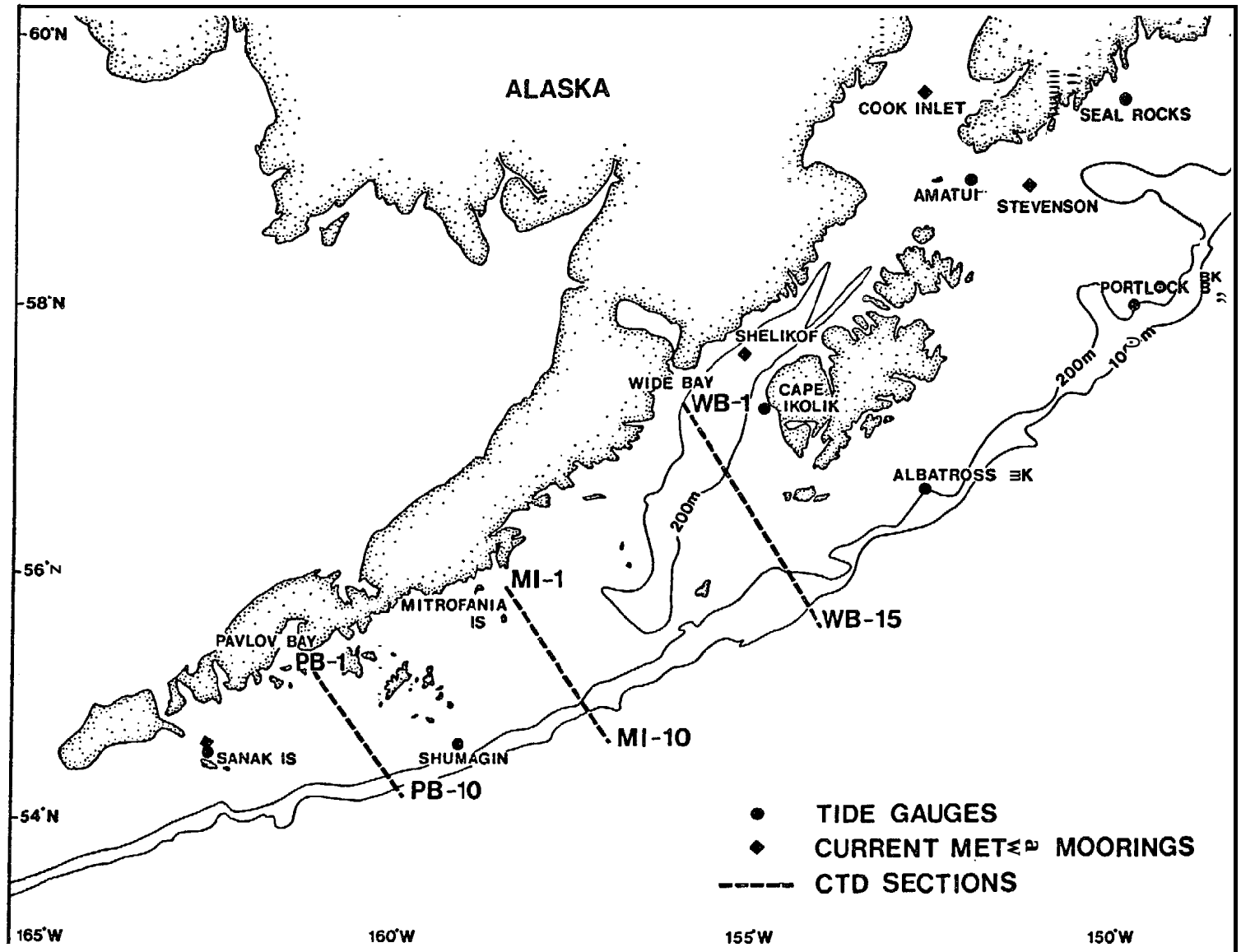

Figure 2.1 - Location chart for salinity, temperature, and sigma-t cross sections

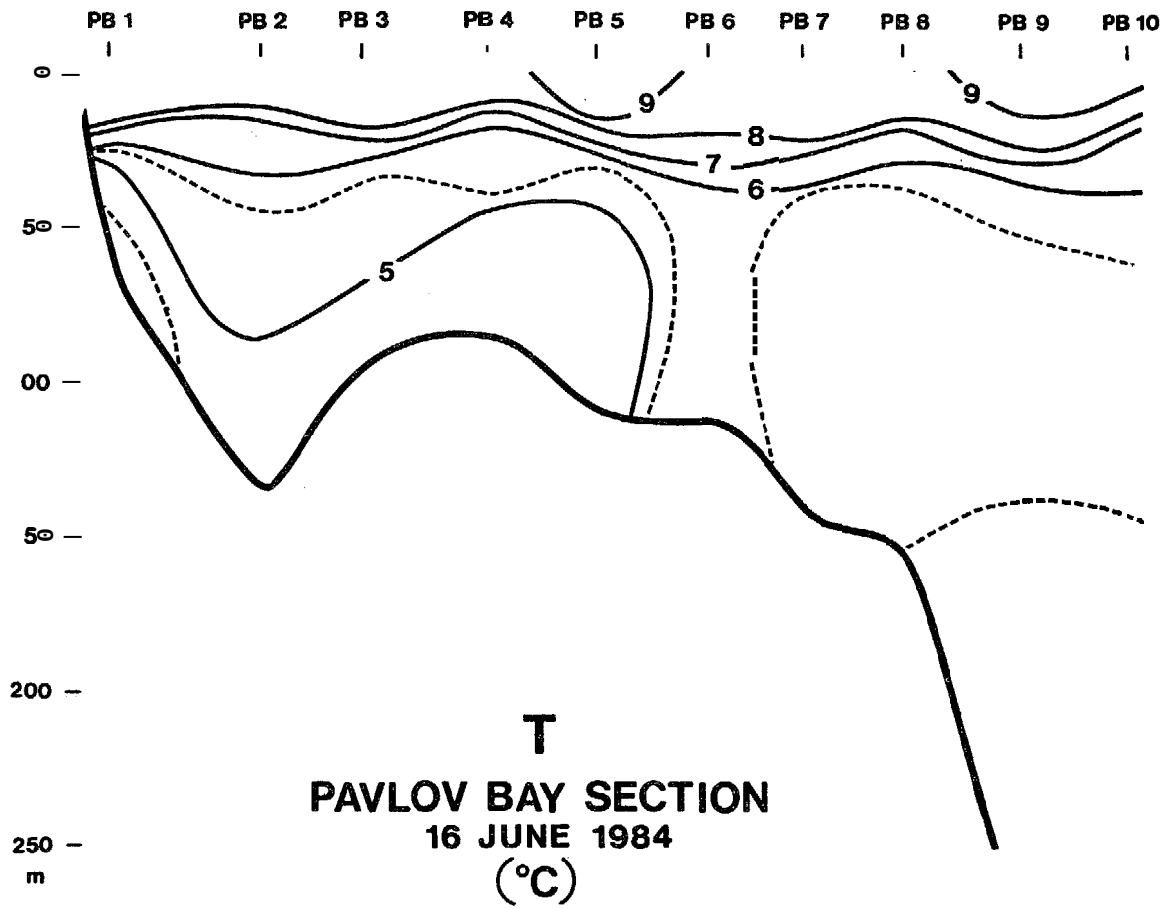

Figure 2.2 - Temperature, Pavlov Bay. June.

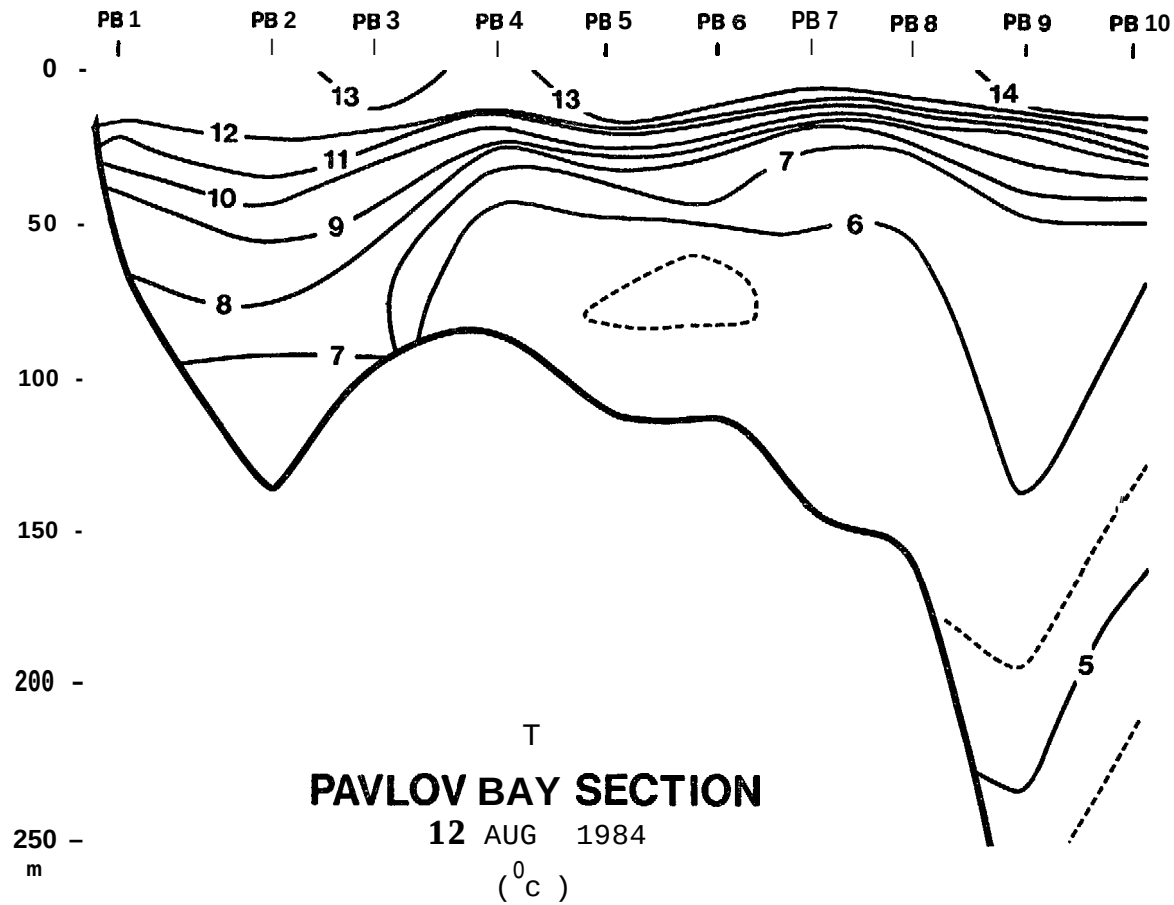

Figure 2.3 - Temperature, Pavlov Bay, August.

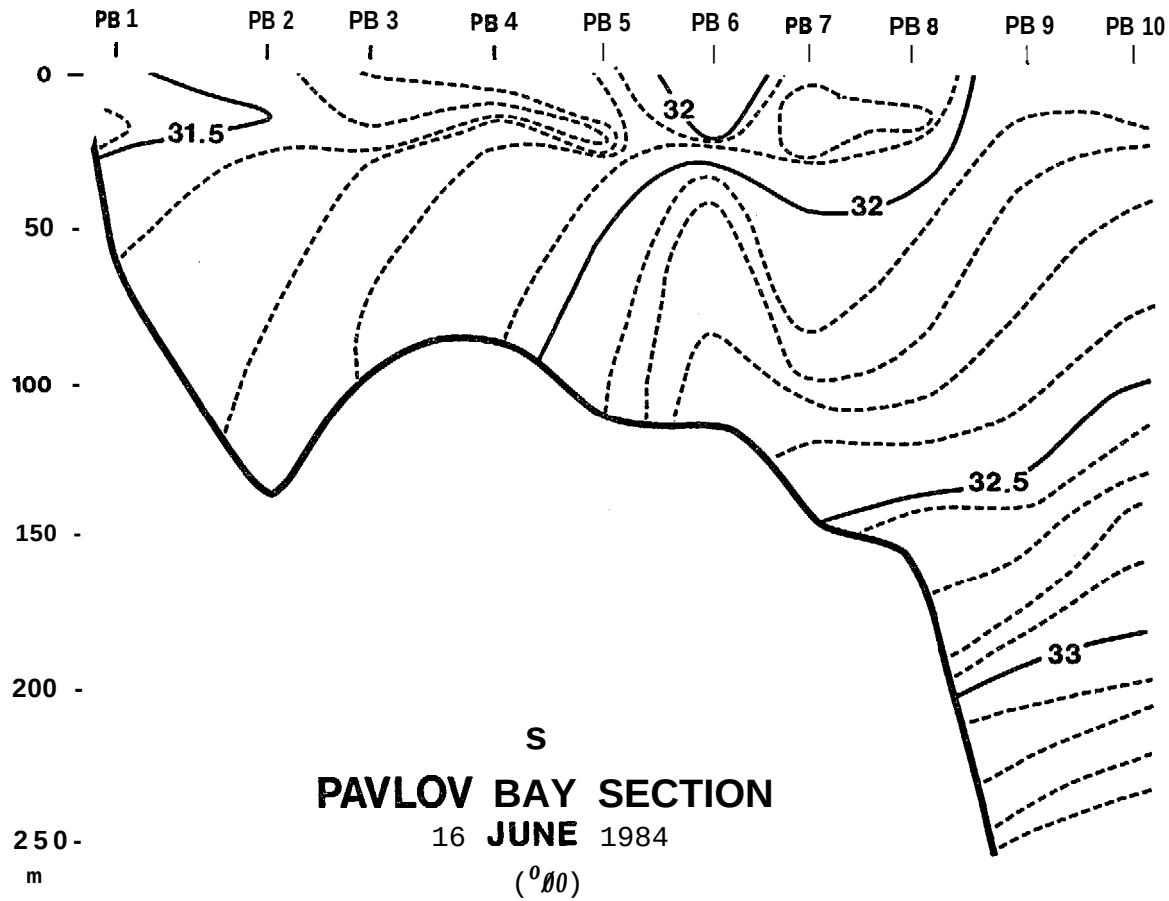

Figure 2.4 - Salinity, Pavlov Bay, June.

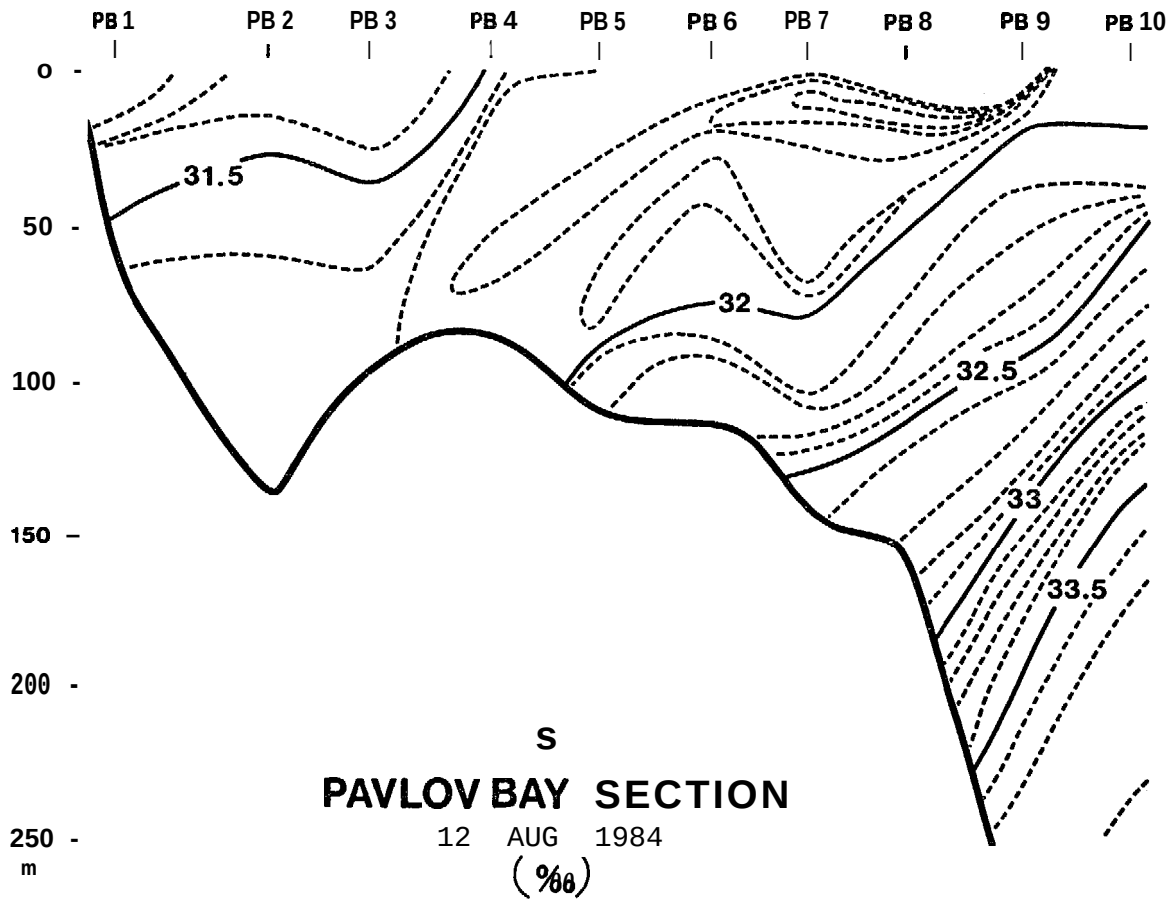

Figure 2.5 - Salinity, Pavlov Bay, August.

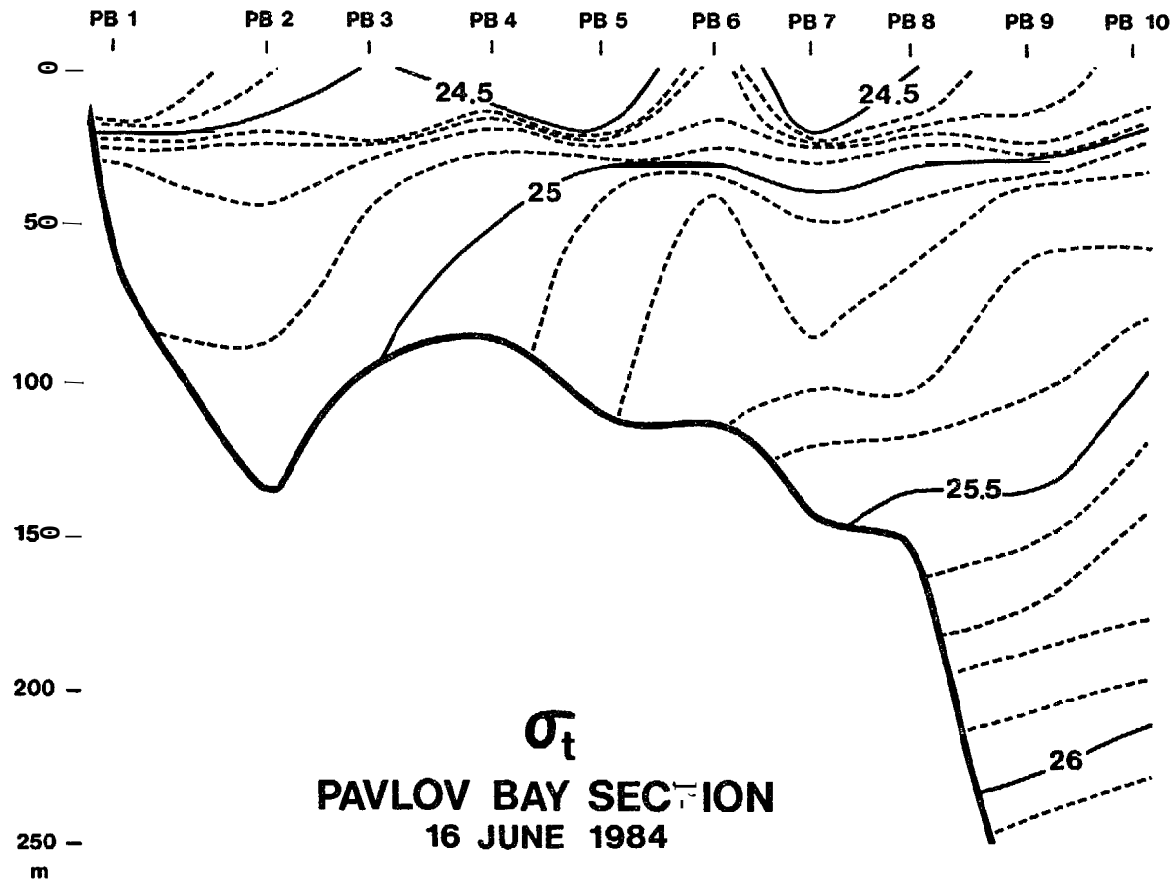

Figure 2.6 - Sigma-t, Pavlov Bay, June.

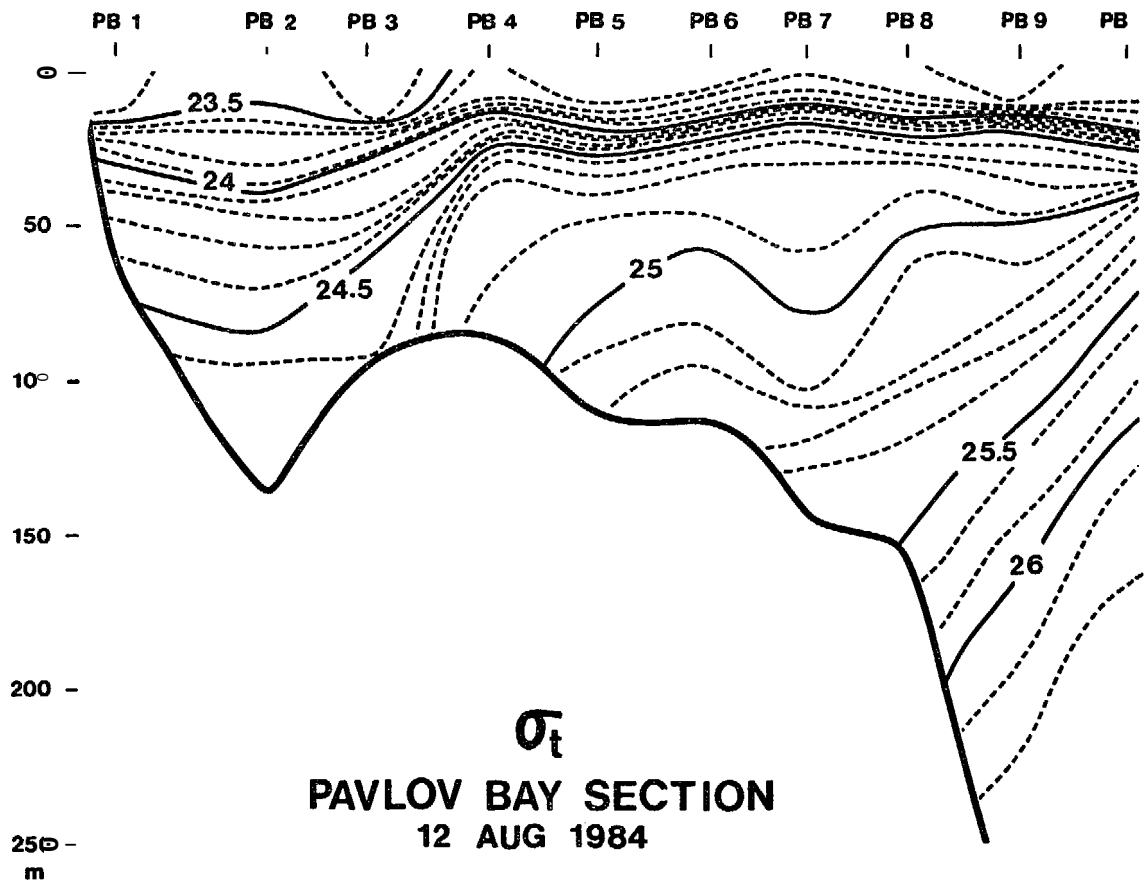

Figure 2.7 – Sigma-t, Pavlov Bay, August.

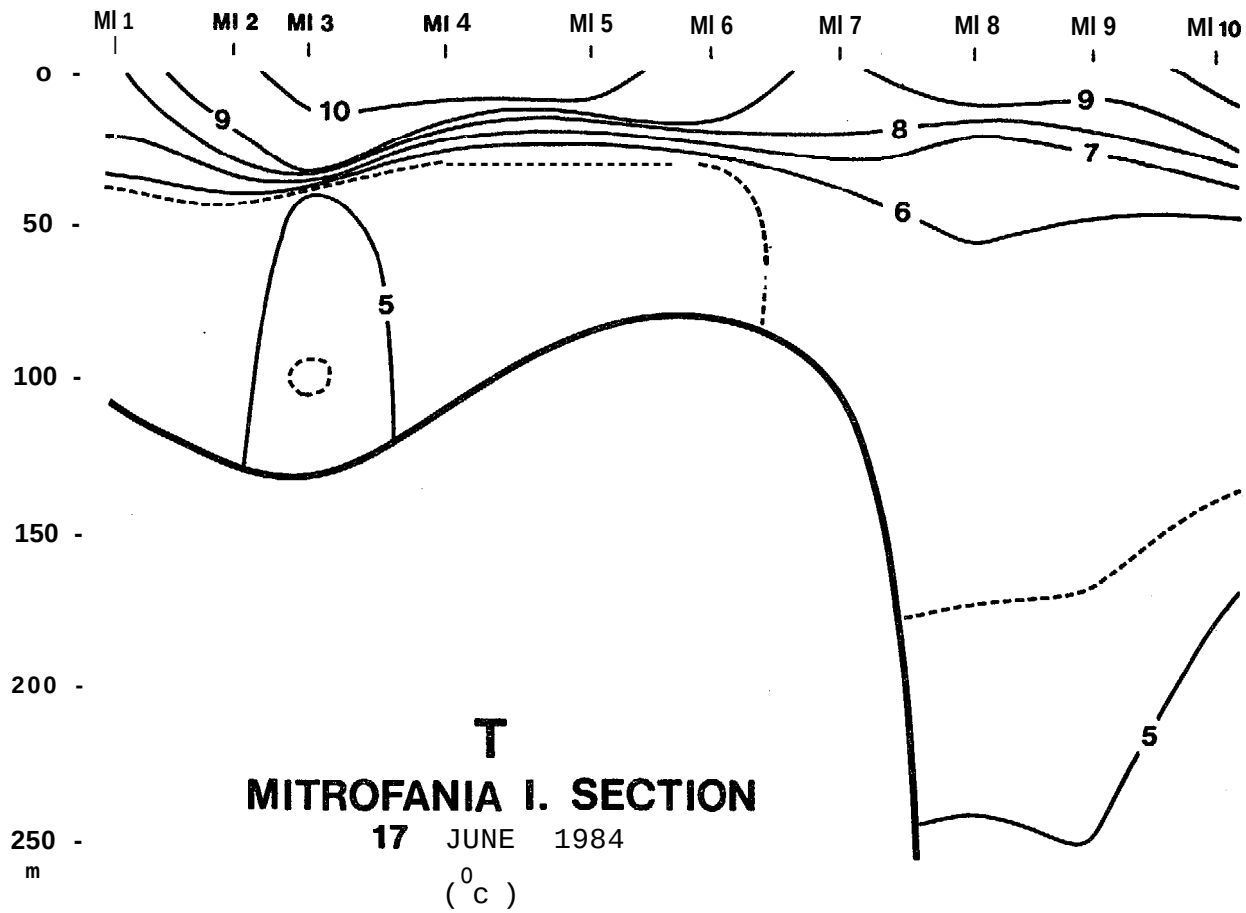

Figure 2.8 - Temperature, **Mitrofania** Island, June.

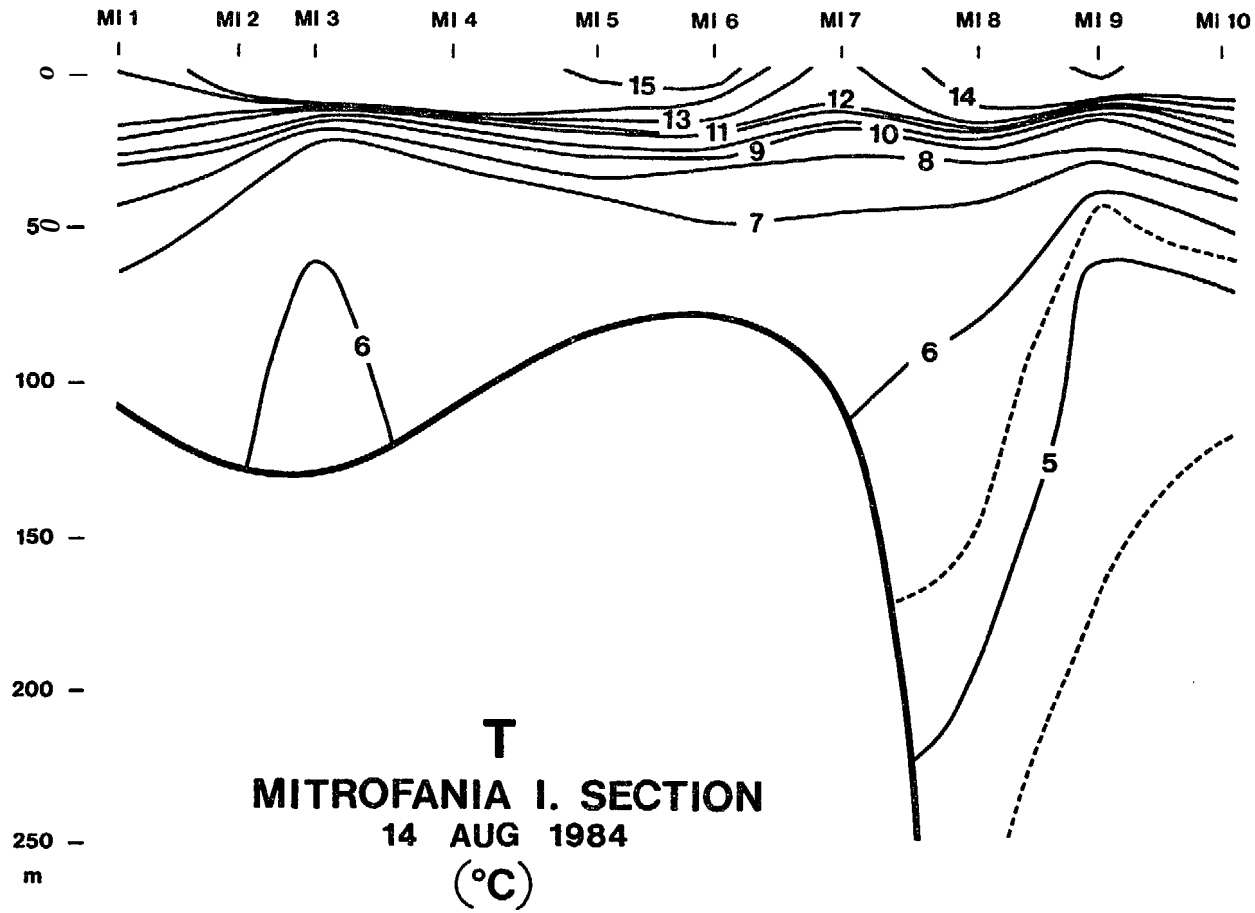

Figure 2.9 - Temperature, Mitrofania Island, August.

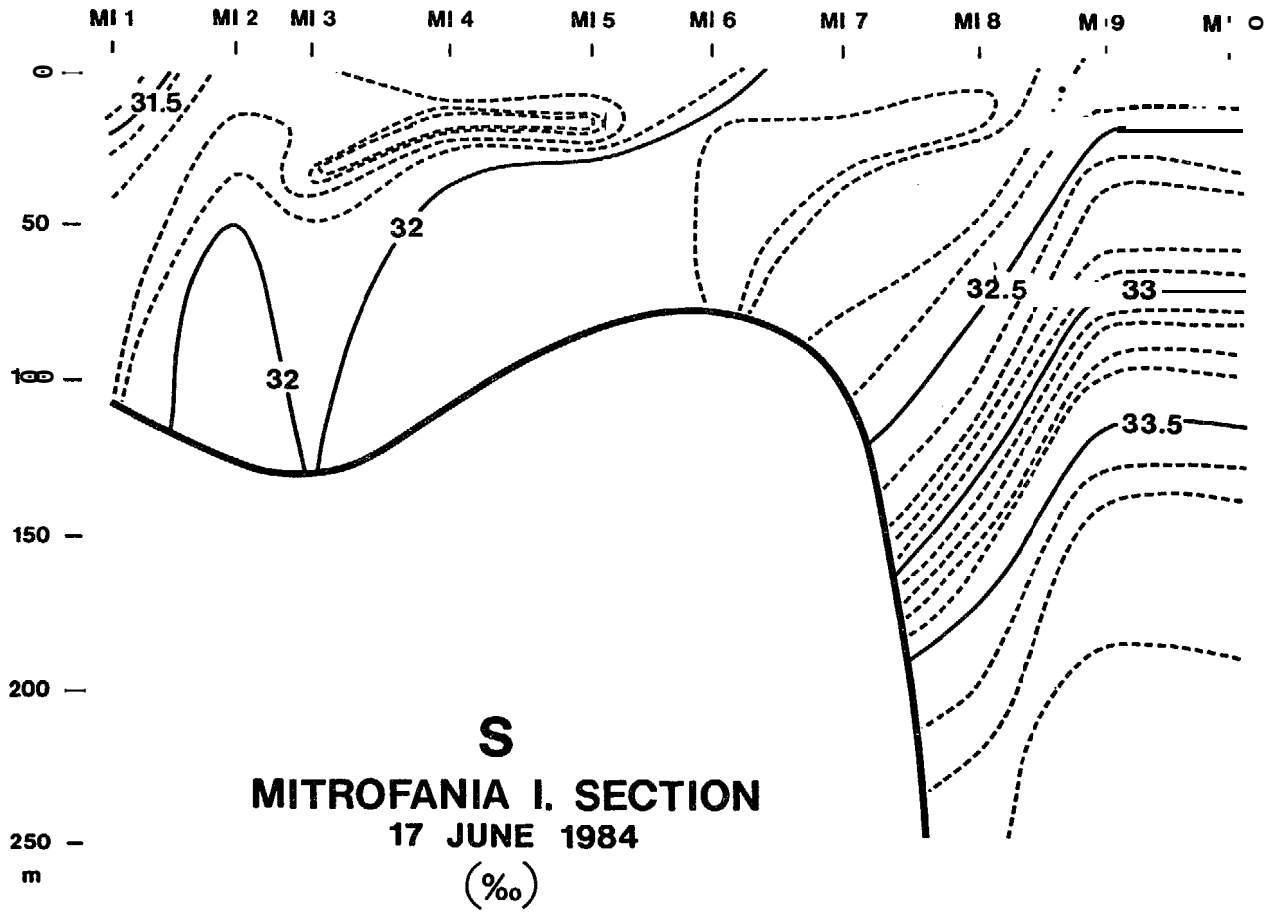

Figure 2.10 – Salinity, Mitrofania Island, June.

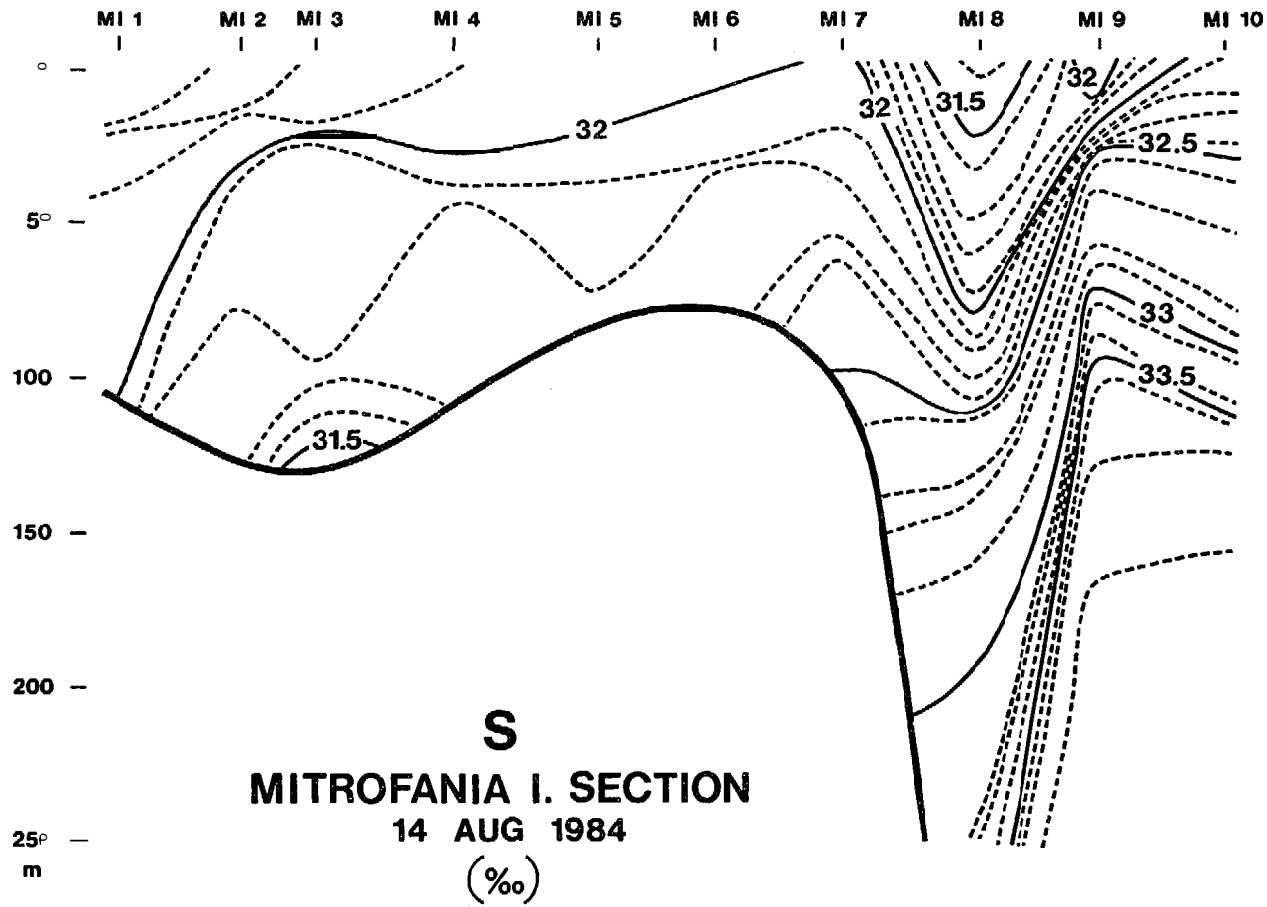

Figure 2.11 – Salinity, Mitrofania Island, August.

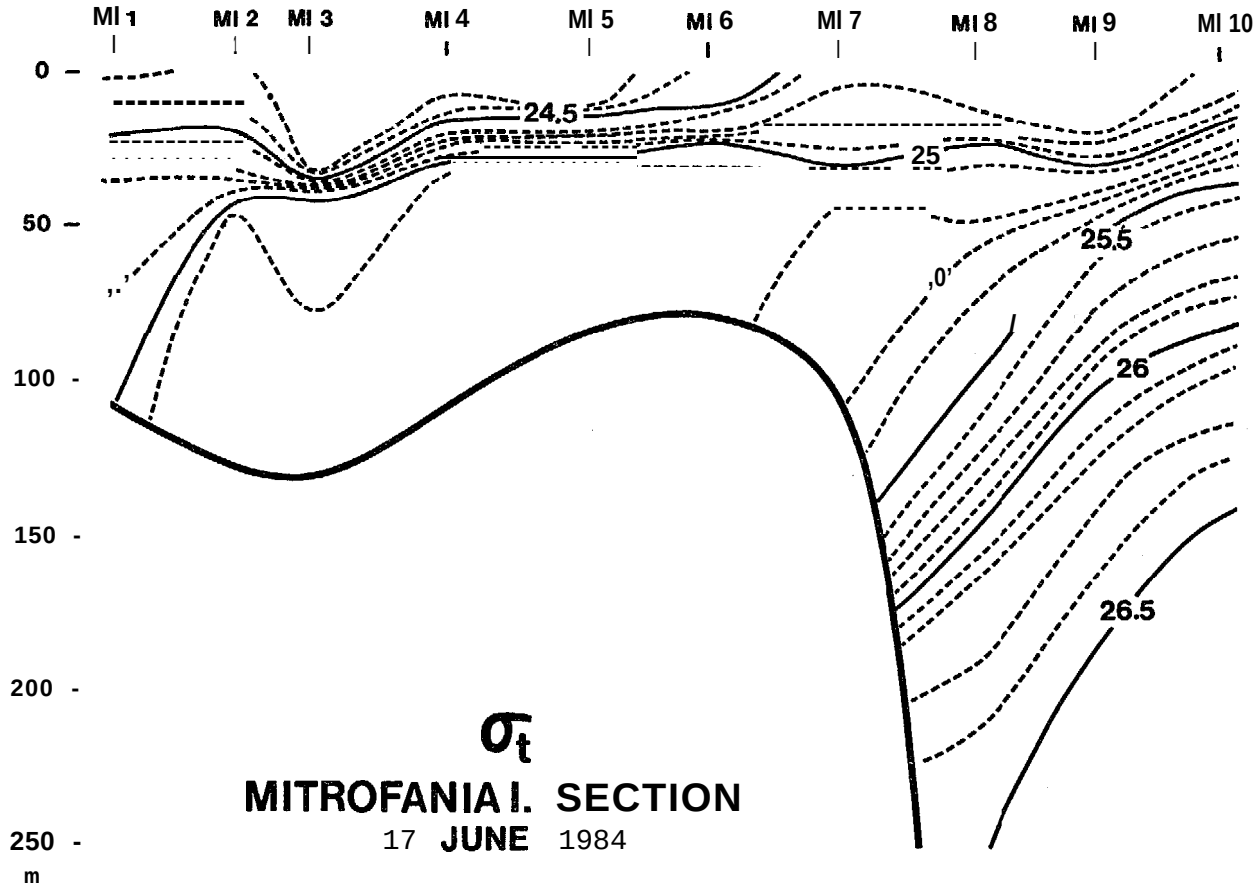

Figure 2.12 - Sigma-t, Mitrof ania Island, June.

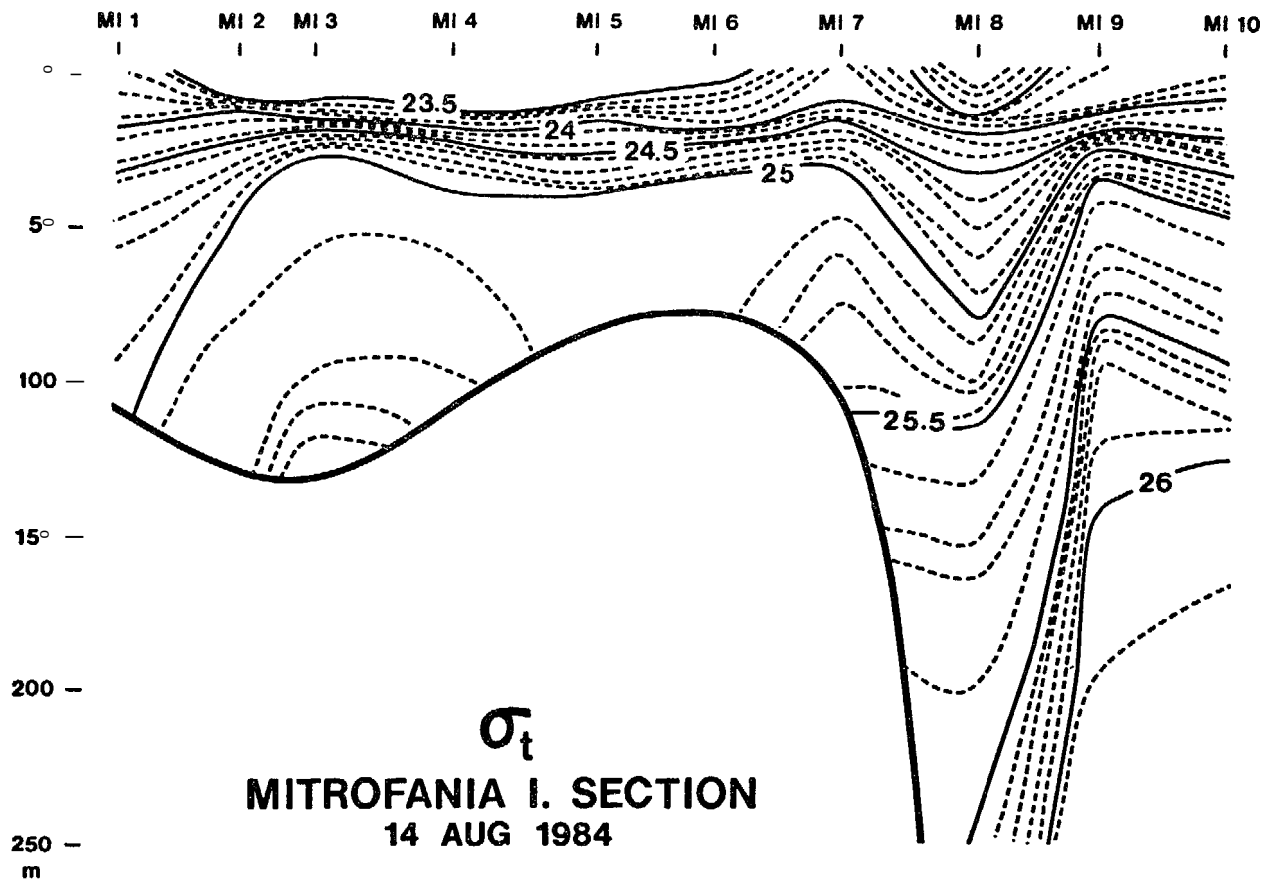

Figure 2.13 – Sigma-t. Mitrofania Island, August.

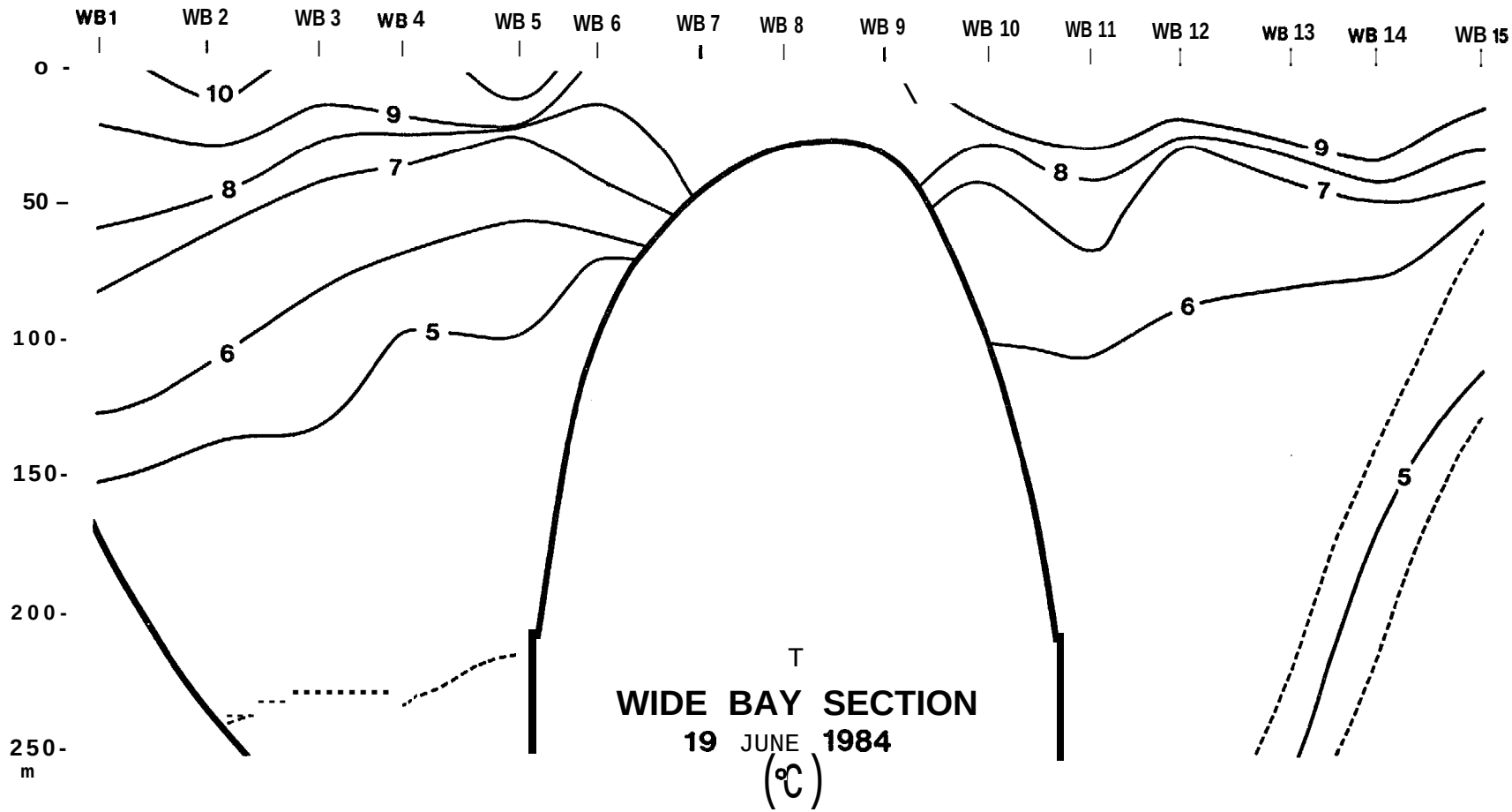

Figure 2.14 – Temperature, Wide Bay, June.

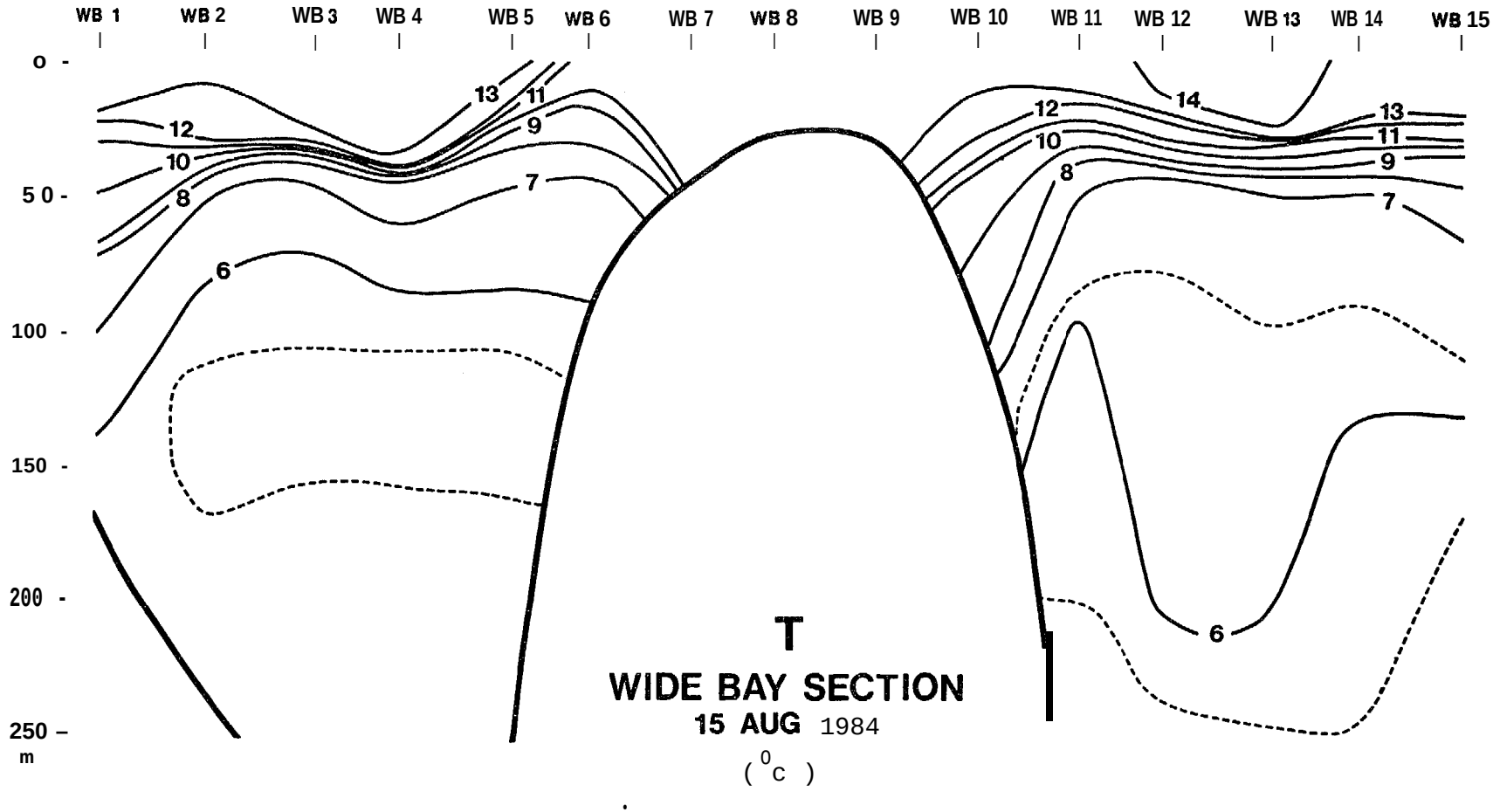

Figure 2.15 - Temperature, **Wide** Bay, August.

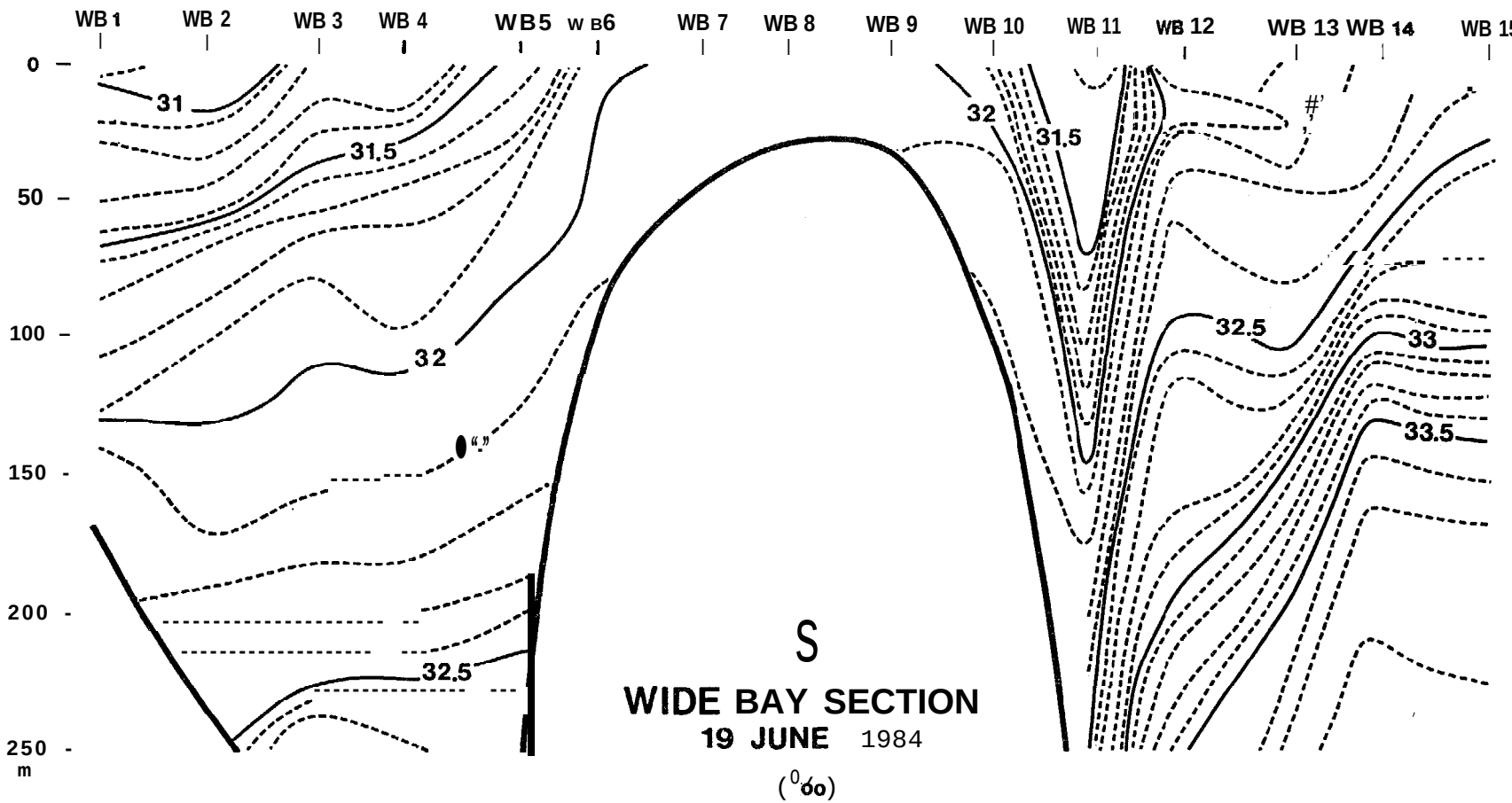

Figure 2.16 - Salinity, Wide Bay, June.

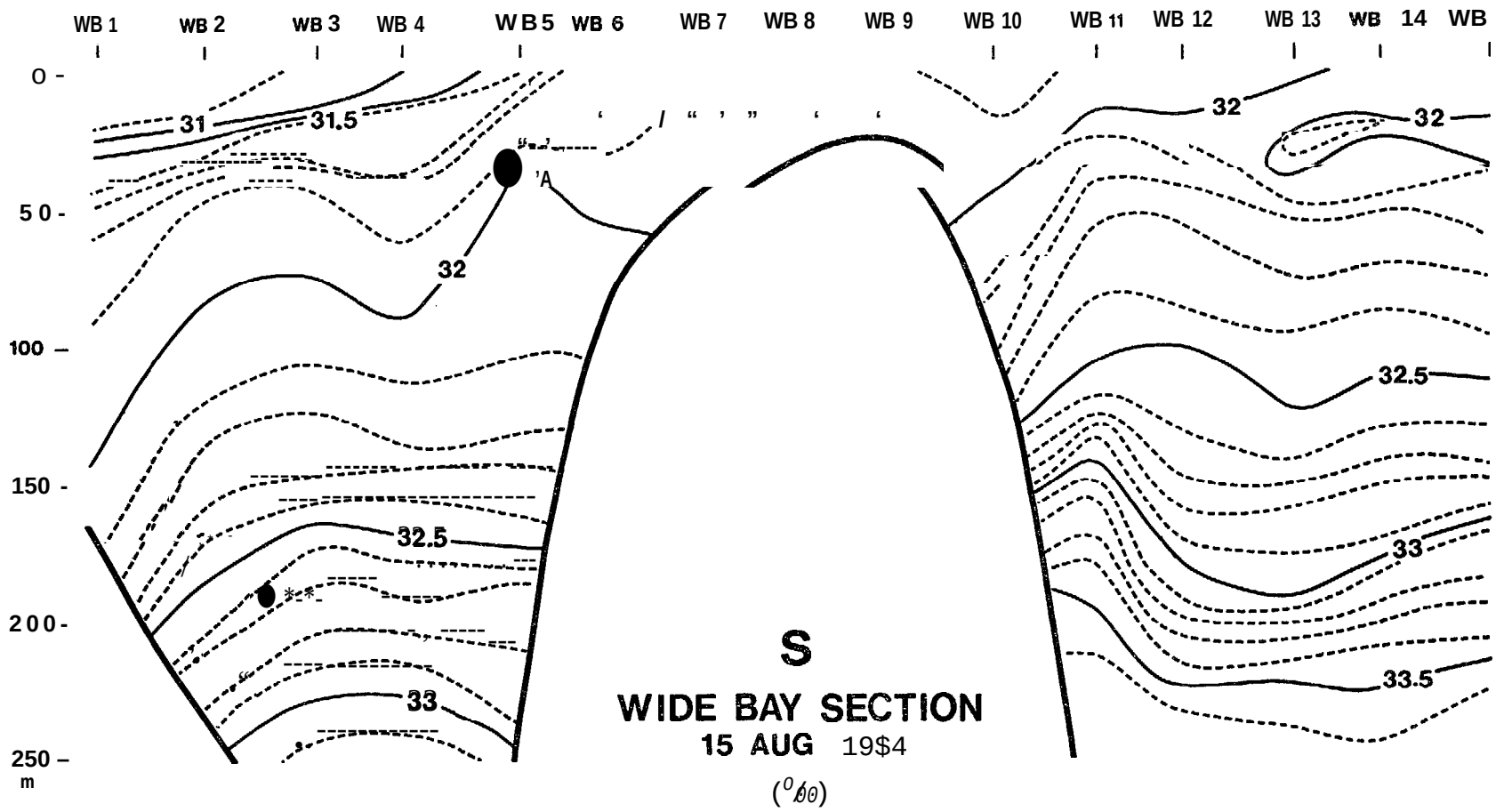

Figure 2.17 - Salinity, Wide Bay, August.

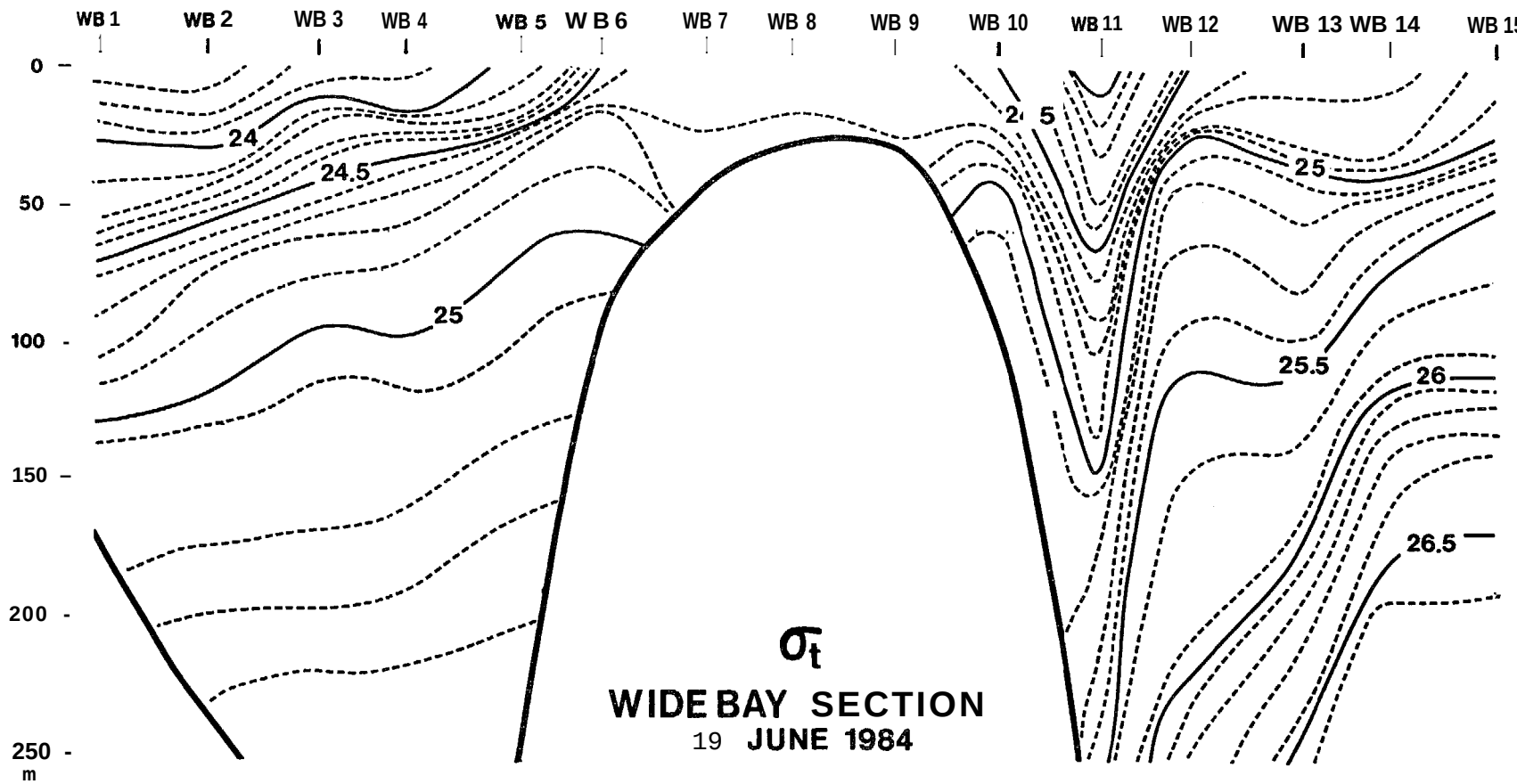

Figure 2.18 - Sigma-t, Wide Bay, June.

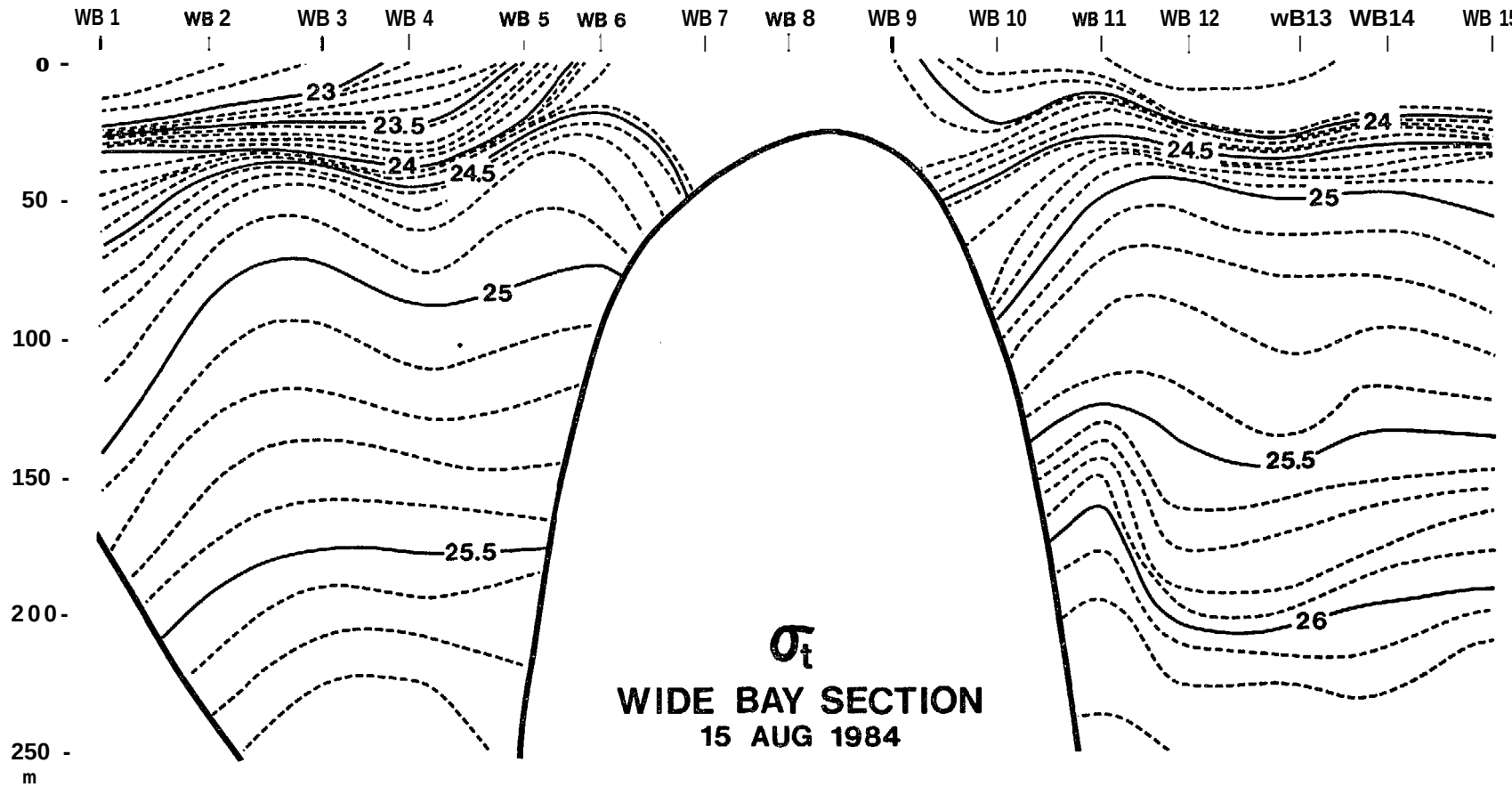

Figure 2.19 - Sigma-t, Wide Bay, August.

tidal mixing in this shallow region. Vertical homogeneity of the water column over Portlock Bank reported by Schumacher et al (1978) and Schumacher and Reed (1980) was also attributed to tidal mixing. It is likely that restratification occurs, at least in the upper layers, during periods of maximum river discharge.

Although the contours have been substantially smoothed, wave-like features still appear on the isotherms particularly at the shallower depths. Such waves are not surprising in light of the strong internal tides (discussed in Section 3.2.2).

2.1.2 Salinity

Unlike the temperature sections, the salinity sections (Figures 2.4, 2.5, 2.10, 2.11, 2.16, 2.17) do not show a pronounced temporal change. There is some indication of freshening over the shelf in the Pavlov Bay section but this process is not apparent in the other two sections. Extremely strong horizontal salinity gradients were measured over the continental slope on the Mitrofania Island section in August (Figure 2.11) and the Wide Bay section in June (Figure 2.14). These gradients are well mirrored in the sigma-t sections, the latter variable being dominated by salinity at low temperatures.

2.1.3 Sigma-t

As a non-linear function of temperature and salinity, sigma-t is more strongly dependent upon salinity at low temperatures and, conversely, more dependent upon temperature at high temperatures. The result in the Western Gulf of Alaska is that sigma--t temporal changes parallel those of temperature in the near surface layers and of salinity in the deeper layers. At all three sections (Figures 2.6, 2.7, 2.12, 2.13, 2.18, 2.19) the density stratification in the upper 50 m approximately doubled between June and August while the deeper stratification remained almost constant. In June very strong horizontal gradients of density were observed over the continental slope in the Wide Bay Section (Figure 2.18). Similarly strong

horizontal gradients were observed over the continental slope in the Mitrofania Island section in August (Figure 2.13). This feature may have been advected, or propagated, along the slope between June and August; the mean advection speed would be about 4 cm s^{-1}. The gradients are suggestive of an anticyclonic (clockwise) eddy of about 13 km in radius. Similar features were described by Favorite and Ingraham (1977) and Schumacher et al, (1979). An eddy whose signature is visible in the mass field should have a radius roughly comparable to the internal Rossby radius which is defined as

$$r = \sqrt{g\frac{\Delta\rho}{\rho}h}/f \qquad \text{(2-1)}$$

where g is gravity, ρ density, h is the thickness of the surface layer and f is the Coriolis parameter over the continental slope. r has a value of between 6 and 12 km so that this eddy-like feature is of appropriate size to satisfy dynamic balances. In particular if the eddy were generated by baroclinic instability it would correspond closely in size to the most unstable (and therefore predominant) wavelength (if wave length = 2r) according to Mysak, et al (1981). The agreement between the apparent eddy radius and the internal Rossby radius supports the observations but does not necessarily imply formation by baroclinic instability.

The presence of anticyclonic (clockwise) eddies over the continental slope raises the possibility of cross-slope exchange of water and nutrients due to instabilities. For example, baroclinic instabilities are characterized by turbulent property exchanges across the mean flow and thus along the mean pressure gradient (Smith, 1976). These cross depth gradient fluxes can be visualized as the breaking of waves on the isopycnal surfaces when the slopes of the surfaces exceed critical values. The "breaking waves" propagate along the initial isopycnal slope, i.e. across the mean flow.

It will be seen in the next sections that the station spacing is not quite small enough to properly resolve spatial variability of the size of the internal Rossby radius. While this drawback has little effect upon

qualitative representation of the distribution of properties, it limits the utility of the dynamic method by which geostrophic currents are computed from horizontal density gradients.

2.2 DYNAMIC HEIGHTS, GEOSTROPHIC CURRENTS

Geostrophic shears can be integrated from an assumed level of no motion to yield estimates of the baroclinic geostrophic current profile. This long-standing method has both its strong adherents and detractors. The latter are critical of some of the assumptions of the "Dynamic Method" and have shown that they do not apply in many regions. For the present data set the most important limitations are lack of synopticity and, to a lesser extent, insufficiently dense station spacing.

The thermal wind equations, from which the dynamic method arises, assume a steady flow. Implicit is that vertical motion of the isopycnals is negligible. In the presence of a strong internal wave field, however, this is simply not the case, Several investigators have surmounted the obstacle of time-varying flows in computations of geostrophic currents by averaging density measurements over a tidal cycle. Such a procedure is extremely consumptive of ship time and was not attempted in our field work. The computed dynamic heights and geostrophic currents therefore neither represent a tidal average nor an instantaneous realization of the flow. We would suggest that where the mean flow energy is small compared to the tidal energy, geostrophic current computations do little more than yield a qualitative view of the flow field.

In order to produce stream lines of the geostrophic flow, the dynamic height anomaly between selected pressure surfaces was plotted and contoured. The charts for June and August are presented on the same page for ease of comparison in Figure 2.20 through 2.23. Figure 2.20 shows the dynamic height topography of the surface relative to 10 decibars. The plots are an indication of the density of the mixed layer; the larger anomalies representing less dense water. The influence of warmer and fresher waters nearshore is shown. The anomalies increased between June

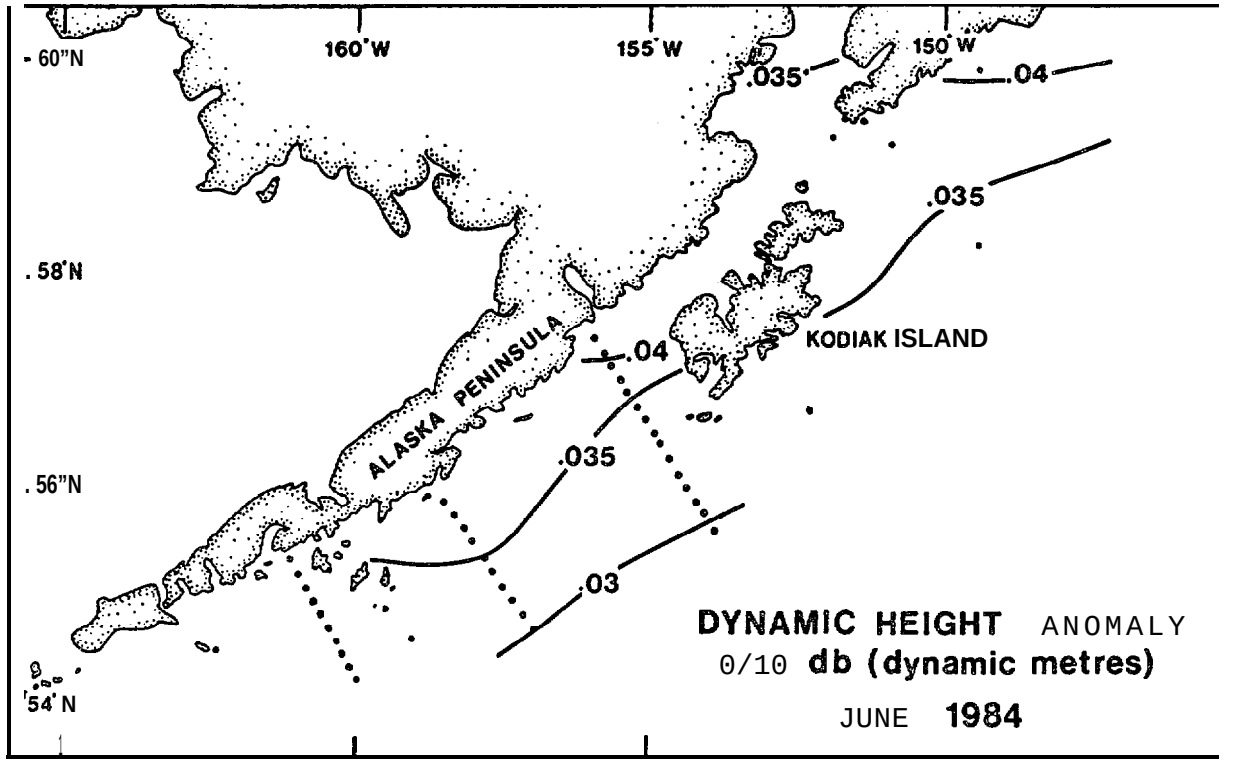

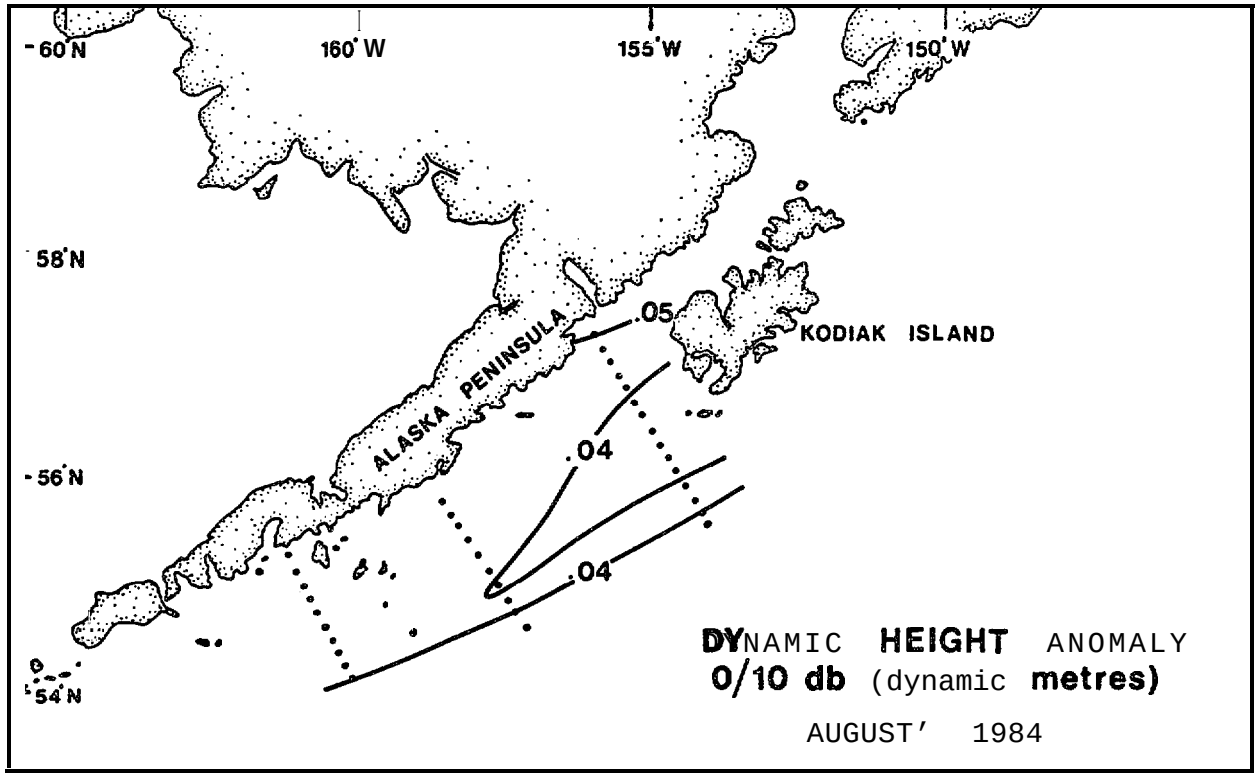

Figure 2.20 - Dynamic height topography, 0/10 db, June and August 1984.

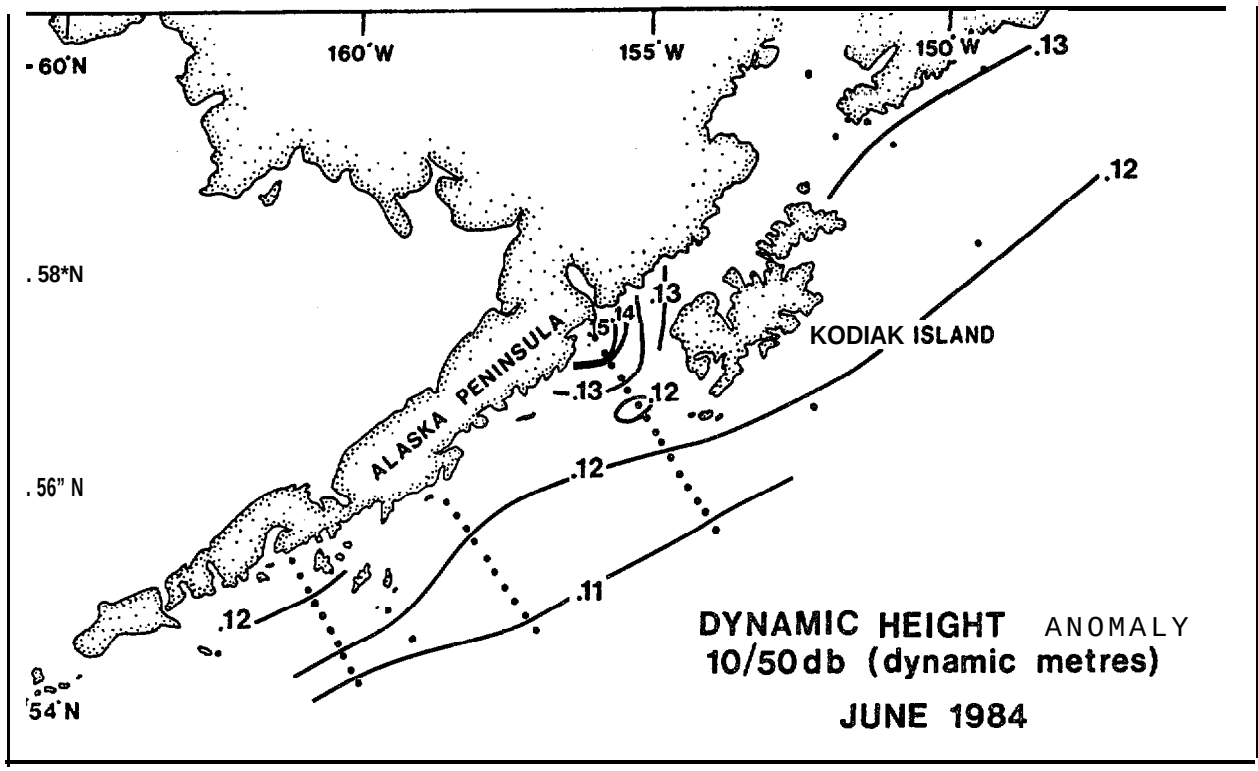

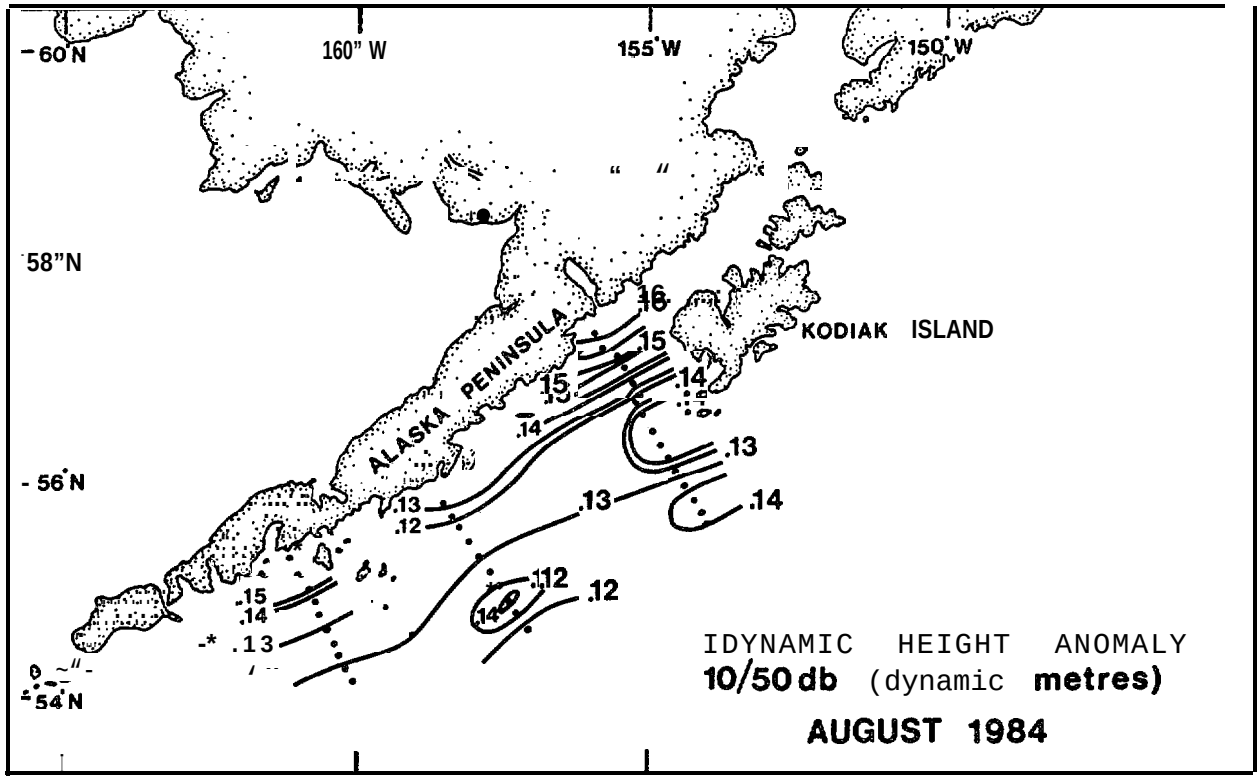

Figure 2.21 - Dynamic height topography, 10/50 db, June and August 1984.

and August due to continued insolation. Figures 2.21 and 2.22 represent the topography of the 10 and O db surfaces relative to 50 db. The geostrophic flow field in the upper 50 m is thus portrayed.

The velocity differences between surfaces can be computed by

$$Au = \frac{l\ O_{A\ D}}{fL} \qquad (2\text{-}2)$$

where Au is the velocity difference, AD is the difference in dynamic height anomaly between two stations, f is the Coriolis parameter and L is the distance between stations. The 10/50 db and 0/50 db charts show that the geostrophic velocity shear in the upper layers was generally less than 10 cm s^{-1} and on average across the shelf about 3 cm S-l. The 10/50 and 0/50 db charts are virtually identical demonstrating the density gradients in the upper 10 m contributed little to the geostrophic flow field. Considerably more horizontal structure was present in August than in June above the 50 decibar surface probably due to increased river discharge toward the end of summer which introduced fresher water. Both the freshening itself and the enhanced stratification promoting heating of the surface layers would have contributed to the contrast between June and August . However, the mean flow (for example through the Wide Bay or eastern most section) changed little between June and August. The mean velocity in the upper 50 m was southwestward at a speed of about 2 or 3 cm s^{-1} relative to 50 db.

Figure 2.23 shows the dynamic topography of the 10 db surface relative to 100 db. Vertical velocity shear is most apparent along and near the shelf break where vertical velocity differences in June are on the order of 8 cm s-f and the direction of flow is to the southwest. In August the flow along the shelf break is about 4 cm s^{-1} and generally directed toward the northeast. An outflow on the order of 5 cm s^{-1} is directed southwestward from Shelikof Strait in both June and August. This *figure is in* fairly good agreement with the mean flow measured over the two month period at the current meter at 46 m depth in Shelikof Strait.

In all the dynamic height topography charts the mean flow from the shore to the shelf break is directed toward the southwest in agreement with the contemporary view of the Alaska Coastal Current regime, e.g. Royer (1981).

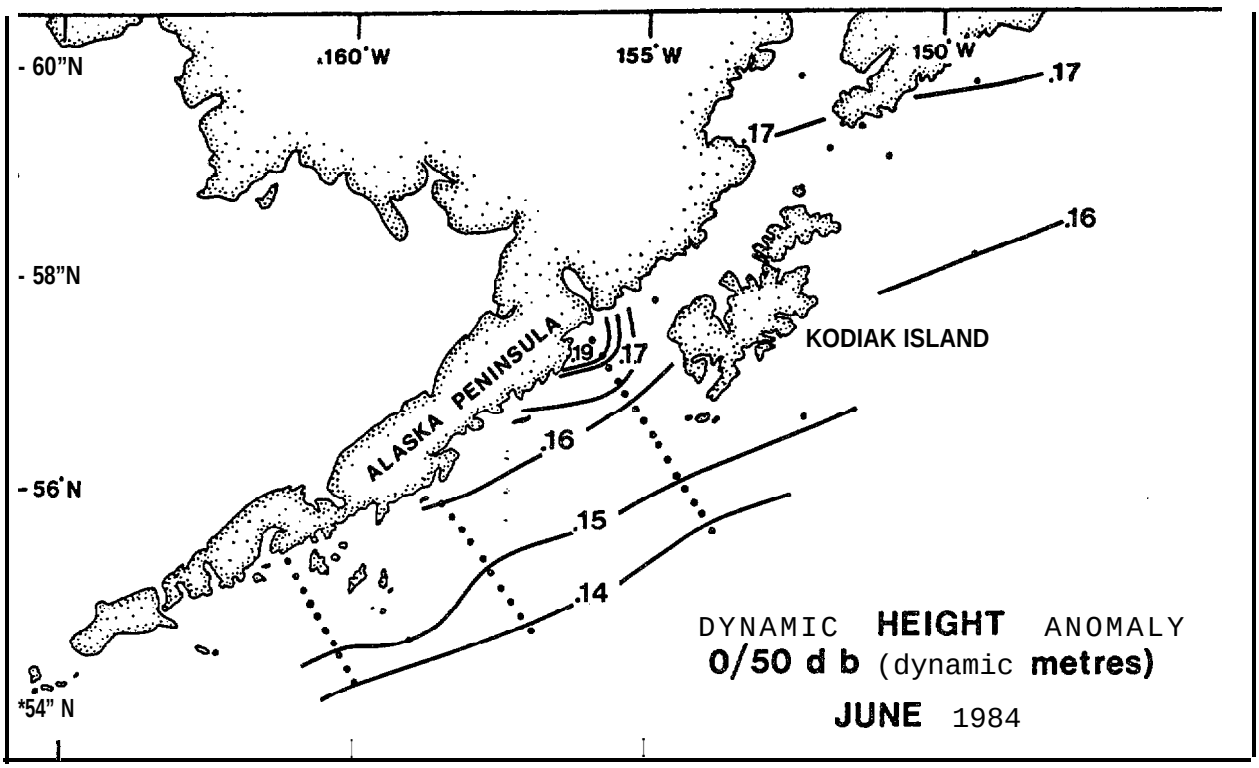

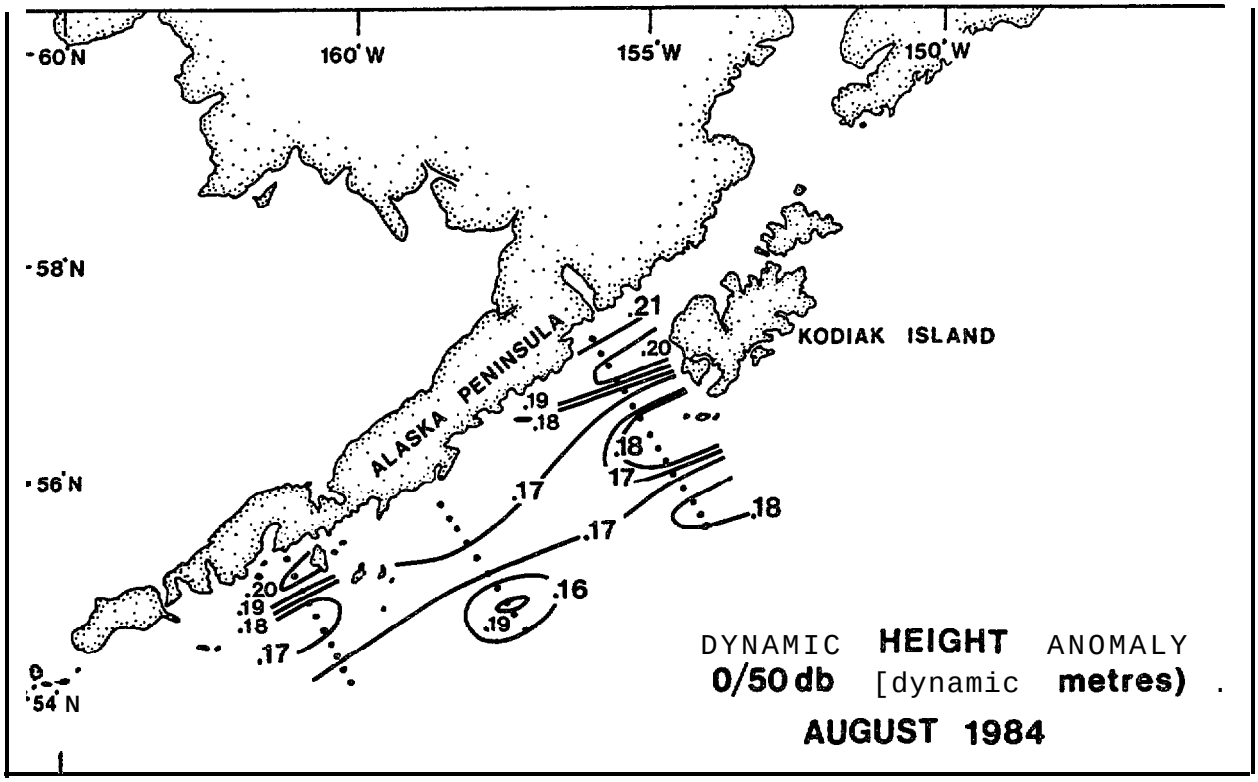

Figure 2.22 - Dynamic height topography, 0/50 db, June and August 1984.

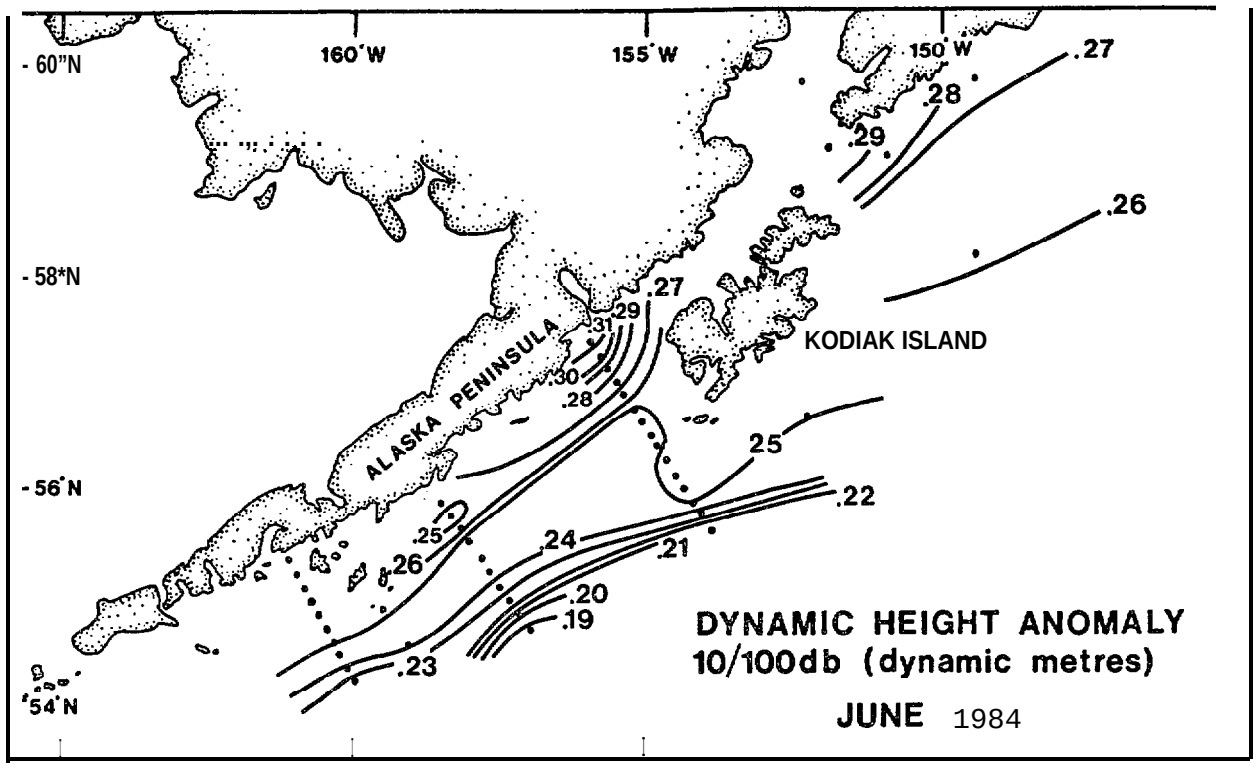

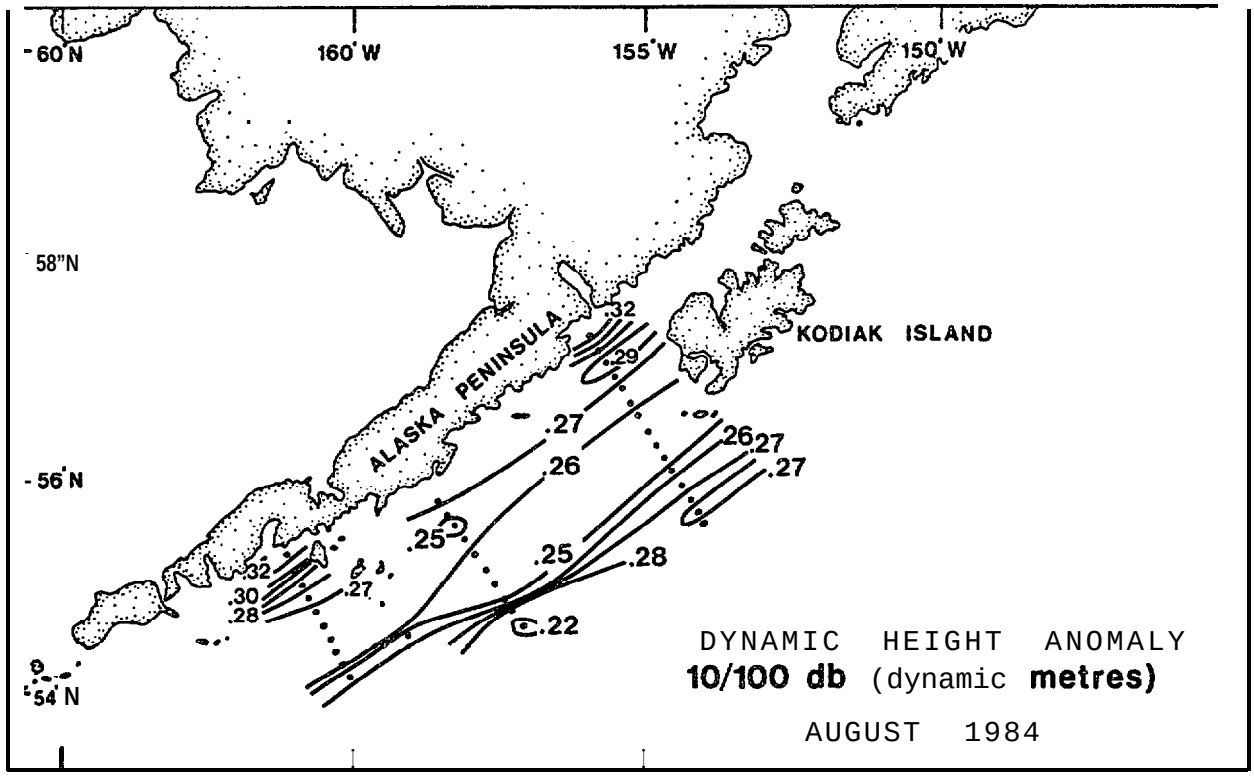

Figure 2.23 - Dynamic height topography, 10/100 db, June and August 1984.

An attempt was made to establish a level of no motion across the shelf and to unify the geostrophic shears into cross section of velocity. In author's view the procedure is more artistic than quantitative. Such cross sections of velocity do, however, give a sense of structure of the velocity field. Isotachs for June and August are presented for each of the sections in Figure 2.24 through 2.29. The details of the structure are clearly limited by the station spacing which was somewhat larger than the internal Rossby radius of deformation. In addition, the quality of the CTD data is rather poor and spurious structures may have been introduced to these cross sections.

2.3 SURFACE SALINITIES AND TEMPERATURES

Charts of the surface salinity and temperature distributions during June and August are shown in Figures 2.30 through 2.33.

The 32.0 ppt surface isohaline appears to follow the shelf break during both June and August. Values are similar to those reported by Reed et al, (1979). There is an indication of the freshening of the surface waters in Shelikof Strait during the summer, but the sampling stations were very sparse in that region. The salinity increased monotonically offshore in agreement with the concept of a runoff driven southwesterly flow along the shelf. No salinity minimum was found over the shelf break as has been reported by Favorite and Ingraham (1977) or Royer and Muench (1977) for Spring conditions. It appears, rather, that summer conditions prevailed during the period June through August 1984.

The surface temperature charts show mainly a general increase in temperature due to insolation over the summer. There is an indication of the presence of cooler surface waters near-shore than offshore in both months probably due to relatively cold river discharge. The cross-shelf horizontal temperature gradients remain almost constant between June and August.

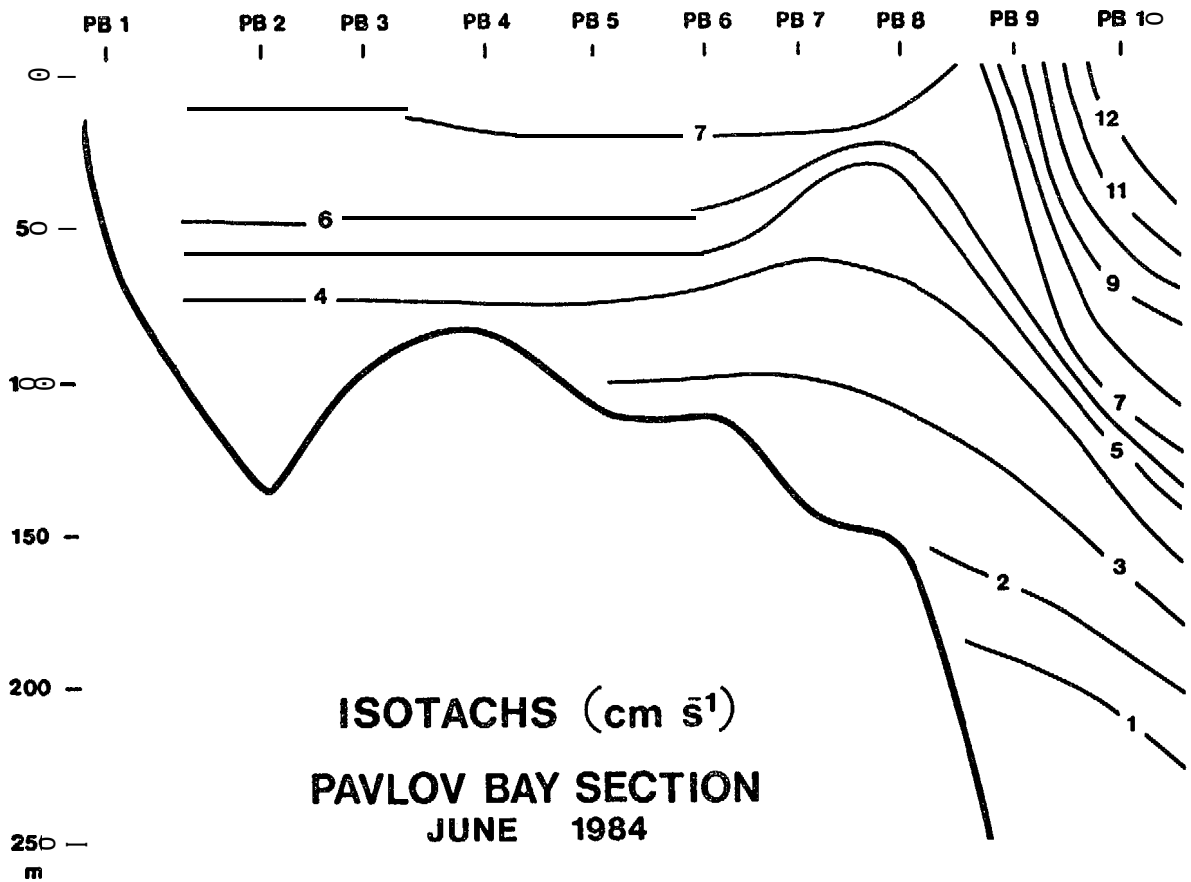

Figure 2.24 - Isotachs, Pavlov Bay, June. Positive flows are out of the page; i.e., to the southwest.

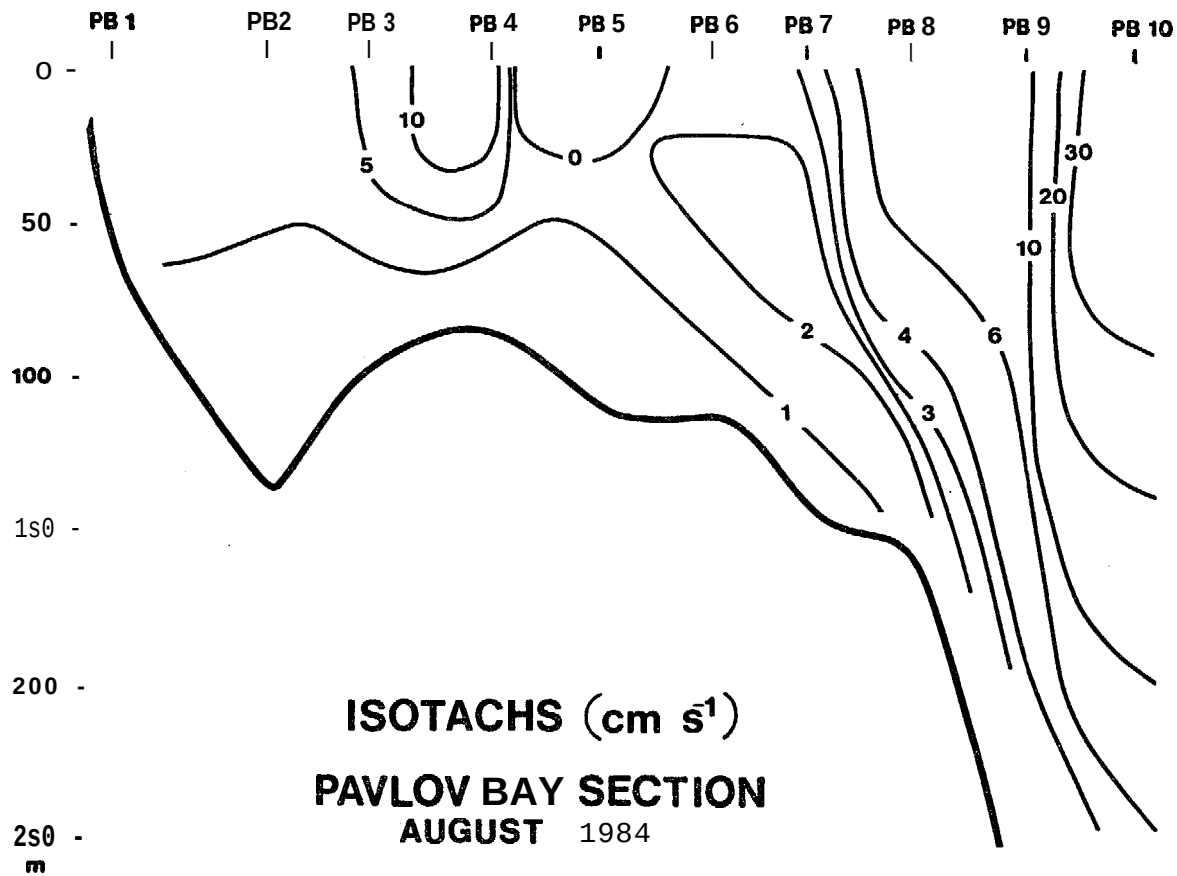

Figure 2.25 - **Isotachs,** Pavlov Bay, August. Positive flows are out of the page; i.e., to the southwest.

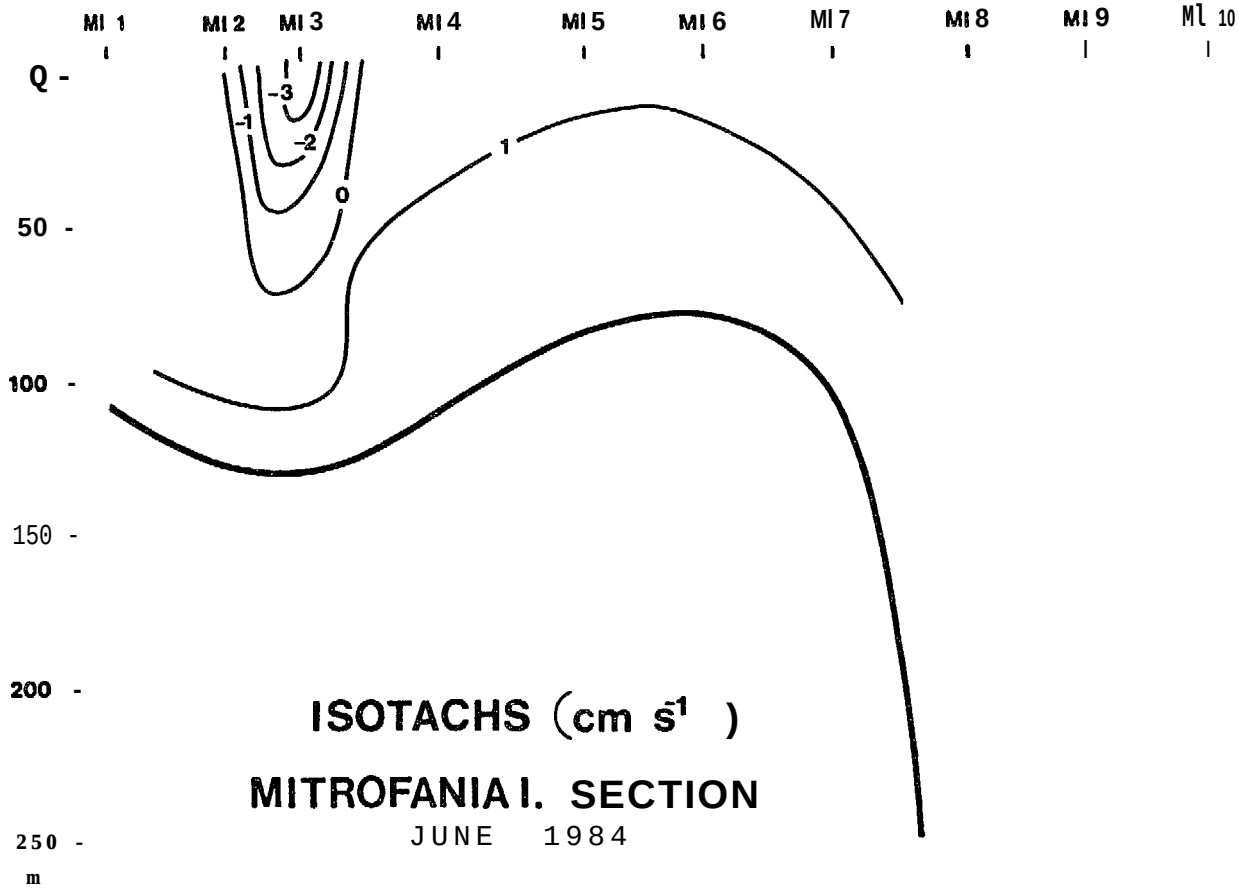

Figure 2.26 - Isotachs, Mitrofania Island, June. Positive flows are out of the page; i.e., to the southwest.

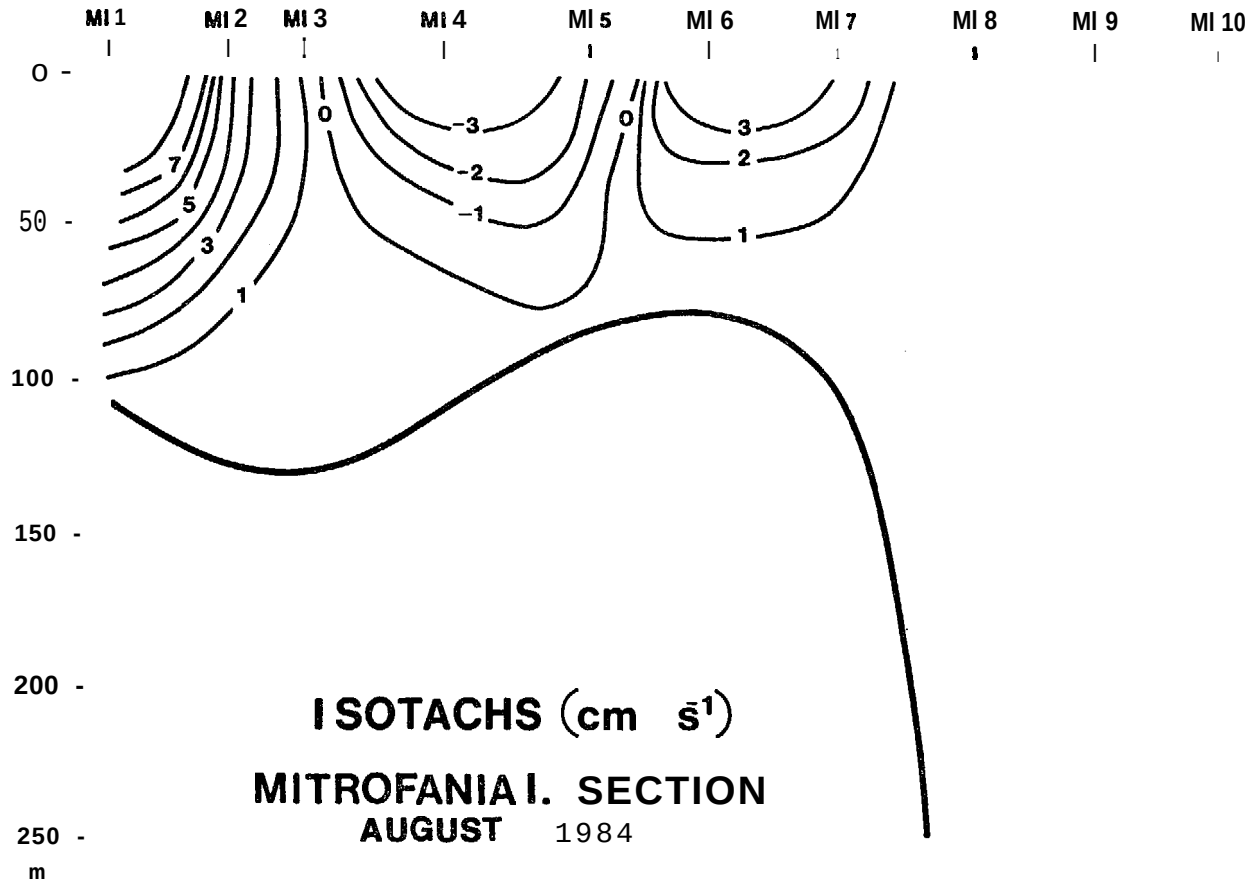

Figure 2.27 -- Isotachs, Mitrofania Island, August. Positive flows are out of the page; i.e., to the southwest.

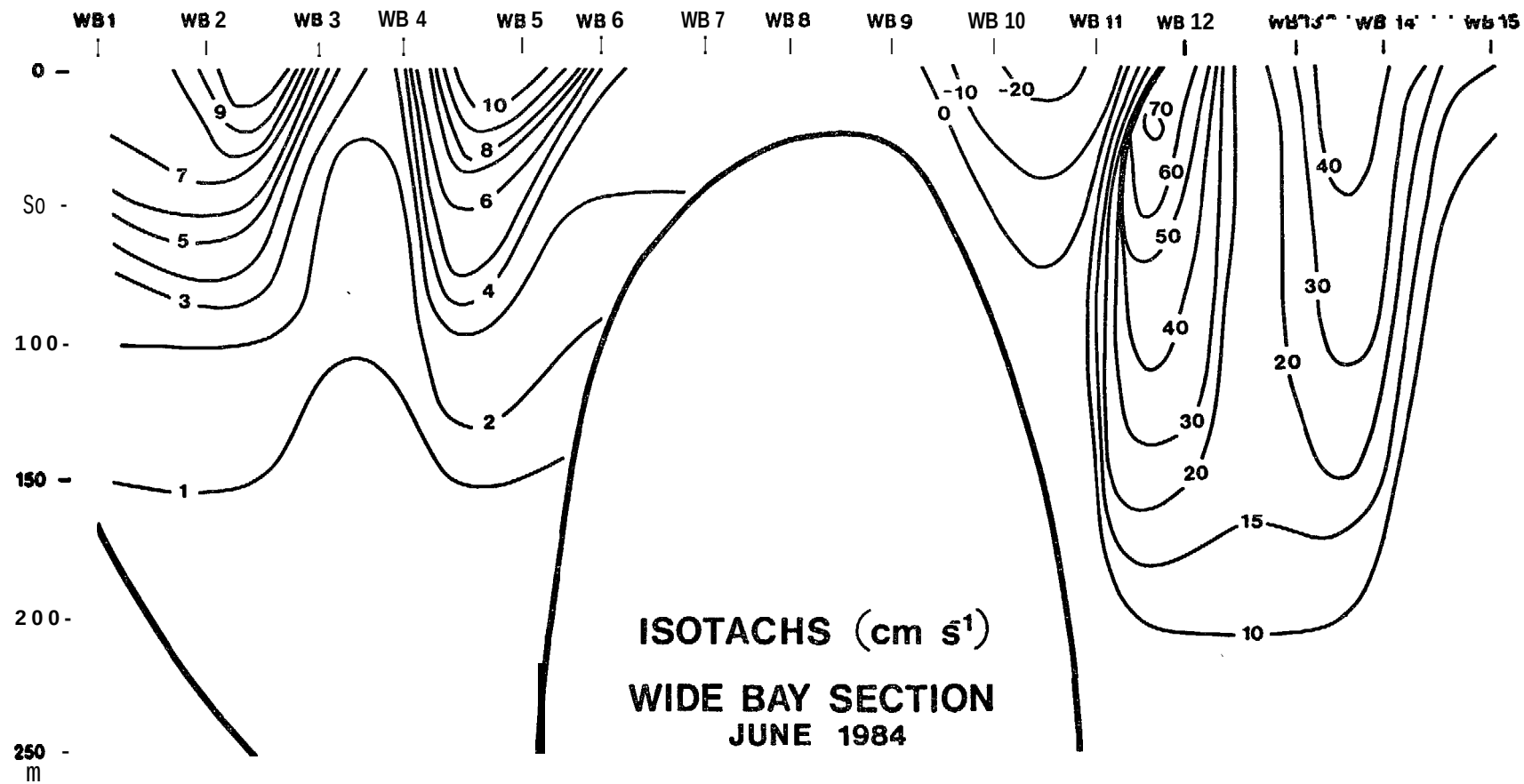

Figure 2.28 - Isotachs, Wide Bay, June. Positive flows are out of the page; i.e., to the southwest.

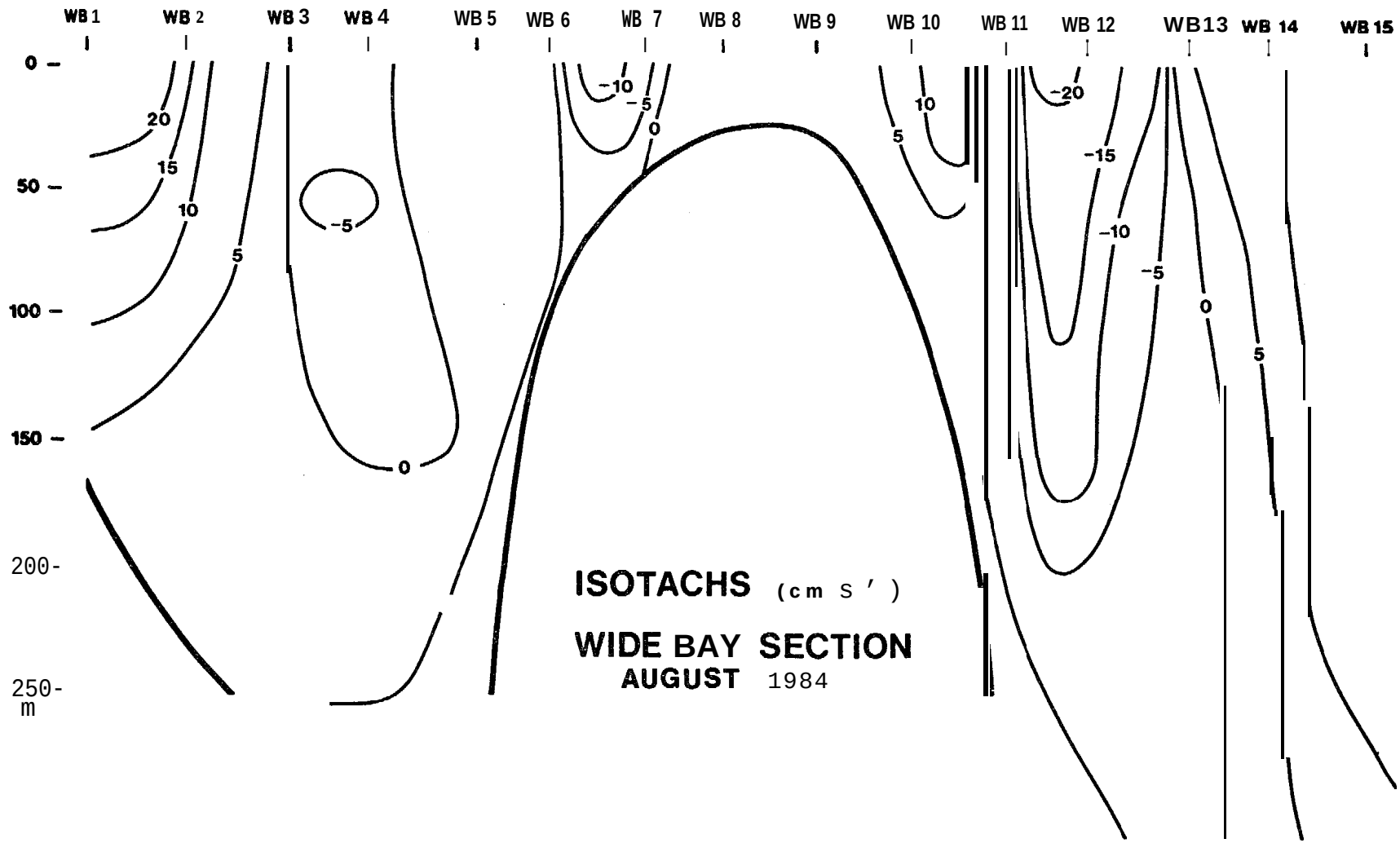

Figure 2.29 - **Isotachs,** Wide Bay, August. Positive flows are out of the page; **i.e.,** to the southwest.

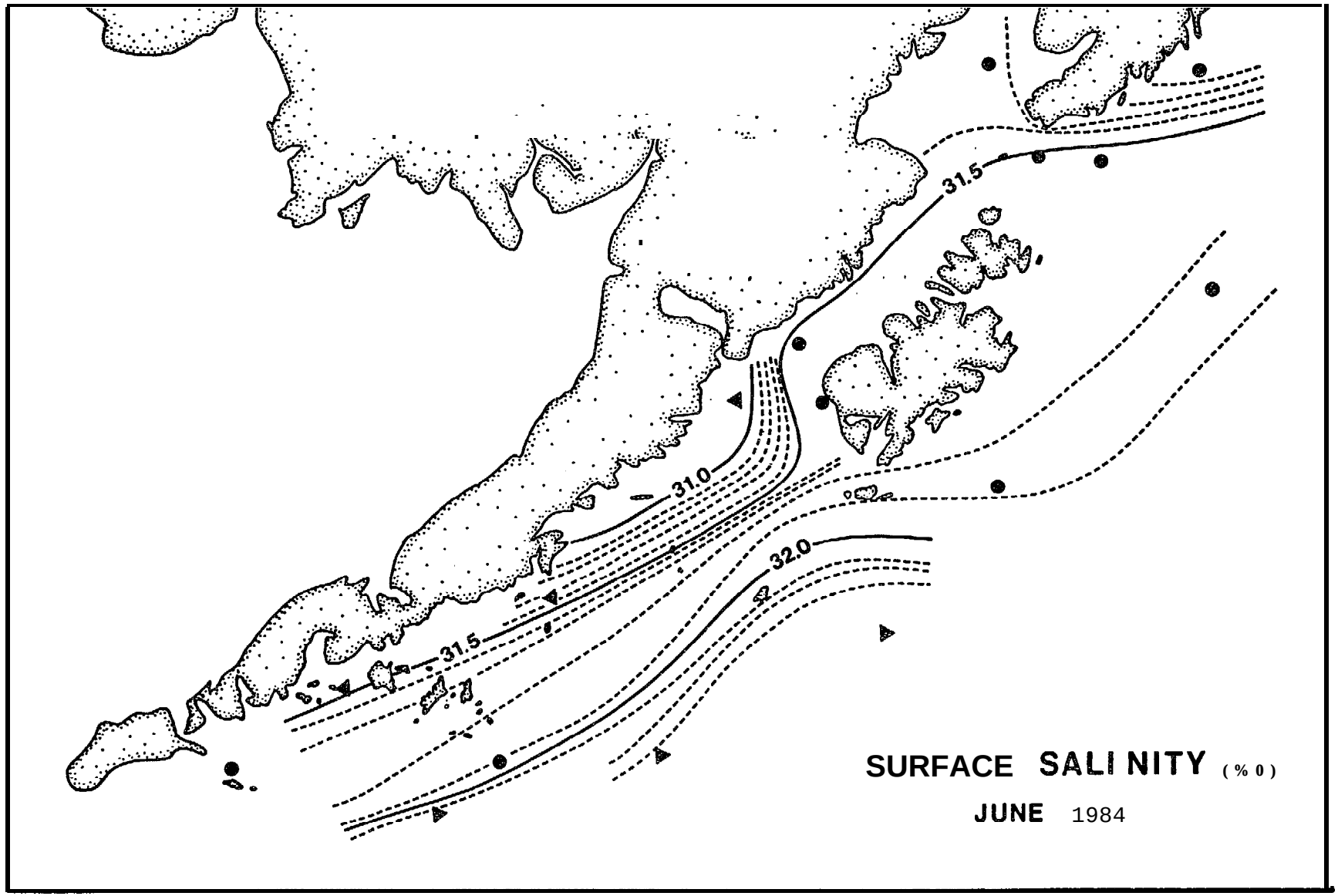

Figure 2.30 - Surface salinity, June.

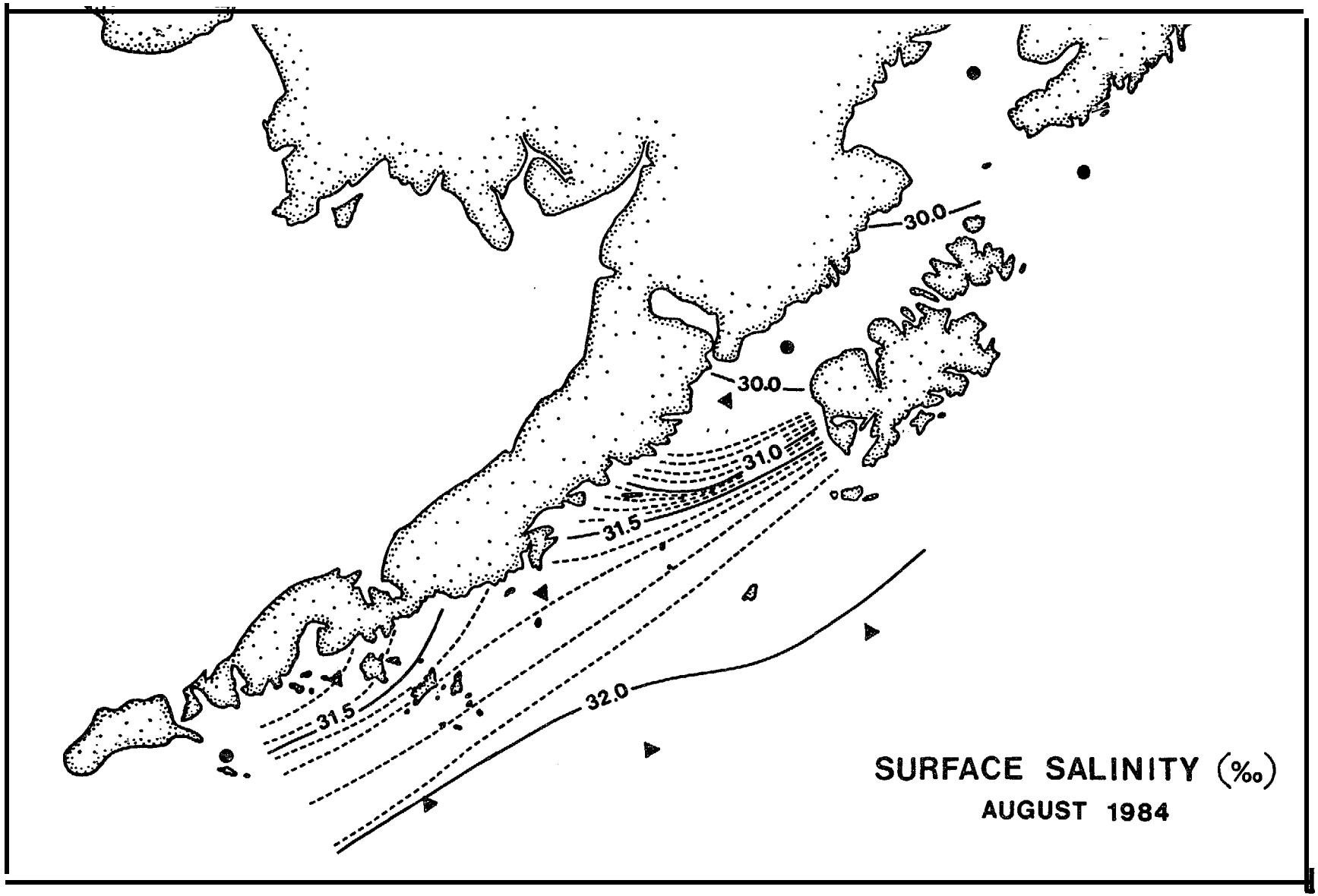

Figure 2.31 - Surface salinity, August.

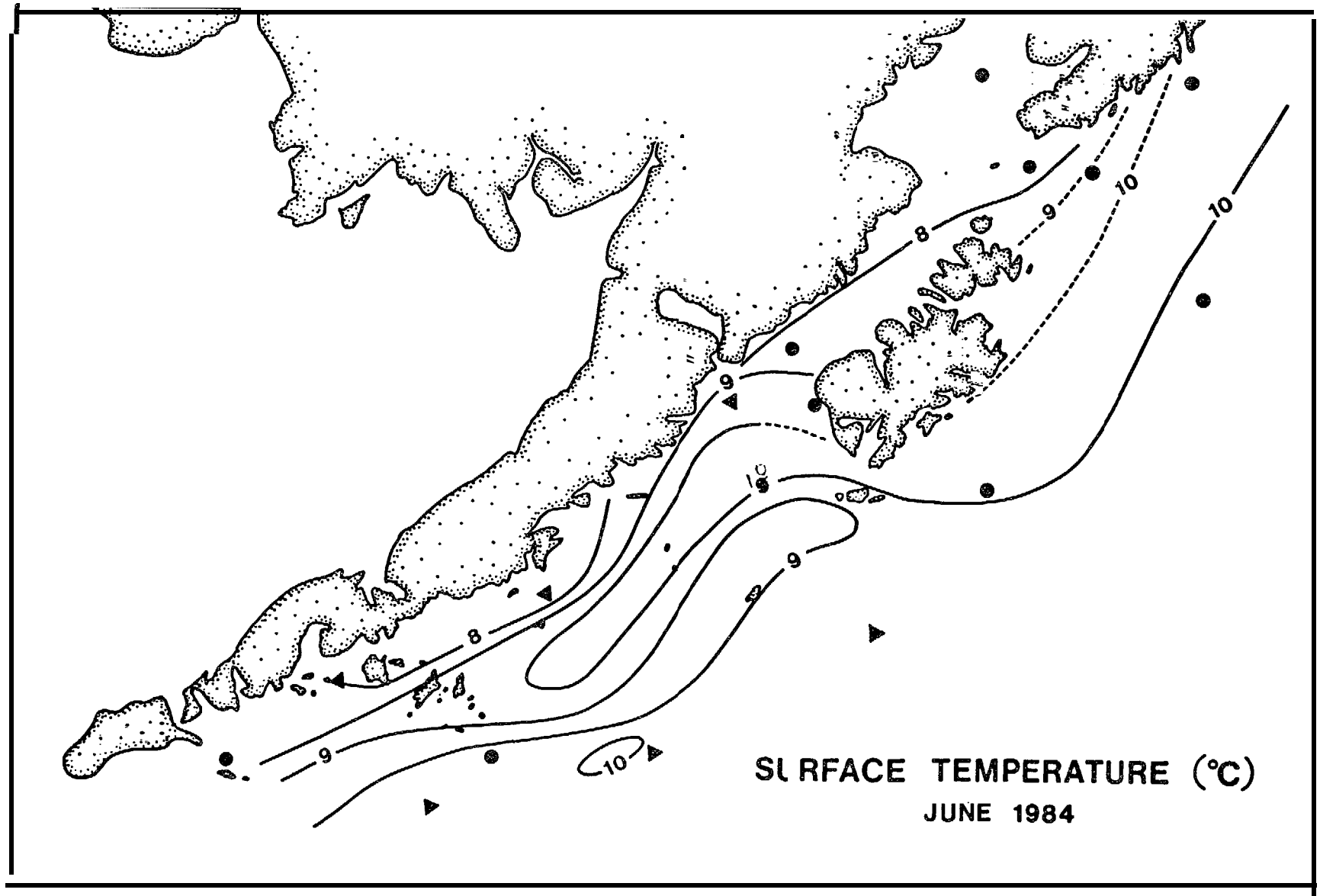

Figure 2.32 - Surface temperature, June.

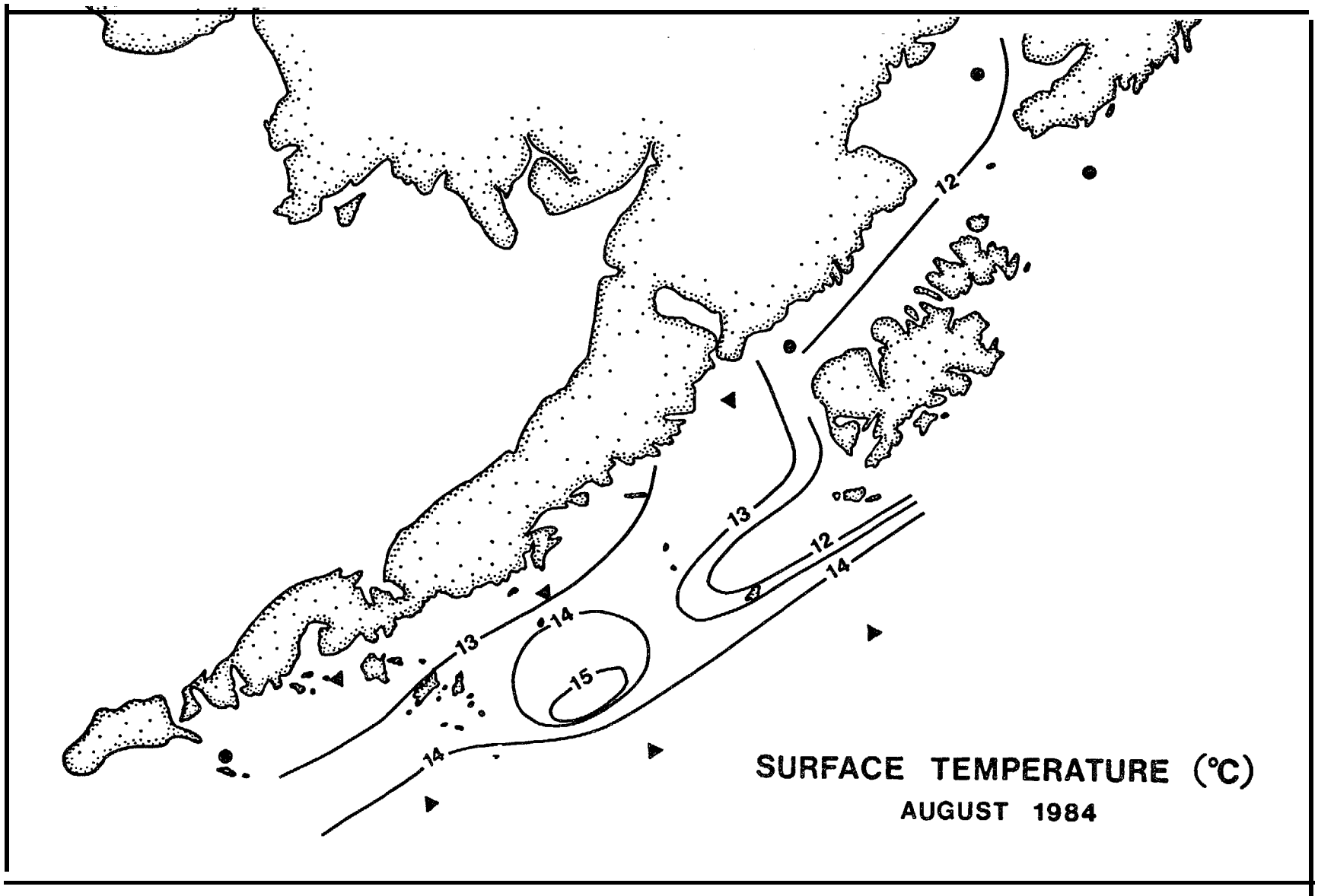

Figure 2.33 - Surface temperature, August.

3. TIDAL OSCILLATIONS

In this report we examine the tidal and subtidal components of the spectra of sea surface and current oscillations separately. The forcing function for the tides is deterministic and well understood so the tidal section of the report can be quantitative in nature. On the other hand, sub-tidal oscillations, including the mean flow may be forced or maintained through a variety of mechanisms so that several statistical procedures have been employed. These are discussed in Section 4.

3.1 TIDAL HEIGHT

The tidal analyses show that the tides in the region are mixed, mainly semi-diurnal. Form numbers (the ratio of the two largest diurnal to the two largest semi-diurnal components) vary between 0.51 and 0.98. Since the relative magnitudes of the tidal constituents vary substantially among the seven tide gauge locations, it is useful to examine the total tidal oscillation as represented by the spring tidal range.

The largest tides of the year occur when the K_1 component is in phase with the M_2 and S_2 components (usually around the solstices). A good approximation of the maximum tidal range can be computed from

$$R_{max} = 2(M_2+S_2+N_2+K_1+O_1). \qquad (3\text{-}1)$$

These ranges are listed below in Table 3.1 along with the estimated maximum ranges at Anchorage and Kodiak.

The highest tides in the region of study occur at Seal Rock, Cape Ikolik and Amatuli Island. The causes for these high ranges are likely shoaling and the reflection of substantial tidal energy from the coast with the attendant formation of partially standing tide waves. Tidal energy propagation is addressed in Section 3.2.

Table 3.1 Maximum Tidal Ranges

Location	Range (m)
Sanak	3.39
Portlock Bank	4.61
Seal Rock	5.10
Cape Ikolik	5.88
Shumagin	3.54
Albatross Bk.	4.25
Amatuli 1s.	6.33
Anchorage (estimate)	11.3
Kodiak (estimate)	4.0

Cotidal charts for the four largest constituents have been plotted and are presented in Figures 3.1 through 3.4. These charts show lines of equal Greenwich phase (cophase lines) and equal amplitude (corange lines). In all cases the tide appears to propagate from northeast to southwest, but there is a suggestion (from the sparse data points) that the tidal propagation is onto the shelf west of Kodiak Island. In non-dissipative (frictionless) systems the corange lines should be normal to the cophase lines. This is roughly the case for the M_2 constituent on the outer shelf. The amplitude of the M_2 constituent increases toward Cook Inlet indicating either pronounced shoaling or that some of the tidal energy is reflected in that area. However the Tide Tables show a six hour phase lag between Seldovia and Anchorage indicative of a progressive wave and little reflection. The increase in amplitude in Cook Inlet is, therefore, probably due solely to the decrease in depth.

The S_2, K_1 and O_1 cotidal charts display cophase and corange lines which are parallel - suggestive of a progressive wave in which *energy* is transported, eventually being dissipated by bottom friction.

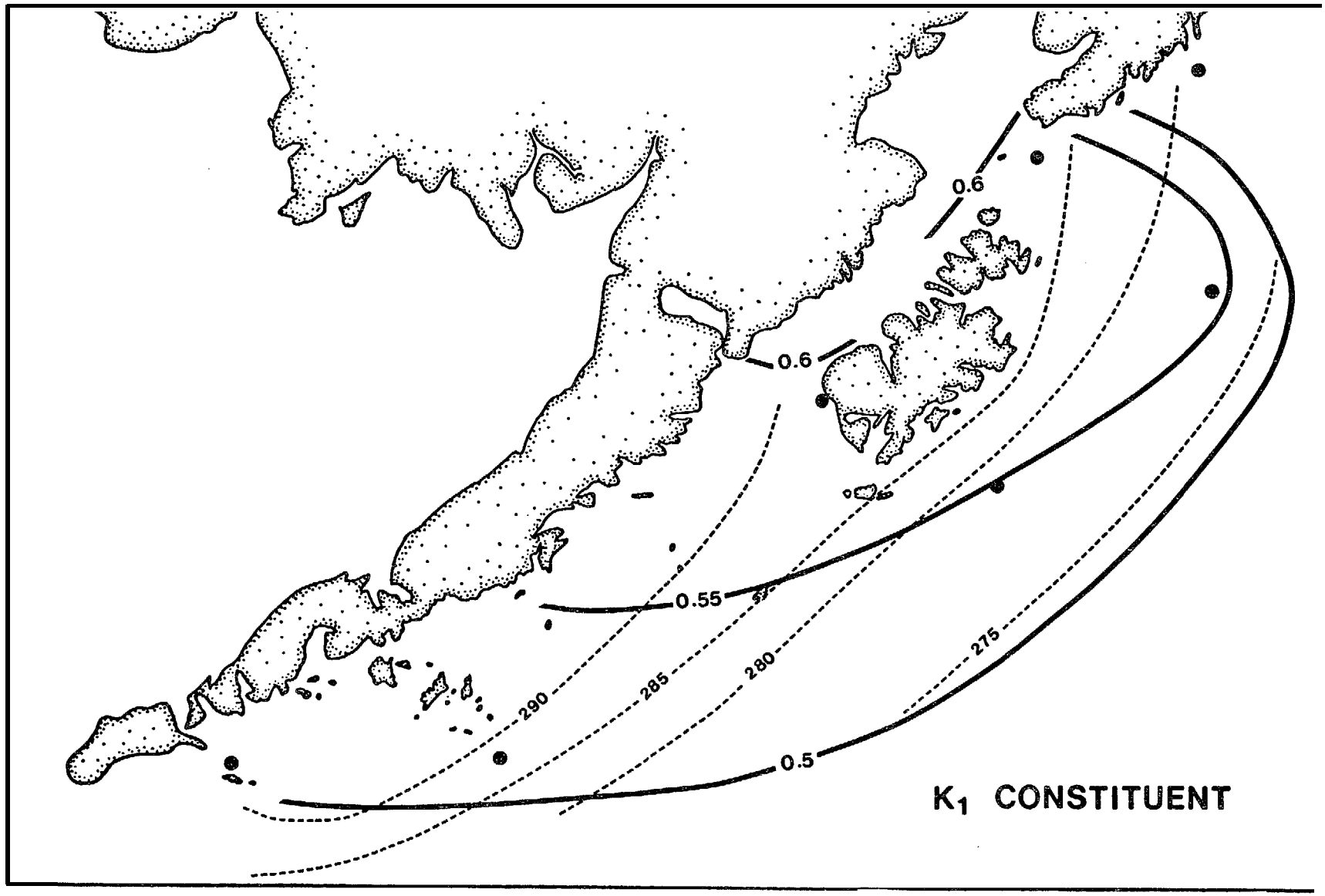

Figure 3.1 - Cotidal chart for the K_1 constituent. Corange line (solid) in meters, cophase lines (dashed) in degrees relative to Greenwich.

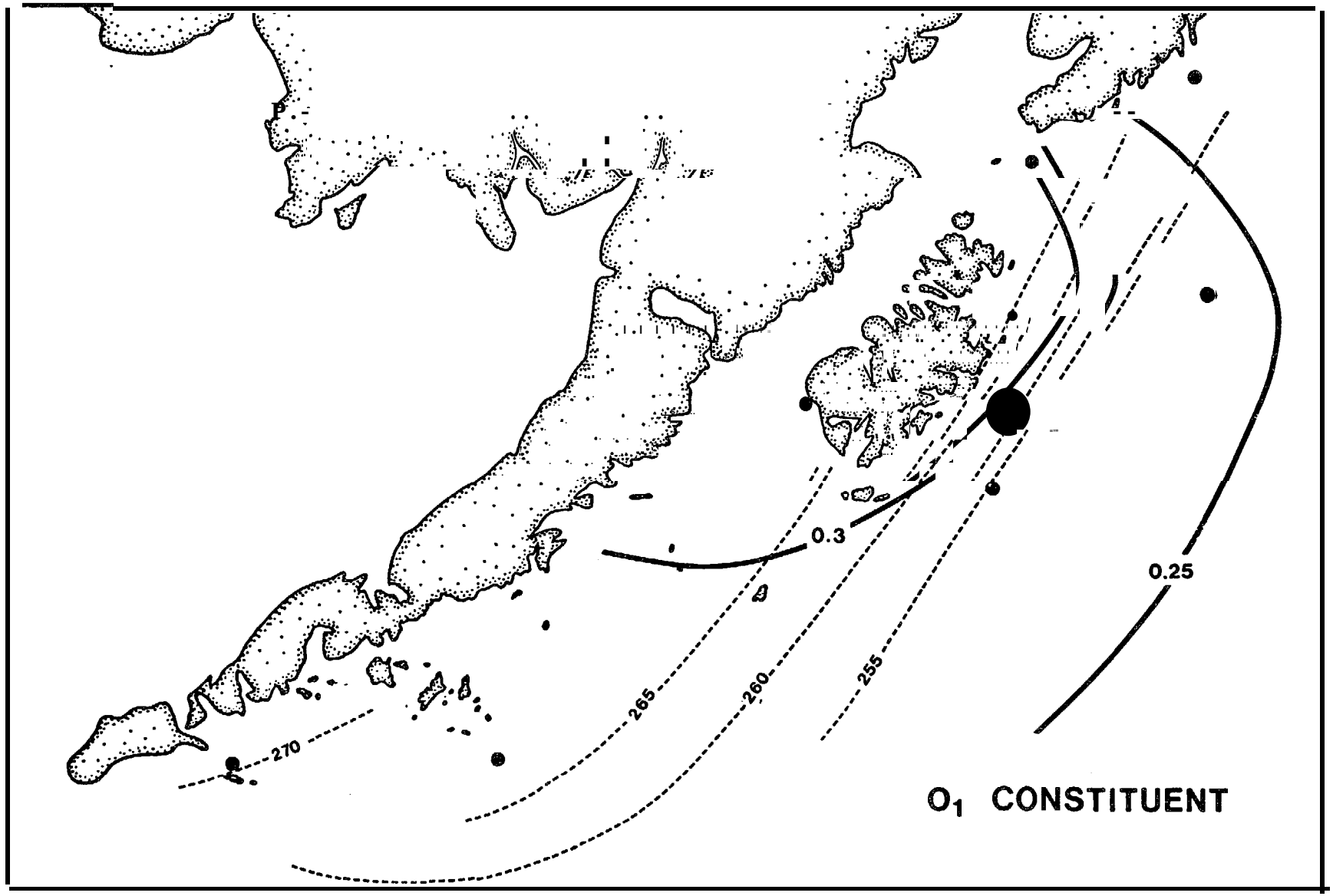

Figure 3.2 - Cotidal chart for the O_1 constituent. Corange line (solid) in meters, cophase lines (dashed) in degrees relative to Greenwich.

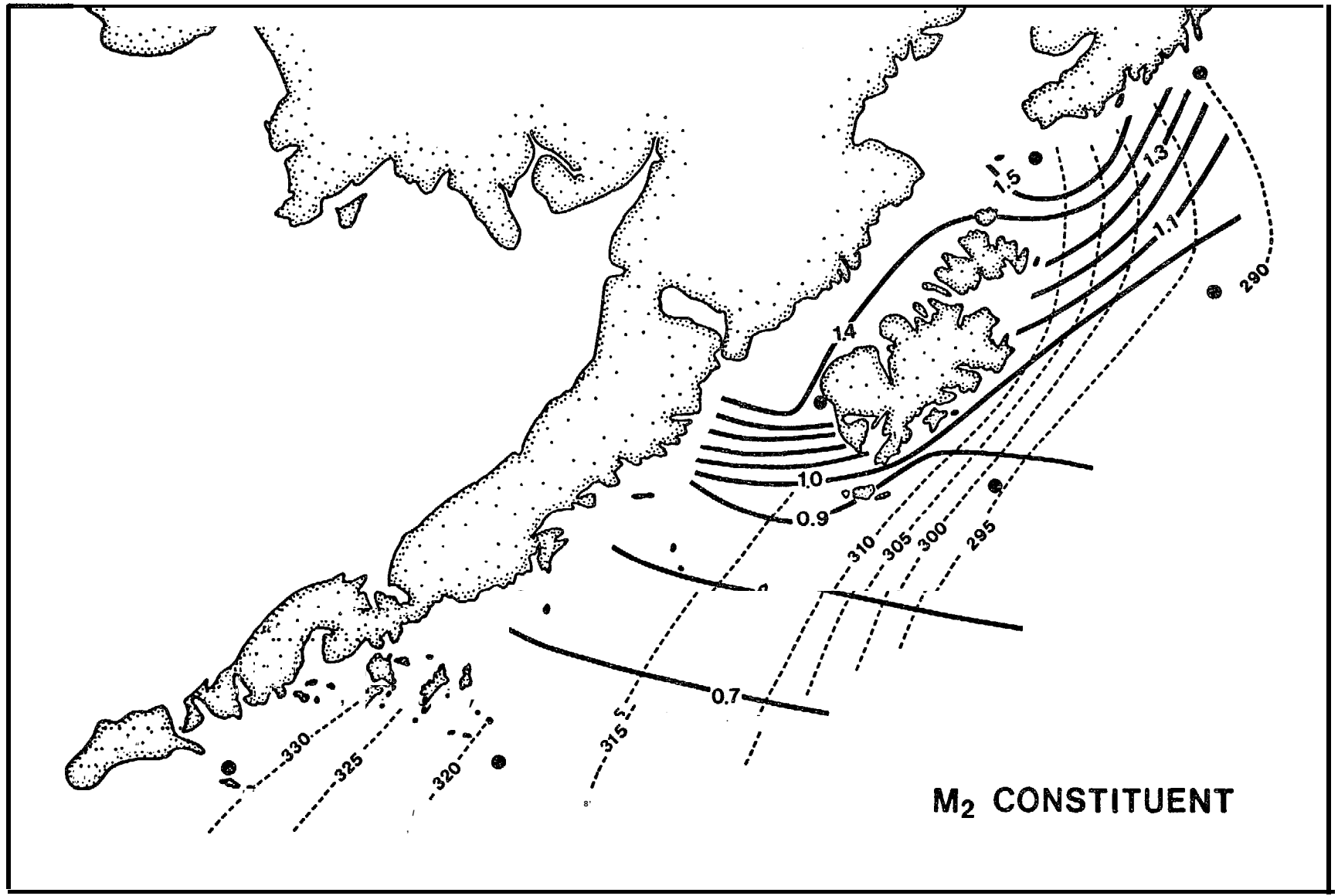

Figure 3.3 - Cotidal chart for the M_2 constituent. Corange line (solid) in meters, cophase lines (dashed) in degrees relative to Greenwich.

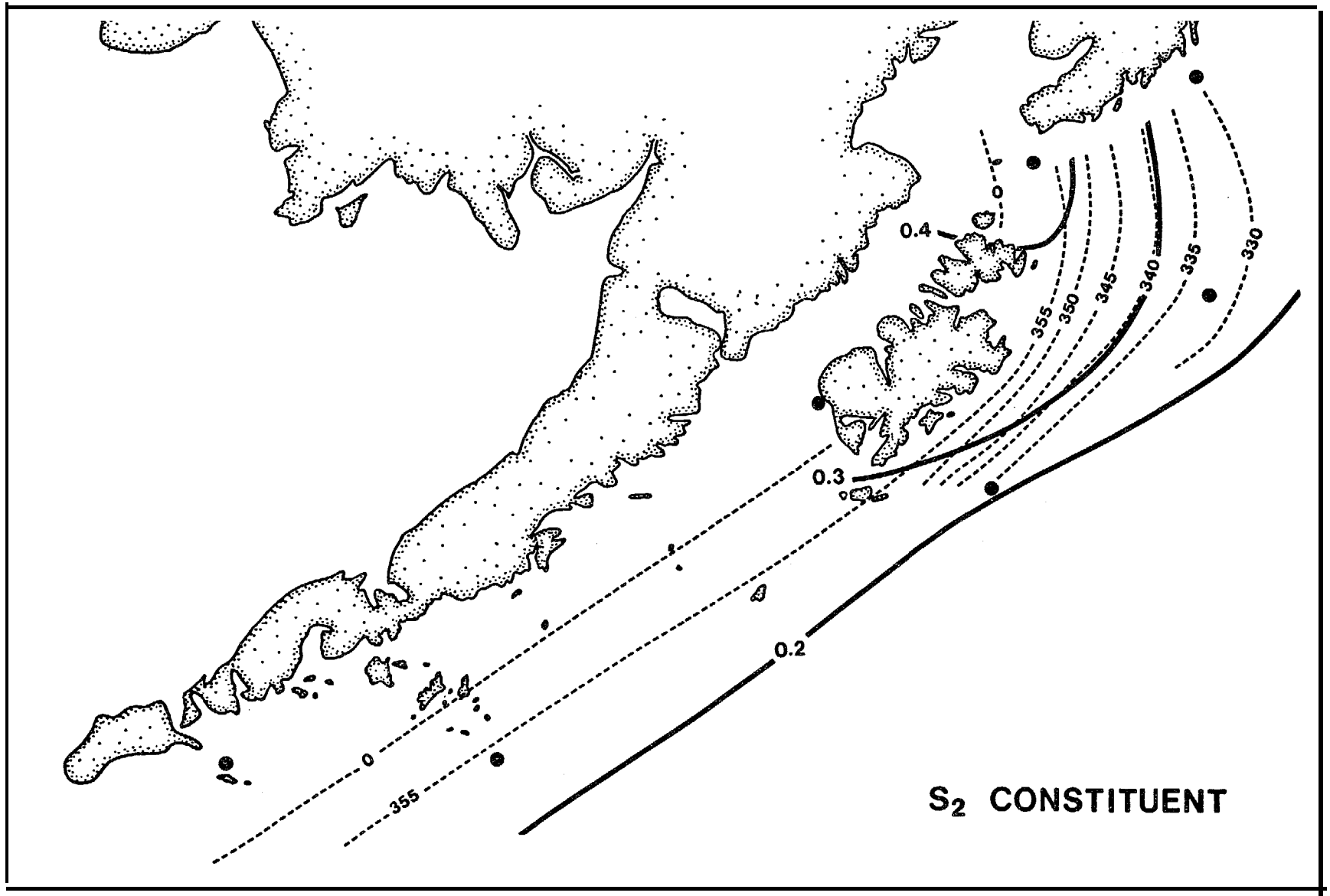

Figure 3.4 - Cotidal chart for the S_2 constituent. Corange line (solid) in meters, cophase lines (dashed) in degrees relative to Greenwich.

Although the cotidal charts are very rough, one can gain some confidence in them by noting that for the M_2, S_2 and K_1 constituents the bottom topography is quite well reflected in the speed of the waves as determined by the distance between cophase lines: the propagation speed is lower over Portlock Bank than in other areas.

3.2 TIDAL CURRENTS

3.2.1 Tidal Energy Propagation

The power propagated per unit width of a tide wave or energy flux can be computed using the results of the tidal stream and tidal height analyses. The energy flux per unit width integrated over depth and over the tidal period for any constituent is

$$E = \rho g h \frac{1}{2\pi} \int_0^{2\pi} A \cos(nt) V \cos(nt + \theta) dt \qquad (3\text{-}2)$$

(e.g. Platzman, 1971) where E is the energy flux, ρ is the density of sea water, g is gravity, h is the depth, A is the amplitude of the tidal height oscillation, V is the amplitude of the tidal current, n is the frequency of the constituent and 6′ is the phase difference between the tidal height and tidal current. Integration of equation 3-2 yields

$$E = 1/2 \rho g h A V \cos\theta. \qquad (3\text{-}3)$$

Thus when the tidal current is in phase with the tidal height (maximum current at high water) a purely progressive wave is present, there is no reflection, and all tidal energy is propagated in the direction of the major axis of the tidal ellipse. When the current is 90° out of phase with the tidal height, then the tide wave is purely standing in character, there exists complete reflection and no net energy flux.

Visual comparison of the current and pressure time series from the Cook Inlet mooring (harmonic analysis of the pressure record from the current meters is inadvisable due to limited resolution) yields a near zero phase difference implying progressive tide waves which dissipate much of their

energy on the extensive flats in Cook Inlet. On the other hand, the tidal height and current are about 66° out of phase at the Shelikof Strait mooring; characteristic of little energy propagation and a tide wave nearly standing in character.

The practical significance of these observations is that maximum currents occur roughly mid-way between low and high tide in Shelikof Strait but closer to low and high tide in southern Cook Inlet.

Quantitative evaulation of the energy flux by equation 3-3 is possible where tide gauges and current meters are in close proximity. The pressure sensors on the current meters were not of great enough precision to permit reliable tidal analyses. We have computed the tidal energy flux per meter of channel width for the four largest constituents. It should be noted that the direction of energy propagation is along the major axis of the tidal ellipse. This direction is given in the tidal stream analysis with a $\pm$ 180° ambiguity, but the current phase is computed according to the direction of the semi-major axis specified. If a negative energy flux resulted from the calculation for Table 3.2, then a 180° correction was applied to the direction of the semi-major ellipse axis given in the tidal analyses. The DIR column of Table 3.2 therefore shows the actual direction of tidal energy flux.

The tidal current constituents used in the computations were approximately the barotropic components of the tidal current constituents (exactly for M_2). The barotropic component was computed from knowledge of the modal structure and the tidal currents at two depths (see section 3.2.2). The most confidence can be placed on the results from Sanak where the current meters and tide gauges were on the same mooring. The Cape Ikolok tide gauge and Shelikof Strait current meter appear to yield logical results while the Amatuli Island gauge and Stevenson Entrance meters display a peculiar phase lag.

Table 3.2 **Tidal Energy Flux**

Location	A (m)	v (m/s)	e (°)	h (m) (Approx)	DIR (“True)	Power (kw/m)
O_1						
Sanak	0.27	**0.029**	- 10	*45*	091	1.8
Ikolik-Shelikof	0.31	**0.016**	50	200	046	3.2
Amatuli-Stevenson	O*3I	**0.036**	245	100	176	2.4
K_1						
Sanak	O*50	0.056	153	45	104	5.0
Ikolik-Shelikof	0.59	0.032	54	200	045	11.4
Amatuli-Stevenson	**0.58**	0.065	249	100	**166**	7.0
M_2						
Sanak	**0.63**	.034	36	45	*349*	4.0
Ikolik-Shelikof	1.39	.145	68	200	*048*	77.3
Amatuli-Stevenson	1.55	,287	241	100	*173*	111.6
S_2						
Sanak	**0.16**	.011	64	*45*	*37*	0.2
Ikolik-Shelikof	1.39	.044	65	200	*46*	7.2
Ametuli-Stevenson	0042	.101	239	100	**179**	11.3

Tidal energy propagation for all the constituents appears to be north-eastward into Shelikof Strait. The mean phase lag between the tidal heights and currents at the southwestern end of Shelikof Strait is about 60 degrees which implies that about half the tidal energy is reflected.

At Sanak, tidal energy is propagated to the north and east (between 349o and 104° true). The diurnal constituents propagate nearly eastward while the semi-duirnal constituents nearly northward. There appears to be no consistency among constituents regarding the standing/progressive nature of the tide waves.

At Stevenson Entrance all four tidal constituents appear to propagate energy to the south. The current meters at. this site exhibit comparable Greenwich phases and the phase difference between heights and currents is nearly constant. An error in timing is therefore very unlikely. Also unlikely is the presence of an amphidrome on Portlock Bank for all the tidal constituents. The phase differences between the Amatuli gauge and the Cook Inlet current meters are less than 10° for the semi-duirnal constituents thus consistent will the notion of a progressive wave in southern Cook Inlet and substantial tidal energy dissipation over the shallows there (independent confirmation of our current measurements in Cook Inlet exist in the report of Patchen et al, (19S1)). At this writing we are unable to explain the apparent anomalous southward propagation of tidal energy in Stevenson Entrance.

The magnitude of the tidal energy flux in the vicinity of Kodiak Island is about 90 kilowatts per meter of channel width. Using 25 km as an appropriate width for Shelikof Strait, this amounts to about 2.25 x 10^9 watts, about 0.1% of the tidal energy in the world ocean (LeBlond and Mysak, 1978). The data appear to indicate that the tidal energy flux is northeastward into Shelikof Strait. Presumably much of this energy is dissipated in Cook Inlet but the apparent southward energy flux at Stevenson Entrance is still puzzling.

3.2.2 Internal Tides

Internal tides may be generated on the continental slope and can account for substantial phase differences between near surface and deep flows. In addition to the velocity signature of such oscillations, there exist concomitant vertical oscillations of the density surfaces. Unlike the surface or barotropic tides, the internal tides are characterized by velocity and displacement fields which are functions of depth.

The vertical velocity can be represented as:

$$w = W(z) \exp [i (k\% - nt)] \qquad (3\text{-}4)$$

where w is the vertical velocity, W(z) is the depth varying amplitude of the velocity fluctuation, k is a horizontal wave number vector and n is the angular frequency of the wave. The vertical mode structure can be found from the linearized internal wave equation:

$$\frac{\partial^2}{\partial t^2}(\nabla^2 w) + N^2(z)\nabla_h^2 W + f^2 \frac{\partial^2 \ldots}{\partial z^2} = 0 \qquad (3\text{-}5)$$

where N (z) is the Vaisala frequency $= \sqrt{-\frac{g}{\rho}\frac{\partial \rho}{\partial z}}$, and f is the Coriolis parameter. Substitution of eq 3-4 into eq 3-5 yields

$$\frac{d^2 W}{dz^2} + \left[\frac{\sim(z) - \text{“}^2}{n^2 - f^2}\right] k^2 \quad W = 0 \qquad (3\text{-}6)$$

(Further details of internal wave dynamics can be found in Phillips, 1966.) Solution of eq. 3-6 can be performed numerically if the distribution of density with depth is known. Such solutions yield a vertical structure of vertical velocities. The Z derivative of the vertical velocity is proportional to the horizontal velocity so that a normalized distribution of horizontal velocity amplitude as a function of depth can be computed.

Mode structures were computed from the June and August CTD data taken at the current meter moorings.

The structures of the first modes for vertical displacements and horizontal velocities for the M_2 constituent are shown in Figure 3.5 along with the density structure in Cook Inlet in August. Note that the maximum horizontal velocity associated with internal tides occurs at the surface and that zero horizontal velocity occurs at a depth of 25 meters where the vertical excursion of the isopycnals and the vertical velocity are the greatest.

The modal structures for the horizontal velocities yield relative magnitudes of the internal oscillation at various depths. For example, at the Cook Inlet mooring in August the amplitudes of the internal velocity oscillations at the two current meters are in the ratio of -0.27/-0.36. The amplitudes of the first internal (baroclinic) and surface (barotropic) tidal oscillations can be computed from this mode structures and the tidal stream analyses of two current time series.

For a given tidal frequency, n, the combined amplitude and phase of the oscillations at the current meters is obtained from the tidal stream analyses. If only the oscillations along the major axes of the tidal ellipses are considered then the oscillations may be represented by

$$'_i = Ai \cos (nt - G_i) \qquad \textbf{(3-7)}$$

where i = 1,2 for shallow, "deep, V_i are the total tidal velocities, A_i are the amplitudes of these velocities and G_i are the Greenwich phases. If m_i are the normalized amplitudes of the velocity fluctuations then the amplitudes and phases of the baroclinic and barotropic oscillations can be computed. These are:

$$BT = \frac{m_1 A_2 \sin \varphi}{(m_1 - m2) \sin s} \qquad \text{(barotropic amplitude)} \qquad (3\text{-}8)$$

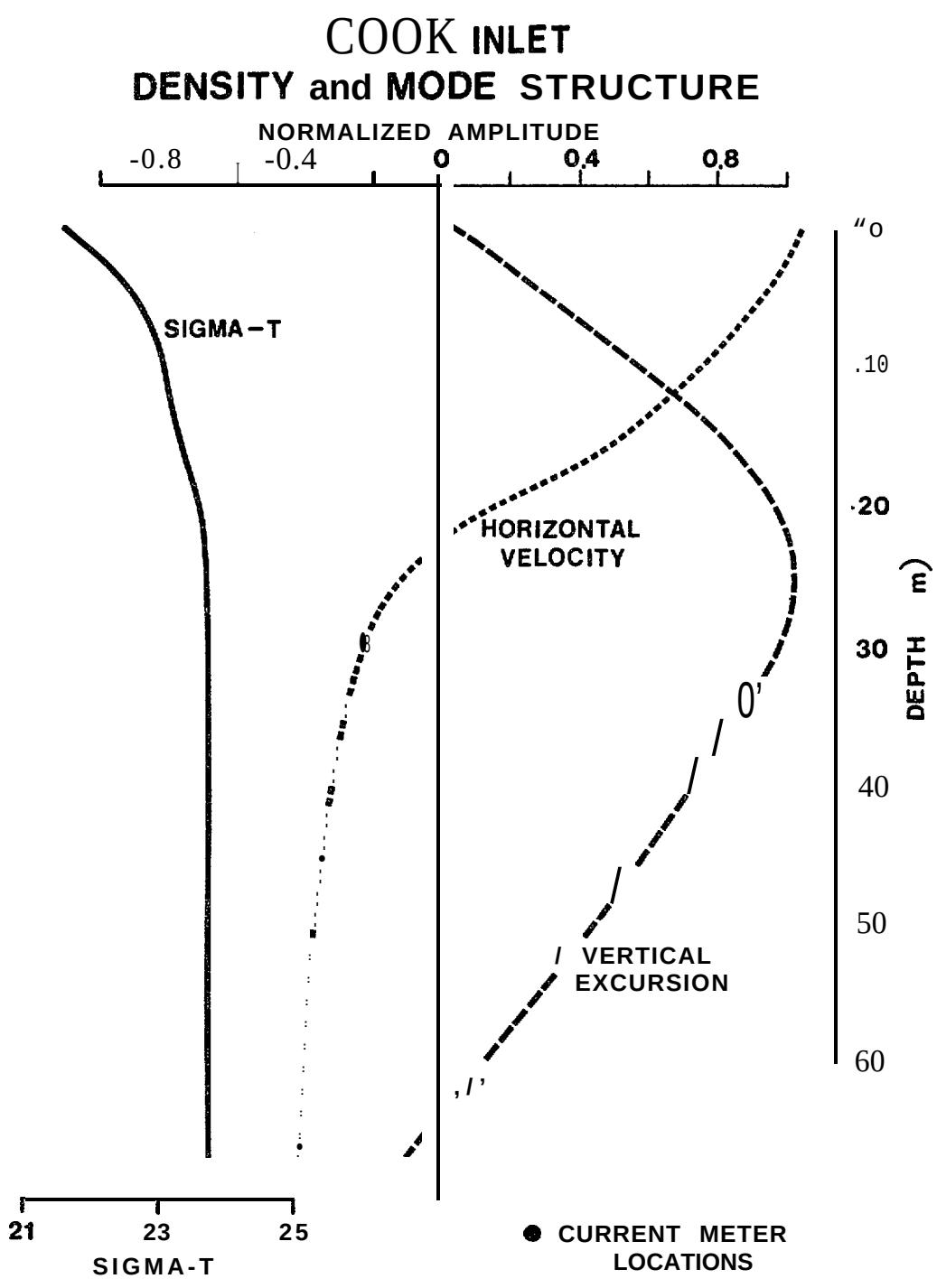

Figure 3.5 - Lowest internal mode structure for the M_2 constituent in Cook Inlet.

$$\tan \alpha = \frac{m_1 A_2 \sin \varphi}{m1\ A2 \cos \varphi - m2\ A_1} \quad \text{(barotropic phase)} \quad (3\text{-}9)$$

$$BC = \frac{A_2 \sin \varphi}{(m_2 - m_1) \sin \beta} \quad \text{(baroclinic amplitude]} \quad (3\text{-}10)$$

$$\tan \beta = \frac{A_2 \sin \varphi}{A_2 \cos \varphi - A_1} \quad \text{(baroclinic phase)} \quad (3\text{-}11)$$

where $\varphi = G_1 - G_2$ and α and β are phases relative to G_1.

Where possible we used the average stratification (June and August) at the mooring sites to compute the mode structures. These often varied considerably due to the vertical oscillation of the isopycnals. Ideally the density data from which the modes were computed would have been measured over a tidal cycle and averaged. Recognizing the limitations of our density profile data we computed the baroclinic and barotropic modes for the largest (M2) tidal constituent to obtain an estimate of the internal oscillations, these are listed in Table 3.3.

By far the largest internal tides appear to occur at the Cook Inlet mooring. Indeed examination of the temperature and salinity time series from the meter at 35 m depth in Cook Inlet shows temperature and salinity oscillations of about 0.4° and 0.4°/00, respectively. Using the temperature and salinity gradients measured in June and August we can estimate the height of the internal tide

$$H \simeq \frac{\Delta T}{\partial T/\partial Z} \simeq \frac{\Delta S}{\partial S/\partial Z} \quad (3\text{-}12)$$

where H is the height of the internal tide and ΔT and AS are the tidal excursions of the temperature and salinity values (assuming negligible horizontal gradients). Equation 3-12 yields values of about 30 meters for the vertical excursion of a water parcel at a mean depth of 35 m in Cook Inlet. Such a vertical excursion would produce a horizontal velocity which can be approximated by:

Table 3.3 Barotropic and **Baroclinic** Velocities For The M_2 Tidal **Constitutent** (Amplitudes **in cm/s)**

Cook Inlet

BT = 96.2 cos (nt -2.8° - G_1)

BC = -58.6 cos (nt -12.8° - G_1)

Shelikof Strait

BT = 14.5 cos (nt +1.7° - G_1)

BC = -1.3 cos (nt +30.9° - G_1)

Stevenson

BT = 28.7 cos (nt -3.5° - G_1)

BC = 17.4 cos (nt -47.6° - G_1)

Sanak

BT = 3.4 cos (nt -3.5° - G_1)

BC = -1.6 cos (nt -67.2o - G_1)

$$V_{(internal)} = \left(\frac{g}{h}\right)^{1/2} \left(\frac{\Delta\rho}{\rho}\right)^{1/2} \eta \qquad (3\text{-}13)$$

where ρ is the density, g gravity, η the amplitude of the internal wave and h the depth over which $\Delta\rho$ is computed. Eq. 3-13 yields a value of about 35 cm s^{-1} for the fluid velocity associated with internal waves of tidal period in Cook Inlet. This is in qualitative agreement with the amplitude presented in Table 3.3; surprisingly so. Clearly an internal wave of 30 m height in 65 m water depth is no longer a small amplitude wave and many of the assumptions of the theory are inadequate,

Our conclusion here is that substantial internal wave energy of tidal period is present in Cook Inlet. Without tidally averaged CTD data, we cannot confidently ascribe precise amplitudes to these oscillations; however, our observations as well as our computations show that internal tides are present in Cook Inlet. It is therefore unlikely that a purely barotropic tidal model will adequately represent this region.

4. SUBTIDAL OSCILLATIONS

In this section the energy associated with subtidal oscillations is discussed and an attempt made to relate it to atmospheric driving forces. The region is, of course, dominated by tidal oscillations, the tidal kinetic energy accounting for between 50% and 95% of the total kinetic energy. The spectral distribution of energy is shown for the longshore velocity component in Shelikof Strait in Figure 4.1. In Cook Inlet, for example, the mean flows are about 5 cm s^{-1} while the tidal flows exceed 80 cm s^{-1}. For the purposes of this section the tidal oscillations can be considered "noise" and thus for the subtidal oscillations the signal to noise ratio is generally poor. For example any effect due to sea breezes of diurnal period would be completely masked by the tidal flows.

4.1 MEAN FLOWS

The mean velocities recorded over the two month deployment period are shown in Table 4.1. At Stevenson Entrance a weak mean flow to the southeast at depth and south southwest at mid-depth may be due to outflow from the Cook Inlet area. The vertical shear of the alongshore velocity is in the same sense as that measured in Shelikof Strait however, so that the Stevenson Entrance regime could be considered to be linked to Shelikof Strait. It should be noted that mean westerly flow in Stevenson Entrance is suggested in the dynamic topographies of Favorite and Ingraham (1977). In Cook Inlet the mean flow is east northeast at both depths, differing in direction by about 45° from the orientation of the Inlet. It is probable that the recorded mean flows in Cook Inlet are due largely to rectification of strong tidal flows. Such rectification is indicated in the presence of "shallow water" tidal constituents of substantial size. The MK3 and M4 components (terdiurnal and quarter-diurnal respectively) are both of comparable magnitude to the mean flow. The presence of these "difference frequencies" indicates that non-linear effects also produce "sum frequencies". For example the M4 constituent (lunar quarter-diurnal) is a

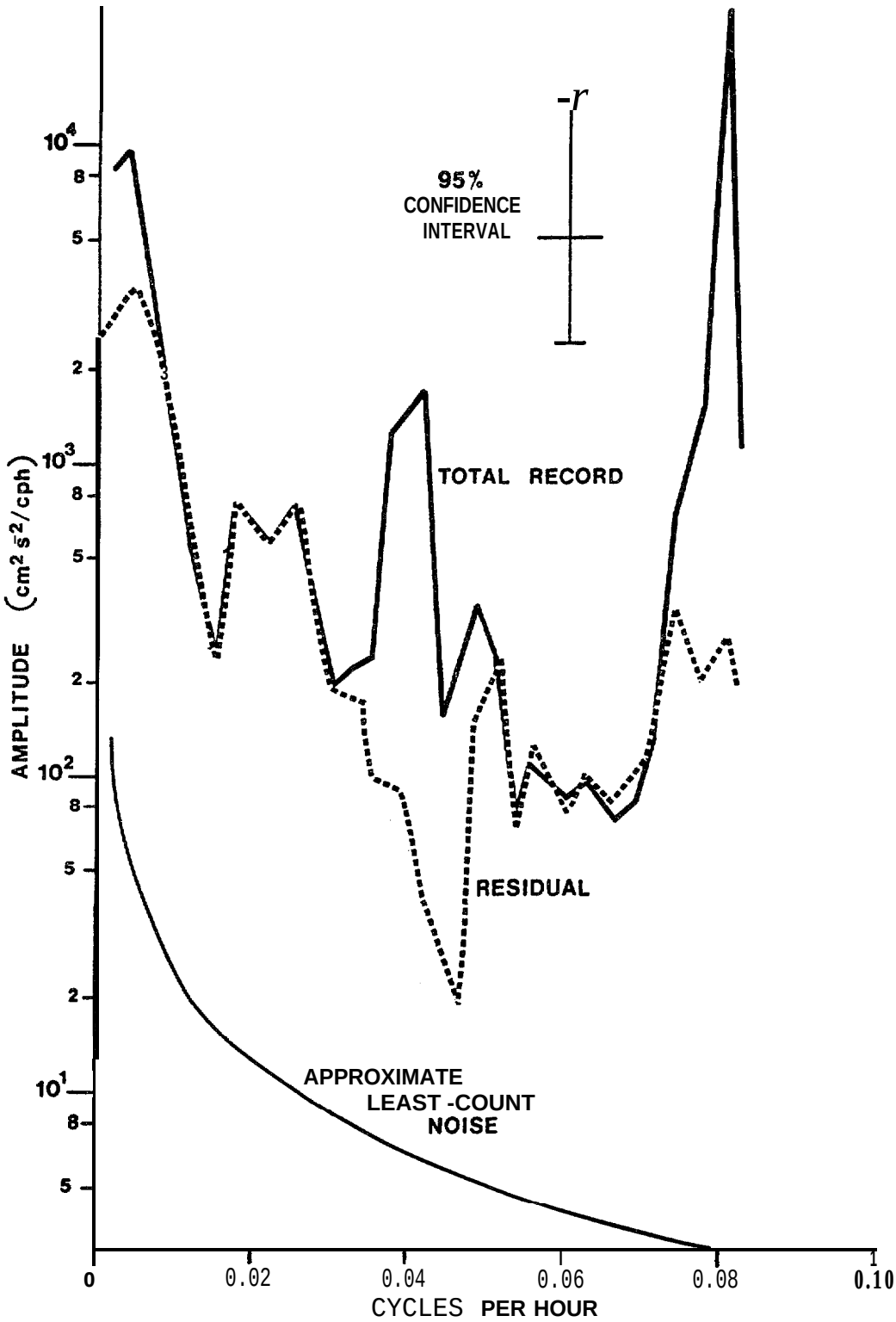

Figure 4.1 - Autospectrum alongshore (225° T) component, 46 m depth in Shelikof Strait.

Table 4.1 Mean Velocities at the Eight Current Meters

Location	Instrument Depth (m)	Water Depth (m)	Speed (cm s-1)	Direction ° True
Stevenson	54	113	201	212
Entrance	82		2.6	135
Cook	35	66	4.3	078
Inlet	52		5.6	064
Sanak	20	50	2.3	254
Island	41		3.1	299
Shelikof	46	250	3.8	210
Strait	157		1.3	037

manifestation of the shoaling of the M_2 constituent. Also associated with the generation of the M_4 constituent is the generation of a DC (mean flow component). The process is perhaps best envisaged as the beating of two tidal constituents. The beat frequencies are the sum and difference of the two frequencies. In the limit as the two constituents approach an identical frequency, oscillations of twice the fundamental frequency and zero frequency are produced.

At Sanak, where the tidal amplitudes are much smaller, the shallow water tidal constituents are of negligible size and the mean flows at both 20 and 41 meters depth are directed roughly toward the west. This mean flow is generally reflective of the flow of the coastal current.

In Shelikof Strait moderate tidal currents and deep water *combine* to minimize non-linear tidal effects. The shallow water constituents are small and the mean flows are representative of quasi-steady processes. At the shallow meter the flow is toward the southwest, while at the lower meter it is toward the northeast. Such a velocity distribution is characteristic of an estuarine flow in which the fresher lighter waters move seaward compensated by a slower, but vertically more extensive return flow* Schumacher et al, (1978) suggested that the inflow of deep water into Shelikof Strait occurs to balance the loss of deep water entrained by the outflowing surface waters. Further observations will be necessary to fully describe the estuarine-like flow in Shelikof Strait.

4.2 LOW FREQUENCY FLOWS

The region within about 20 km of the southern Alaska Coast is dominated by the Alaska Coastal Current according to Royer (1981). Maximum speeds can be over 60 cm s^{-1} and transports can exceed 1 x 10^6 m^3 s^{-1}. Royer attributed the variations in the current to variations in freshwater discharge and found wind stress to be a very minor influence. The annual cycle of increasing stratification in early fall and decreasing stratification in late winter changes the magnitude of the internal Rossby

radius. Royer mentioned this variation but did not seem to link it with the width of the current itself. In fact, as the stratification increases, the coastal current will become wider.

The Shelikof Strait current meter mooring of the present study was located approximately 14 km offshore of the Alaska Peninsula. The internal Rossby radius in Shelikof Strait during the deployment was between 3.5 km in June and 6.5 km in August. Data from Xiong and Royer (1984) indicate that the maximum internal Rossby radius that might be encountered in Shelikof Strait is about 16 km and would occur in fall at the peak of the freshwater discharge. If the intensity of the flow is proportional to

$$\exp(-y/r_i) \qquad (4\text{-}1)$$

where y is the offshore distance then the strength of the current from its centerline to the mooring would be reduced by a factor between 10 and 50. It is, therefore, unlikely that flow or flow variations associated with the Alaska Coastal Current would have been measured at the Shelikof Strait mooring or at any of the others deployed during this study.

In order to test the above hypothesis, we employed data for the daily discharges of the Knik and Susitna Rivers (kindly supplied by Professor Royer) to represent the freshwater discharge along this section of the coast. The combined discharge of these rivers peaks in July-August at about 1000 m3 s^{-1}. The daily mean discharges of these rivers and the alongshore velocity component at 46 m depth in Shelikof Strait are plotted in Figure 4.2. There is no apparent correlation between the discharge and the current; certainly the reversals of the current are not reflected in discharge. The possibility, of course, exists that the currents are driven by freshwater discharge far "upstream", for example, along the coast of southeast Alaska. However, the lengths of the present current records do do not permit comparison over the monthly time scales which would be required to investigate such a driving mechanism.

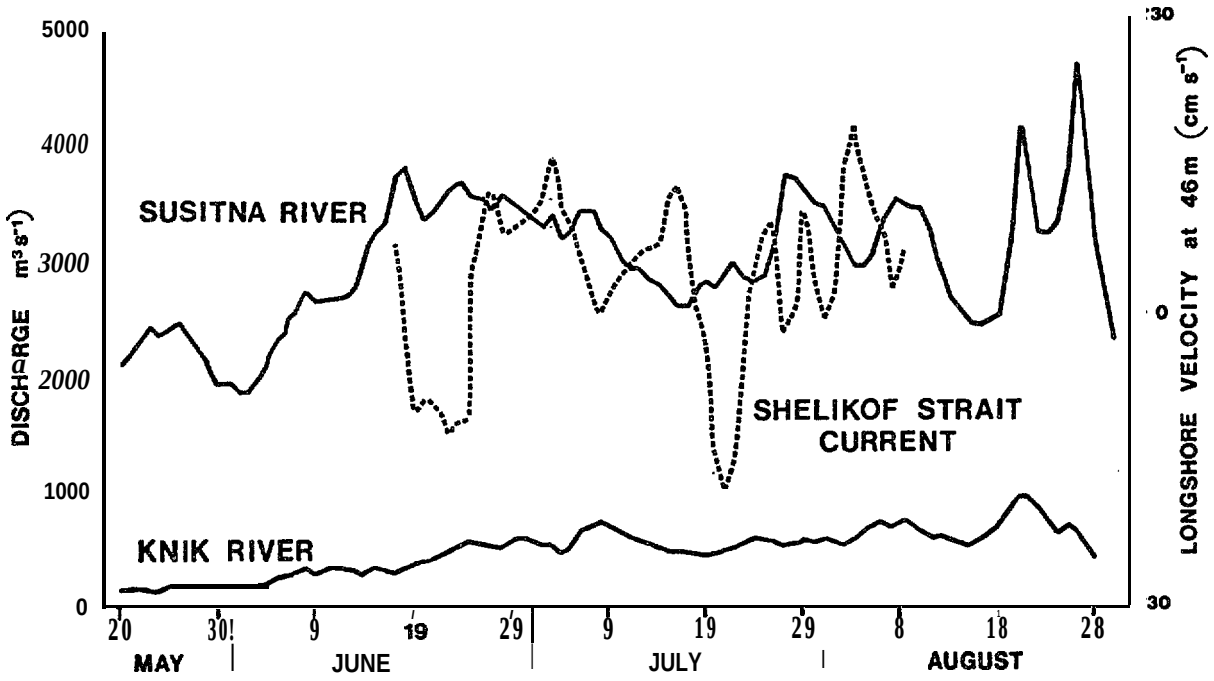

Figure 4.2 - Daily discharge of the Knik and Susitna Rivers (solid lines) and the mean daily alongshore component of flow at 46 m depth in Shelikof Strait (broken line) .

The well defined variations in the flow through Shelikof Strait are apparent in either the time series data (Appendix 2) or the tidal analyses (Appendix 1). Energy at the MM (lunar monthly) and MSF (luni-solar fortnightly) is relatively high and not reflective of the ratios of the astronomical forcing functions at these frequencies to that at the M2 frequency (9% and less than 1% of M2 respectively). Presence of energy at these frequencies more properly indicates long period oscillations.

In that there appeared to be no correlation between the Shelikof Strait currents and freshwater discharge, we investigated possible atmospheric driving of the currents.

Figure 4.1 shows the autospectra of the alongshore (225° T) velocity component for the raw time series and for the time series with the tidal oscillations removed (residual). The principal tidal frequencies are in the region of 0.04 and 0.08 cycles per hour. The curve at the bottom of the figure represents the noise level due to the resolution limitations of the current meter. The 95% confidence interval is shown. For the spectrum of the residual currents there is significant energy near 0.02 cph (50 hours) as well as at the very low end of the spectrum (periods of about 15 to 20 days).

For the lowest frequencies we cannot precede with a meaningful cross-spectral analyses since only three or four realizations of oscillations of these periods occur in our two month records. We have, however visually compared the velocity time series with time series based upon the sea surface atmospheric pressure data obtained from the Naval Fleet Numerical Oceanography Center at Monterey.

Using the six hourly pressure grid (grid spacing approximately 300 km) we computed geostrophic winds. These winds were then decomposed into alongshore and offshore components. In addition, we computed surface wind stress by 1) rotating the geostrophic velocity vector 20° counter-clockwise to account for Ekman turning; 2) taking 70% of the geostrophic velocity to simulate the frictional dissipation in the boundary layer; 3) squaring the wind speed and 4) applying a drag coefficient of 1.2×10^{-3}. These procedures can be expressed as:

$$\vec{\tau} = \vec{\tau} \exp(i'\gamma) = p_a C_D (0.7W)^2 \exp[i(\delta + 20°)] \quad (4\text{-}2)$$

where $\vec{\tau}$ is the surface wind stress vector, pa is the density of air, CD the drag coefficient, W the geostrophic wind speed δ the direction of the geostrophic wind vector anti clockwise from east γ and the direction of the surface stress vector. It should be borne in mind that the precise magnitudes of the drag coefficients, air density and the ratio of 10 m wind speed to geostrophic wind speed are unimportant in coherence computations.

The longshore and offshore components of the surface stress vector were then plotted versus time. Comparison of current, wind and wind stress component time series yielded no striking correlation. Time series plots of the current velocity components in Shelikof Strait and the atmospheric pressure gradient, windspeed and wind stress are shown in Appendix 2. Although long period variations spanning about 10 days are clearly present in the current records these are not mirrored in the meteorological records. Either these variations are not locally driven, are driven by a non-meteorological process, the surface pressure grid is too coarse to resolve the Shelikof Strait winds, or an agency other than wind stress is responsible for the current oscillations. The oscillation are probably not attributable to baroclinic instabilities since these are thought to have periods in Shelikof Strait of about four days (Mysak et al, 1981).

4.3 SUBTIDAL OSCILLATIONS OF PERIOD LESS THAN SEVEN DAYS

In this range of the spectrum we have enough realizations to apply cross-spectral techniques. Since we are dealing with synoptic scale atmospheric pressure maps, however, wavelengths greater than 600 km only can be rigorously addressed. Table 4.2 lists the periods at which coherence above the 95% confidence level were found between variables.

The fluctuations in the cross-shelf sea surface slope (between Ikolik and Albatross Bank) were coherent with the longshore wind stress at periods of about 35 hours. The alongshelf (Ikolik-Amatuli) sea surface slope was coherent in this range of periods with both the longshore and offshore wind stress.

Table 4.2 Periods for Which Significant Coherence Were Pound

	Alongshore Wind Stress	Onshore Wind Stress
Shelikof Strait		
47 m Current Components		
alongshore	5 days	
offshore		
Shelikof Strait		
157 m Current Components		
alongshore	7 days, 3 days	5 days
offshore	35 hours	
Cross-shelf Pressure Gradient (Ikolik-Albatross)	35 hours	
Along-shelf Pressure Gradient (Ikolik-Amatuli)	35 hours	35 hours

Clearly, the cross-shelf sea surface slope (Ikolik-Albatross) responds to alongshore shore wind-stresses of periods of just over one day (the time lag is about 12 hours). The alongshore sea surface slope however (Ikolik-Amatuli) responds significantly to both alongshore and onshore wind stress.

The shallow alongshore currents appear to respond primarily to alongshore stress oscillations of about five day period while the deeper alongshore currents appear to respond to both alongshore and offshore stresses.

If we assume that both current meters are located within the geostrophic interior of the fluid, that is outside the surface and bottom Ekman layers, then the behavior of the cross-shelf pressure gradient should mirror that of the alongshore current component. Inspection of Table 4.2 reveals that this is not the case. Additionally, it is difficult to explain the high coherence between the onshore wind stress and the along-shelf pressure gradient.

Unfortunately, we cannot draw conclusions from the observed coherence. We can only speculate that the geostrophic winds are not a good indication of the atmospheric forcing over Shelikof Strait. It is likely that the local topography greatly alters the wind field, e.g., as described by Kozo (1980).

The oscillations in Shelikof Strait, therefore, are still unexplained. It is extremely unlikely that they are *driven* by coastal freshwater discharge so that the remaining mechanisms are the atmospheric pressure field, wind stress or wave-like instabilities.

5. SUMMARY

5.1 PROPERTY FIELDS

Between June and August 1984, the surface temperature increased by about 5°C in the Western Gulf of Alaska due to insolation. Cross sections of density revealed an eddy-like feature of dimensions comparable with the internal Rossby radius which propagated (or was advected) westward at a speed of about 4 cm s^{-1}. If the feature was associated with baroclinic instability, then a mechanism for cross slope exchange of water and nutrients was present.

The station spacing and the lack of synopticity of the CTD limit the the utility of the computed geostrophic currents. In general, however, westerly flows as high as 60 cm s^{-1} were computed over the continental slope while westerly flows up to 10 cm s^{-1} were computed over the continental shelf.

The property distributions were similar to those reported by previous investigators.

5.2 TIDAL OSCILLATIONS

The tides in the region are mixed, mainly semi-diurnal with spring tide ranges of between 3.5 and 6.5 m. Cotidal charts show the major tidal constituents propagating from northeast to southwest with some suggestion of shoreward propagation west of Kokiak Island. Computations of tidal energy flux are generally consistent with the cotidal charts with the exception of the Stevenson Entrance location. At this site, southward propagation of energy is computed.

Substantial tidal period internal wave energy was computed for the M_2 constituent in Cook Inlet. Internal tide waves have associated velocity,

amplitudes and heights of about 50 cm S-l and 30 m respectively. The implication is that a 60 m height internal tide wave is present at spring tide. In 65 m water depth such an oscillation is extremely unlikely without strong non-linearities in the flow field. A purely linear-barotropic tidal model will, therefore, likely be inadequate to predict the flow field in Cook Inlet.

5.3 SUBTIDAL OSCILLATIONS

The current data collected during this study were inadequate to address variations in the Alaska Coastal Current for two reasons: first, the records are only two months long and, "second, the moorings were located no closer than 15 km to the coast. The offshore length scale of the current during June-August is expected to be between 3 and 7 km so that the current meters would not have sensed the coastal current.

Mean flows ranged between 1.3 and 5.6 cm s^{-1}, and were directed generally southwestward along the shelf with two important exceptions. In Shelikof Strait, the mean flow at depth was northeastward implying an estuarine type of flow regime there. In Cook Inlet the mean flows was east by northeast nearly across the inlet. The Cook Inlet mean flows are probably a manifestation of a secondary circulation the most likely driving force for which is tidal rectification.

No success was achieved in relating the variations in the geostrophic winds with the variations in the flow on the continental shelf. We speculate that this is due to ageostrophic atmospheric flow caused by the presence of coastal mountains.

6. REFERENCES CITED

Favorite, F and W.J. Ingraham, Jr., 1977. On flow in northwestern Gulf of Alaska, Nay 1971. Journ. Oceanogr. Sot. Japan, 33:67-81.

Foreman, M.G.G., 1977. Manual for Tidal Heights Analysis and Prediction. Pacific Marine Science Report 77-10. Institute of Ocean Sciences, Patricia Bay, Victoria, B.C.

Forman, M.G.G., 1978. Manual for Tidal Currents Analysis and Prediction. Pacific Marine Science Report 78-6. Institute of Ocean Sciences, Patricia Bay, Victoria, B.C.

Greisman, P., 1984. Data Report. Oceanographic Data and Circulation, Western Gulf of Alaska prepared for NOAA, Ocean Assessment Division, Anchorage. Dobrocky Seatech Ltd., 382 pp.

Kozo, T.L., 1980. Mountain Barrier Baroclinicity Effects on Surface Winds Along the Alaskan Arctic Coast. Geophys. Res. Letrs. 7(5):377-380.

Le Blond, P.H. and L.A. Mysak, 1978. Waves in the Ocean. Elsevier, Amsterdam. 602 pp.

Mysak, L.A., R.D. Muench and J.D. Schumacher, 1981. Baroclinic Instability in a Downstream Varying channel: Shelikof Strait, Alaska. Journal of Physical Oceanography, 11 (7):950-969.

Patchen, R.C., J.T. Bruce and M.J. Connolly, 1981. Cook Inlet Circulatory Survey: 1973-75. NOS Oceanographic Circulatory Survey Report No. 4. U.S. Department of Commerce, NOAA. 89 pp.

Phillips, O.M., 1966. The Dynamics of the Upper Ocean. Cambridge University Press. 261 pp.

Platzman, G.W., 1971. Ocean Tides and Related Waves. In Mathematical Problems in the Geophysical Sciences, pt. 2. (W.H. Rein cd.), Lectures in Applied Math. V. 14, Am. Math. Sot. Providence, R.I. 239-291.

Reed, R.K., R.D. Muench and J.D. Schumacher, 1979. On the baroclinic transport of the Alaska Stream near Kodiak Island.

Royer, T.C. and R.D. Muench, 1977. On the ocean temperature distribution in the Gulf of Alaska 1974-1975. Journ. Phys. Oceanogr. 7:92-99.

Royer, T.C., 1979. On the effect of precipitation and runoff on coastal circulations in the Gulf of Alaska, Journ. Phys. Oceanogr. 9:555-563.

Royer, T.C., 1981. Baroclinic Transport in the Gulf of Alaska, Part II. A freshwater driven coastal current. Journ. Mar. Res. 39(2):251-266.

Schumacher, J.D., R. Silcox, D. Dreeves and R.D. Muench, 1978. Winter Circulation and Hydrography Over the Continental Shelf of the Northwest Gulf of Alaska. NOAA Tech. Rep. ERL 404-PMEL 31.

Schumacher, J.D., R.K. Reed, M. Grigsby and D. Dreeves, 1979. Circulation and Hydrography Near Kodiak Island September to November 1977. NOAA Tech. MeIn. ERL PMEC-13.

Schumacher, J.D. and R.K. Reed, 1980. Coastal Flow in the Northwest Gulf of Alaska: The Kenai Current. Journal of Geophysical Research 85: 6680-6688.

Smith, P.C., 1976. Baroclinic Instability in the Denmark Strait Overflow. Journ. Phys. Oceanogr. 6:355-371.

Xiong, Q and T.C. Royer, 1984. Coastal Temperature and Salinity in the Northern Gulf of Alaska, 1970-1983. Journal of Geophysical Research, 89(5):8061-8068.

Appendix 1

Tidal Analyses

GULF OF ALASKA

ANALYSIS OF HOURLY TIDAL HEIGHTS

S◁N. AMATULI ISLAND
DEPTH: 167 M
START: 2300Z 13/ 6/84
NO.OBS. = 1360 NO.PTS.ANAL.= 1460

LAT: 59 0 7.8 N
LONG: 151 50 1.8 W
END: 1400Z 9/ 8/84
MIDPT: 600Z 12/ 7/84

	NAME	FREQUENCY (CY/HR)	A (M)	G
1	Z0	0.000000	166.2659	0.00
2	MM	0.00151215	0.0257	145.38
3	MSF	0.00282193	0.0323	328.20
4	ALP1	0.03439657	0.0068	62.74
5	2Q1	0.03570635	0.0137	303.66
6	Q1	0.03721850	0.0468	271.60
7	O1	0.0 8 3 65	0.3082	262.95
8	NO1	0.04026860	0.0214	331.62
9	K1	0.04178075	0.5834	287.24
10	J1	0.04329290	0.0200	324.87
11	OO1	0.04483084	0.0092	293.79
12	UPS1	0.04634299	0.0033	270.03
13	EPS2	0.07617730	0.0068	169.58
14	MU2	0.07768947	0.0470	213.74
15	N2	0.07899922	0.3011	297.41
16	M2	0.08051139	1.5548	312.60
17	L2	0.08202355	0.0125	294.06
18	S2	0.08333331	0.4184	357.54
19	ETA2	0.08507365	0.0199	302.03
20	MO3	0.11924207	0.0127	194.15
21	M3	0.12076712	0.0022	46.03
22	MK3	0.12229216	0.0171	218.41
23	SK3	0.12511408	0.0059	219.66
24	MN4	0.15951067	0.0070	322.32
25	M4	0.16102278	0.0163	359.70
26	SN4	0.16233259	0.0010	356.16
27	MS4	0.16384470	0.0084	58.07
28	S4	0.16666669	0.0037	37.73
29	2MK5	0.20280355	0.0058	211.90
30	2SK5	0.20844740	0.0013	50.83
31	2MN6	0.24002206	0.0016	359.03
32	M6	0.24153417	0.0045	53.37
33	2MS6	0.24435616	0.0021	146.80
34	2SM6	0.24717808	0.0012	88.31
35	3MK7	0.28331494	0.0010	265.07
36	M8	0.32204562	0.0014	272.69

ANALYSIS OF HOURLY TIDAL HEIGHTS

STN: ALBATROSS BANK LAT: 56 33 28.8 N
DEPTH : 165 M LONG: 152 26 57.0 W
START : 1200Z 12/ 6/84 END: 400Z 8/ 8/84
NO.OBS.= 1361 NO.PTS.ANAL.= 1361 MIDPT: 2000Z 10/ 7/84

	NAME	FREQUENCY (CY/HR)	A (M)	G
1	ZO	0.00000000	164.4422	0.00
2	MM	0.00151215	0.0206	165.74
3	MSF	0.00282193	0.0155	333. 31
4	ALP1	0.03439657	0.0045	170.37
s	2Q 1	0.03570635	0.0096	320.29
6	Q1	0.03721850	0.0432	256.19
7	O1	0.03873065	0.2905	255.04
8	NO 1	0.04026860	0.0154	318.87
9	K1	0.04178075	0.5528	278.29
10	J1	0.04329290	0.0243	312.61
11	001	0.044s3084	0.0089	315. 17
12	UPS1	0.04634299	0.0011	211.94
13	EPS2	0.07617730	0.0077	203.52
14	MU2	0.0776SS47	0.0177	17$3.66
15	N2	0.07899922	0.1698	279.03
16	M2	0.08051139	0.8940	294.57
17	L2	0.0S2023S6	0.0142	313.45
18	S2	0.08333331	0.2171	334 .37
19	ETA2	0.08507365	0.0094	275.77
20	MO3	0.11924207	0.0021	%32.30
21	M3	0.12076712	0.0017	230.21
22	MK 3	0.12229216	0.0025	226. 88
23	SK3	0.12511408	0.0009	1S2.34
24	MN4	0.15951067	0.0004	55.15
25	M4	0.16102278	0.0007	216.40
26	SN4	0.16233259	0.0006	344.03
27	MS4	0.16384470	0.0009	99.80
28	S4	0.16666669	0.0011	191.48
29	2MK5	0.20200355	0.0009	163.82
30	2SK5	0.20844740	0.0008	282.14
31	2MN6	0.24002206	0.0001	163.15
32	M6	0.24153417	0.0013	150.91
33	2MS6	0.24435616	0.0011	2SS.46
34	2SM6	0.24717808	0.0003	271.15
35	3MK7	0.28331494	0.0006	252.30
36	M8	0.32204562	0 .0003	316.73

ANALYSIS OF HOURLY TIDAL HEIGHTS

STN: SHUMAGIN LAT : 54 31 55.8 N
DEPTH: 193 M LONG: 158 58' 4.8 W
START : 2000Z 15/ 6/84 END : 19002 11/ 8/84
NO.OBS. = 1368 NO.PTS.ANAL. = 1368 MIDPT: 700Z 14/ 7/84

	NAME	FREQUENCY (CY/HR)	A (M)	G
1	ZO	0.00000000	192.0029	0.00
2	MM	0.00151215	0.0148	176.47
3	NSF	0.002S2193	0.0232	0.27
4	ALP 1	0.03439657	0.0052	293.93
5	2Q 1	0,0357063S	0.0066	292.27
6	Q1	0.03721850	0.0510	271.5 7
7	O1	0.03873065	0.2769	266. SO
8	NO 1	0.04026860	0.0244	322.55
9	K1	0.04178075	0.5175	289.08
10	J1	0.04329290	0.0129	310.28
11	00 1	0.04483084	0.0106	279.33
12	UPS i	0.04634299	0.0042	316.70
13	EPS2	0.0?6%?730	0.0037'	239 · 89
14	MU2	0.07769947	0.0173	188.56
15	N2	0.07899922	0.1371	302.39
16	M2	0.08051139	0.6713	317.25
17	L2	0.08202356	0.0147	351.66
18	S2	0.08333331	0. 1690	353.99
19	ETA2	0.08507365	0. 0083	322.62
20	MO3	0.11924207	0.0014	352. ?3
21	M3	0.12076712	0.0017	222.90
22	MK3	0.12229216	0.0006	250.66
23	SK3	0.1251140S	0.0007	215.00
24	MN4	0.15951067	0.0003	199.91
25	M4	0.16102278	0.0011	232.74
26	SN4	0.16233259	0.0002	58. 20
27	MS4	0.16384470	0.0003	112.42
28	S4	0.16666669	0.0017	1'39.84
29	2MK5	0.20280355	0.0020	197.44
30	2SK5	0.20844740	0.0002	195. 38
31	2MN6	0.24002206	0.0009	266. 61
32	M6	(3.24%53417	0.0014	318. 15
33	2MS6	0.24435616	0.0014	346.82
34	2SM6	0.24717808	0 . 0005	43.08
35	3MK7	0.2S331494	0.0010	268.95
36	M8	0.32204562	0.0009	301.68

ANALYSIS OF HOURLY TIDAL HEIGHTS

STN: CAPE IKOLIK LAT: 57 15 0.0 N
DEPTH: 62 M LONG: 154 45 18.0 W
START: 100Z 15/ 6/84 END: 2300Z 10/ 8/84
NO.OBS.= 1367 NO.PTS.ANAL.= 1367 MIDPT: 1200Z 13/ 7/84

	NAME	FREQUENCY (CY/HR)	A (M)	G
1	Z0	0.00000000	61.2714	0.00
2	MM	0.00151215	0.0183	154.76
3	MSF	0.00282193	0.0260	1.68
4	ALP1	0.03439657	0.0032	352.93
5	2Q 1	0.03570635	0.0113	306.23
6	Q1	0.037218S0	0.0515	271.30
7	O1	0.03S73065	0.3070	265.70
8	NO 1	0.04026860	0.0245	327.00
9	K1	0.041?8075	0.5928	2S9.37
10	J1	0.04329290	0.0192	329.15
11	OO1	0.044$30s4	0.0116	274.81
12	UPS1	0.04634299	0,0047	307.11
13	EPS2	0.07617730	0.0062	289.65
14	MU2	0.0776S947	0.0261	212. 33
15	N2	0.07$99922	0.2770	303.52
16	M2	0.0%051139	1. 3889	317.00
17	L2	0.08202356	0.0202	319.81
18	S2	0.08333331	0..3757	1.87
19	ETA2	0.08507365	0.0201	315.96
20	MO3	0.11924207	0.0054	99.62
21	M3	0.12076712	0.0054	11.05
22	MK 3	0.$2229236	0.0167	355.14
23	SK3	0.12511408	0.0096	202.21
24	MN4	0.15951067	0.00S6	199.64
25	M4	0.16102278	0.0299	220.50
26	SN4	0.16233259	0.0036	241.71
27	MS 4	0.16384470	0.0127	207.22
28	S4	0.16666669	0.0054	317.39
29	2MK5	0.202S0355	0.0040	169.34
30	2SK5	0.20844740	0.0011	266.61
31	2MN6	0.24002206	0.0024	141.08
32	M6	0.24153417	0.0043	152.29
33	2MS6	0.2443S616	0.0031	212.66
34	2SM6	0.2471780S	0.0008	153.50
35	3MK7	0.28331494	0.0008	336.89
36	M8	0.32204562	0.0014	9.47

GULF OF ALASKA

ANALYSIS OF HOURLY TIDAL HEIGHTS

STN: SEAL ROCKS LAT: 59 29 55.8 N
DEPTH : 114 M LONG: 149 29 34.2 W
START : 1000Z 13/ 6/84 END: 4002 9/ 8/84
NO.OBS.= 1363 NO.PTS.ANAL.= 1363 MIDPT: 1900Z 11/ 7/84

	NAME	FREQUENCY (CY/HR)	A (M)	G
1	ZO	0.00000000	113.3633	0.00
2	MM	0.00151215	0,0234	133.86
3	MSF	0.002S2193	0.0403	356.06
4	ALP1	0.03439657	0.0061	90030
5	2Q1	0.0357063S	0.0117	308.39
6	Q1	0.03721850	0.0410	263.84
7	O1	0.03873065	0.2846	256 .09
8	NO 1	0.04026S60	0.0172	325.07
9	K1	0.04178075	0.5431	279.69
10	J1	0.04329290	0 . 0209	316.09
11	OO1	0.04483084	0.0088	302. 19
12	UPS1	0.04634299	0.0021	252.49
13	EPS2	0.07617730	0.0053	148.33
14	MU2	0.0776S947	o . 0340	176.16
15	N2	0.07899922	0.2216	274.53
16	M2	0.08051139	1.1975	289 .94
17	L2	0.08202356	0.0109	305.84
18	S2	0.08333331	0.3016	331.25
19	ETA2	0.08507365	0.0121	273.02
20	MO3	0.11924207	0.0036	179.$7
21	M3	0.12076712	0.0012	298.42
22	MK3	0.12229216	0.0043	191.79
23	SK3	0.12511408	0.0031	162.93
24	MN4	0.15951067	0.0013	33.4.68
25	M4	0.16102278	0.0085	13.66
26	SN4	0.16233259	0.0015	3.70
2?	MS4	0.16384?0	0.0042	114.67
28	S4	0.16666669	0.0007	290.37'
29	2MK5	0.20280355	0.0018	245.35
30	2SK5	0.20844740	0.0015	268.12
31	2MN6	0.24002206	0.0022	320. 85
32	M6	0.24153417	0.0062	41.30
33	2MS6	0.24435616	0.0024	117.96
34	2SM6	0.24717808	0.0014	38.02
35	3MK7	0.28331494	0.000?	328 .63
36	M8	0.32204562	0.0013	336.99

ANALYSIS OF HOURLY TIDAL HEIGHTS

STN: PORTLOCK BANK LAT : 58 O 1.8 N
DEPTH : 178 M LONG: 149 29 34.8 W
START : 100Z 13/ 6/84 END: 16002 8/ 8/84
NO.OBS.= 1360 NO.PTS.ANAL.= 1360 MIDPT: 800Z 11/ 7/84

	NAME	FREQUENCY (CY/HR)	A (M)	G
1	ZO	0.00000000	177.0711	0.00
2	MM	0.00151215	0.0272	156.61
3	MSF	0.00282193	0.0218	341.60
4	ALP1	0.03439657	0.0041	112.08
5	2Q 1	0.03570635	0.0104	312.84
6	Q1	0.03721S50	0.0424	258. 27
7	01	0.03873065	0.2916	252.72
8	NO 1	0.04026S60	0.0171	318.75
9	K1	0.04178075	0.5572	276.60
10	J1	0.04329290	0.0227	313.52
11	001	0.04483084	0.0094	30$.53
12	UPS1	0.04634299	0.0014	232.87
13	EPS2	0.07617730	0. 0007	153 .79
14	MU2	0.07768947	0.0273	184.22
15	N2	0.07S99922	0.1902	278. S7
16	M2	0.08051139	1.0140	293. 48
17	L2	0.08202356	0.0094	299.76
18	S2	0.08333331	0.2499	334.36
19	ETA2	0.0S507365	0.0093	278.84
20	MO3	0.11924207	0.0029	263.94
21	M3	0.12076712	0.0027	249.1,6
22	MK 3	0.12229216	0.0014	207.67
23	SK 3	0.12511408	0.0009	112.25
24	MN4	0.15951067	0.0003	293.32
25	M4	0.16102278	0.0015	297.13
26	SN4	0.16233259	0.0015	324.41
27	MS4	0.163S4470	0.0010	49.'75
28	S4	0.16666669	0.0002	17.43
29	2MKS	0.20280355	0.0016	158.97
30	2SK5	0.20S44740	0.0009	288.21
31	2MN6	0.24002206	0.0006	336.75
32	M6	0.24153417	0.0023	61.40
33	2MS6	0.24435616	0.0007	129.92
34	2SM6	0.24717S08	0.0008	55.71
35	3MK7	0.2S331494	0.0008	81.17
36	M8	0.32204562	0.0011	169.50

GULF OF ALASKA

ANALYSIS OF HOURLY TIDAL HEIGHTS

STN: SANAK LAT : 54 35 15.0 N
DEPTH : 51 M LONG : 162 43 46.2 W
START : 1100Z 16/ 6/84 END : 400Z 13/ 8/84
NO.OBS.= 1386 NO.PTS.ANAL. = 1386 MIDPT: 700Z 15/ 7/84

	NAME	FREQUENCY (CY/HR)	A (M)	G
1	Z0	0.00000000	51.0813	180.00
2	MM	0.00151215	0.0097	210.41
3	MSF	0.00282193	0.0220	8.72
4	ALP1	0.03439657	0.0043	256.34
5	2Q 1	0.03570635	0.0040	312.70
6	Q1	0.03721850	0.0476	274.08
7	O1	0.03$73065	0.2691	269.93
8	NO 1	0.04026860	0.0244	324.25
9	K1	0.04178075	0.5041	293.03
10	J1	0.04329290	0.0096	299.74
11	001	0.04483084	0.0113	291.54
12	UPSI	0.04634299	0.0024	341.03
13	EPS2	0.07617730	0. 0038	228.10
14	MU2	0.07768947	0.0173	196.83
15	N2	0.07899922	0.1331	314.13
16	M2	0.08051139	0.6306	330.12
17	L2	0.0S202356	0.0173	347.43
18	S2	0.08333331	0.1579	3.55
19	ETA2	0.08507365	0.0074	337.79
20	MO3	0.11924207	0.0025	13.46
21	M3	0.12076712	0.0023	248.32
22	MK3	0.9.2229216	0.0027	53.03
23	SK3	0.12511408	0.0017	319.22
24	MN4	0.15951067	0.0014	73.10
25	M4	0.16102278	0.0006	89. 53
26	SN4	0.16233259	0.0012	119.45
27	MS4	0.16384470	0.0009	222 .07
28	S4	0.16666669	0.0027	219.48
29	2MK5	0.202S035S	0.0022	181.33
30	2SK5	0.20844740	0.0027	184.51
31	2MN6	0.24002206	0. 0038	128.19
32	M6	0.24153417	0.0095	$39.34
33	2MS6	0.24435616	0.0069	202. 12
34	2SM6	0.24717S08	0.0021	254. 16
35	3MK7	0.28331494	0.0022	303.21
36	M8	0.32204562	0.0016	341.89

GULF OF ALASKA

ANALYSIS RESULTS IN CURRENT ELLIPSE FORM
AMPLITUDES HAVE BEEN SCALED ACCORDING TO APPLIED FILTERS

STN: STEVENSON ENTRANCE — LAT: 58 53 43.8 N
DEPTH : 54 M — LONG: 1S0 57 13.8 W
START : 2000Z 13/ 6/84 — END: 800Z 9/ 8/84

	NAME	FREQUENCY (CY/HR)	MAJOR (CM/S)	MINOR (CM/S)	INC	G	G+	G-
1	Z0	0.00000000	2.111	0.000	57.8	180.0	122.2	237, 8
2	MM	0.00151215	3.924	-2.361	45.0	55.4	10.5	100.4
3	MSF	0.00282193	2.861	-2.021	84.7	68.2	343.6	152.9
4	ALP1	0.03439657	0.476	-0.391	179.0	156.0	337.0	334.9
5	2Q1	0.03570635	0.728	0.126	109.4	93.1	343.7	202.5
6	Q1	0.037218S0	1.000	0.344	97.5	17.0	279.5	114.5
7	O1	0.03873065	3.742	-0.774	98.1	13.7	275.6	111.8
8	NO1	0.04026860	0.2s8	0.040	106.4	156.6	50.2	263.1
9	K1	0.04178075	6.571	-2.157	100.6	40.5	300.0	141.1
10	J1	0.04329290	0.558	0.430	126.2	?'5.9	309.8	202.1
11	OO1	0.04483084	0.450	-0.140	75.4	349.8	274.5	65.2
12	UPS1	0.04634299	0.395	0.087	7.3	12.6	5.3	19.9
13	EPS2	0.07617730	1.338	0.774	74.1	304.2	230.2	13.3
14	MU2	0.0776$947	2.474	0.503	67.2	31.8	324.6	98.9
15	N2	0.07899922	5.889	1.478	93.5	50.5	317.0	143.9
16	M2	0.08051139	30.198	0.621	102.1	66.3	324.1	168.4
17	L2	0.08202356	1.484	-0.098	116.5	37.0	280.5	153.5
18	S2	0.08333331	10.086	0.591	97.2	112.3	15.1	209.5
19	ETA2	0.08S07365	1.137	0.717	80.1	100.2	20.1	180.3
20	MO3	0.11924207	0.645	0.246	74.4	182.6	108.2	257.1
21	M3	0.12076712	0,545	-0.231	17.1	228.3	211.2	245.4
22	MK3	0.12229216	i.015	0.195	50.4	2s0.5	230.1	331.0
23	SK3	0.12511408	0.417	0.173	25.5	329.1	303.6	354.6
24	MN4	0.15951067	0.141	-0.060	90.3	6.9	268.6	105.2
25	M4	0.16102278	0.691	0.538	5.7	259.3	253.6	265.0
26	SN4	0.16233259	0.415	-0.185	126.4	262.2	135.8	28.5
27	MS4	0.16384470	0.526	-0.342	2.0	357.1	355.0	359.i
28	S4	0.$6666669	0.651	0.354	43.5	319.7	276.3	3.2
29	2MK5	0.20280355	0.922	0.247	55.3	283.3	228.0	336.6
30	2SK5	0.20844740	0.187	0.105	149.7	214.2	64.4	3.9
31	2MN6	0.24002206	0.535	-0.153	15.8	303.1	287.3	318.8
32	M6	0.24153417	0.923	-0.041	36.3	310.8	274.5	347.2
33	2MS6	0.24435616	0.'720	-0.050	58.9	328.8	269.9	27.7
34	2SM6	0.24717808	0.525	0.128	134.0	98.0	323.2	232.7
35	3MK7	0.28331494	0.492	0.110	101.4	233.6	132.2	335.0
36	M8	0.32204562	0.338	0.135	151.1	45.9	254.7	197.0

ANALYSIS RESULTS IN CURRENT ELLIPSE FORM
AMPLITUDES HAVE BEEN SCALED ACCORDING TO APPLIED FILTERS

STN: STEVENSON ENTRANCE — LAT: 58 53 43.8 N
DEPTH : 82 M — LONG: 150 57 13.8 W
START : 2000Z 13/ 6/84 — END: 800Z 9/ 8/84

	NAME	FREQUENCY (CY/HR)	MAJOR (CM/S)	MINOR (CM/S)	INC	G	G+	G-
1	ZO	0.00000000	2.576	0.000	134.9	180.0	45.2	314.9
2	MM	0.00151215	3.302	-0.808	30.9	50.5	19.7	81.4
3	MSF	0.00282193	2.993	-1.034	17.5	149.0	131.5	166.5
4	ALP1	0.03439657	0.221	-0.191	70.4	202.2	131.8	272.6
5	2Q1	0.03570s35	0.424	-0.006	69.0	63.5	354.5	132.5
6	Q1	0.03721850	0.826	0.220	59.6	54.5	354.9	114.1
7	O1	0.03873065	3.456	-1.668	91.3	21.5	290.2	112.8
8	NO1	0.04026860	0.268	0. 138	10.0	109.7	99.7	119.7
9	K1	0.04178075	6.411	-3.464	108.3	35.9	287.6	144.3
10	J1	0.04329290	0.931	0.647	66.9	69.2	2.3	136.2
11	001	0.04483084	0.343	0. 130	82.8	55.6	332.8	138.4
12	UPSI	0.04634299	0.248	0.085	166.1	324.1	158.1	130.2
13	EPS2	0.07617730	1.490	0.759	60.?	357.5	296.8	58.2
14	MU2	0.07768947	2.926	0.764	26.1	57.8	31.7	83.9
15	N2	0.07s99922	5.908	-0.342	94.1	55:1	321.0	149.3
16	M2	0.08051139	36. 348	1.649	91.2	76.0	344.7	167.2
17	L2	0.08202356	3.619	2.749	1.0	%0.6	19.6	21.6
18	S2	0.0s333331	11.5s4	1.104	83.6	126.3	42.7	210.0
19	ETA2	0.0S507365	0.820	0.024	95.6	67.9	332.3	163.5
20	MO3	0.11"924207	0.323	-0.026	60.0	352.2	292.3	52.2
21	M3	0.12076712	0.252	0. 121	136.3	16.3	240.0	152.6
22	MK3	0.12229216	o* 809	-0.112	33.4	40.8	7.4	74.3
23	SK3	0.12511408	0.271	0.036	32.5	85.7	53.2	118.2
24	MN4	0.15951067	0.983	0.046	79.4	92.0	12.6	171.4
25	M4	0.16102278	1.492	0. 128	24.7	127.5	102.8	152.2
26	SN4	0.16233259	1.139	0.294	150.7	238.2	87.6	28.9
27	MS4	0.16384470	0.461	-0.179	57.3	151.4	94-.2	208.7
28	S4	0.16666669	0.672	0.618	107.4	215.4	108.0	322.8
29	2MK5	0.202S0355	0.679	0.233	40.2	7.4	327.2	47.7
30	2SK5	0.20844740	0.125	0.079	96.0	171.2	75.2	267.1
31	2MN6	0.24002206	0.310	-0.054	96.4	85.4	349.0	181.8
32	M6	0.24153417	0.203	0. 167	58.8	320.1	261.3	19.0
33	2MS6	0.24435616	0.474	0.131	41.4	45.7	4.3	87.1
34	2SM6	0.24717$30S	0.220	-0.003	105.0	188.3	03.3	293.3
35	3MK7	0.2s331494	0.558	0.182	140.2	307.0	166.8`	S7.2
36	M8	0.32204562	0.299	-0.172	15.4	88.4	73.1	103.8

ANALYSIS RESULTS IN CURRENT ELLIPSE FORM
AMPLITUDES HAVE BEEN SCALED ACCORDING TO APPLIED FILTERS

STN: COOK INLET
DEPTH: 35 M
START: 500Z 14/ 6/84

LAT: 59 35 1.2 N
LONG: 152 29 0.0 W
END: 1800Z 9/ 8/84

	NAME	FREQUENCY (CY/HR)	MAJOR (CM/S)	MINOR (CM/S)	INC	G	G+	G-
1	ZO	0.00000000	4.304	0. 000	12.1	360.0	347.9	12.1
2	MM	0.00151215	1 .922	1.178	117.8	165.3	47.4	2B3. 1
3	MSF	0.002s22'33	4.297	-1.351	99.1	264.3	165.2	3.4
4	ALP1	0.034%9657	0. 591	-0.411	95.0	26.4	291.4	121.5
5	2Q1	0.03S70635	0. 757	-0.323	108.6	256. 8	148.3	5.4
6	Q1	0.03721850	1. 892	0.09$	91.8	241.0	149.1	332.8
7	O1	0.03873065	9.482	-0.695	78.5	223.7	145.2	302.3
8	NO1	0,04026860	0.897	-0.069	105.1	290.7	185.6	35.8
9	K1	0.04178075	19.006	-3.527	77.4	243.9	166.5	321.2
10	J1	0.04329290	0.602	0. 184	54.4	292.2	237.8	346.6
11	001	0.044S3084	0 . 837	-0.097	104.2	264.7	160.5	9.0
12	UPS1	0.04634299	0.428	0.020	124.4	237.3	112.9	1.6
13	EPS2	0.07617730	1 . 706	-1.474	51.9	193.8	141.9	245.6
14	MU2	C.07768947	6. 366	-0.209	96.6	199.5	102.9	296.2
15	N2	0.07899922	14.444	-2.391	81.2	285.2	204.0	6.4
16	M2	0.08051139	73.'533	-8. 936	78. 1	308.4	230.3	26.5
17	L2	0.08202356	1 .290	1.098	6*6	357.0	350 .4	3.6
18	S2	0.0s333331	19.821	-2.525	84.1	352.1	268.1	76.2
19	ETA2	0.08507365	1 . 028	-0.461	95.4	278.3	183.0	13.7
20	MO3	0.11924207	1.905	-0.115	70.3	112.1	41.7	182.4
21	M3	0.12076712	1.271	-0.679	74.7	29.7	315.1	104.4
22	MK3	0.12229216	2.642	-o. 081	84.6	145.0	60.4	229.6
23	SK3	0.12511408	1 .306	-0.512	5'?.0	20? .1	150. 1	264.2
24	MN4	0.15951067	0.941	-0.658	92.7	161.7	69.0	254.4
25	M4	0.16102278	2.622	-1.012	65.7	179.0	113.3	244.6
26	SN4	0.16233259	0.362	-0.100	75.8	239.5	163.8	315.3
27	MS4	0.16384470	0. 922	-0.193	77.2	215.0	137.8	292.3
28	S4	0.36666669	0. 867	-0. 480	9.6	23.6	13.9	33.2
29	2MK5	0.202S0355	0.973	-0.022	108. 1	304.2	196.1	52.2
30	2SK5	0.20s44740	0.273	-0.148	44.3	175.9	131.6	220.2
31	2MN6	0.24002206	0.517	-0.007	158.6	194.8	36.2	353.4
32	M6	0.24153417	0.833	-0.077	49.8	101.3	51.6	151.1
33	2MS6	0.24435616	0.593	-0.218	154.4	334.4	180.0	128.7
34	2SM6	0.24717808	0 . 384	-0.044	171.3	352.0	180.6	163.3
35	3MK7	0.28331494	0.531	-0. 118	149.4	109.0	319.5	258.4
36	M8	0.32204562	'0.424	-0.178	4.3	328 .9	324.7	333.2

ANALYSIS RESULTS IN CURRENT ELLIPSE FORM
AMPLITUDES HAVE BEEN SCALED ACCORDING TO APPLIED FILTERS

STN: COOK INLET — LAT: 59 35 1.2 N
DEPTH: 52 M — LONG: 152 29 0.0 W
START: 500Z 14/ 6/84 — END: 2200Z 13/ 7/84

	NAME	FREQUENCY (CY/HR)	MAJOR (CM/S)	MINOR (CM/S)	INC	G	G+	G-
1	ZO	0.00000000	5.464	0.000	25.9	360.0	334. 1	25.9
2	MSF	0.002S2193	3.256	-1.136	110.4	248. 8	138.4	359.2
3	2Q1	0.0357063S	1 . 045	-0. 480	55.8	343.4	287.6	39.2
4	Q1	0.03721050	1.980	-0. 183	70.6	236.5	165.8	307. 1
5	01	0.03873065	7.990	-0.067	69.0	220.4	151.4	2139.4
6	NO1	0.04026S60	0.679	0.122	120.4	323 . 8	203.4	84.2
7	K1	0.04178075	16.570	-3.415	78.0	238. 6	160.7	316.6
8	J1	0.04329290	1.078	0. 115	7.4	286.4	279.0	293.7
9	001	0.04483084	1.061	0.298	114.7	272.9	158.2	27.7
10	UPS1	0.04634299	0.429	-0.256	36.0	220 .9	184.9	257.O
11	N2	0,0?899922	3,3.229	-3.5'30	83.2	278.7	195.6	1.9
12	M2	0.080S1139	59.845	-1.996	74.2	304. 8	230.6	19.0
13	S2	0.08333331	14.814	-%.754	83.6	346.3	262.7	69.9
14	ETA2	0.08507365	1 .$00	-0.948	10.2	260. 2	250 .9	270.4
15	MO3	0.11924207	2.104	-0.622	62.2	112.4	50.2	174.7
16	M3	0.12076712	1.449	-0.530	59.0	53.7	354.7	112.7
17	MK3	0.12229216	2.352	-0. 228	62.8	150.4	87.6	213.3
18	SK3	0.12511408	1.771	-0.904	67.8	213.9	146.1	281.8
19	MN4	0.15951067	1 .277	-0.474	65.1	250.3	185.2	315.4
20	M4	0.1610227S	1 . 528	-o. 846	115.3	105.2	349.9	2%0.6
21	MS4	0.16384470	0.699	0. 146	158.7	206.1	47.3	4.8
22	S4	0.16666669	0. 888	-0. 686	2.8	348 . 5	345.7	351.3
23	2MK5	0.20280355	1.314	0.168	83.1	296.9	213.8	20.0
24	2SK5	0.20S44740	0.517	-0. 108	21.9	200.9	179. 1	222. 8
25	2MN6	0.24002206	0.768	-o. 380	97.5	310.0	212.5	47.5
26	M6	0.24153417	0. 880	-0. 106	14.8	40.9	26.1	55.7
27	2MS6	0.24435616	0.468	-0. 389	133.8	314.6	180.7	88.4
28	2SM6	0.24717S08	0.532	-0.065	45.2	239.6	194.4	284.9
29	3MK7	0.28331494	0.692	-0.296	167.5	116.8	309.3	284.4
30	M8	0.32204562	0.439	-0. 298	55.8	287.3	231.5	343.1

ANALYSIS RESULTS IN CURRENT ELLIPSE FORM
AMPLITUDES HAVE BEEN SCALED ACCORDING TO APPLIED FILTERS

STN: SANAK — LAT: 54 3s 15.0 N
DEPTH: 20 M — LONG: 162 43 46.2 W
START: 1200Z 16/ 6/84 — END: 300Z 13/ 8/84

	NAME	FREQUENCY (CY/HR)	MAJOR (CM/S)	MINOR (CM/S)	INC	G	G+	G-
1	ZO	0.00000000	2.261	0.000	15.7	180.0	164.3	195.7
2	MM	0.00151215	0.426	0.084	94.4	173.3	78.9	267.8
3	MSF	0.002S2193	2.939	-0.146	0.9	146.9	146.0	147.8
4	ALP1	0.0343965?	0.527	0.048	18.6	84.1	65.5	102.7
5	2Q1	0.03570635	0.469	0.091	64.3	117.5	53*3	181.8
6	Q1	0.03721850	0.251	-0.019	54*B	227.3	172.5	282.0
7	O1	0.03873065	2.285	-1.082	176.8	104.7	287.9	261.5
8	NO1	0.04026860	0.488	-0.07'7'	94.7	35.3	300.6	130.0
9	K1	0.04178075	3.981	-1.997	166.9	145.2	338.3	312.1
10	J1	0.04329290	0.726	-0.440	10.2	349.9	339.6	0.1
11	OO1	0.044$3084	0.232	0.197	41.6	38.9	357.3	80.5
12	UPS1	0.04634299	0.345	0.004	32.5	344.0	311.4	16.5
13	EPS2	0.0?6277'30	1.098	-0.810	4.2	112.7	108.5	116.9
14	MU2	0.07768947	0.420	-:.150	12.1	92.8	?0.8	95.0
15	N2	0.07899922	0.684	-0.261	89.9	269.0	179.1	359.0
16	M2	0.08051139	3.121	0.469	112.8	285.1	172.3	37.9
17	L2	0.08202356	0.984	0.133	65.3	341.8	276.5	47.1
18	S2	0.08333331	1.091	-0.110	76.6	335.5	258.9	52.1
19	ETA2	0.08507365	0.403	-0.033	56.0	213.8	157.8	269.8
20	MO3	0.11924207	0.231	0.035	91.2	186.5	95.3	277.7
21	M3	0.12076712	0.153	-0.032	3.8	355.3	351.5	359.2
22	MK3	0.12229216	0.324	-0.227	138.6	237.0	98.4	15.5
23	SK3	0.12511408	0.237	0.001	125.9	195.3	69.5	321.2
24	MN4	0.15951067	0.247	0.013	77.s	295.1	217.6	12.6
25	M4	0.16102278	0.255	-0.045	20.2	117.8	97.6	138.0
26	SN4	0.16233259	0.068	-0.0413	23.1	184.3	161.2	207.4
27	MS4	0.16384470	0.218	-0.133	149.1	30.3	241.1	179.4
28	S4	0.16666669	0.239	-0.025	94.1	231.3	137.2	325.4
29	2MK5	0.20280355	0.092	0.064	75.1	344.7	269.7	59.8
30	2SK5	0.20844740	0.131	0.060	168.8	255.3	86.5	64.0
31	2MN6	0.24002206	0.204	0.050	70.3	46.2	335.9	116.5
32	M6	0.2415342'7	0.349	0.086	108.5	104.4	355.9	212.9
33	2MS6	0.24435616	0.323	-0.023	39.2	100.6	61.3	139.8
34	2SM6	0.24717808	0.127	0.007	179.6	246.0	66.5	65.6
35	3MK7	0.28331494	0.168	-0.042	57.0	200.8	151.7	265.8
36	M8	0.32204562	0.058	-0.004	76.4	141.7	65.3	218.1

ANALYSIS RESULTS IN CURRENT ELLIPSE FORM
AMPLITUDES HAVE BEEN SCALED ACCORDING TO APPLIED FILTERS

STN: SANAK LAT: 54 35 15.0 N
DEPTH : 41 M LONG: 162 43 46.2 W
START: 1200Z 16/ 6/84 END: 200Z 13/ 8/84

	NAME	FREQUENCY (CY/HR)	MAJOR (CM/S)	MINOR (CM/S)	INC	G	G+	G-
1	ZO	0.00000000	3.086	0.000	150.8	360.0	209.2	150.8
2	MM	0.00151215	1.195	-0.687	145.6	307.9	162.3	93.5
3	MSF	0.00282193	1.414	0.176	170.3	329.5	159.2	139.9
4	ALP1	0.03439657	0.421	-0.306	86.3	296.9	210.6	23.3
5	2Q1	0.03570635	0.322	-0.016	9.1	154.6	145.5	163.7
6	Q1	0.03721850	0.659	-0.023	33.7	284.4	250.7	318.1
7	O1	0.03873065	3.465	-0.904	1.0	274.4	273.4	275.4
8	NO1	0.04026860	0.544	0.063	12.6	325.2	312.6	337. 8
9	K1	0.04178075	7.146	-3.135	165.6	135.7	330.2	301.3
10	J1	0.04329290	1 .040	-0.267	160.3	168.7	9.4	328.9
11	001	0.04493084	0.754	-0.216	163.7	152.4	348.7	316.0
12	UPS1	0.04634299	0.271	-0.057	125.2	213.9	88.7	339.0
13	EPS2	0.07617730	0.624	0.063	5.9	285.7	279.8	291.6
14	MU2	0.07768947	0.470	-0.125	16.9	85.3	74.8	112.5
15	N2	0.0?s99922	0.786	-0. 486	64.3	238. 5	174.3	302.$
16	M2	0.08051139	4.121	1.077	89.6	252.6	163.0	342.3
17	L2	0.0S202356	0.731	-0.162	98.1	91.0	352.9	189.1
18	S2	0.08333331	1.476	-0.607	30.1	267.4	237.4	297.5
19	ETA2	0.0s507365	0. 056	0.023	164.1	14.6	210.5	178.8
20	MO3	0.11924207	0.402	-0.135	153.0	256.5	103.5	49.5
21	M3	0.12076712	Oil?	-0.065	76.5	9.2	292.8	85.7
22	MK3	0.12229216	0.394	-0.063	89.0	293.6	204.6	22.5
23	SK3	0.12511408	0.314	-O.10B	9.0	99.0	89.9	108.0
24	MN4	0.15951067	0.322	-0.0$39	35.9	158.8	122.9	194.7
25	M4	0.16102278	0.110	-0.011	65.1	52.3	347.2	117.4
26	SN4	0.16233259	0.180	0.068	55.7	162.1	106.5	217.8
27	MS4	0.16384470	0.123	0.004	112.0	140.9	28.9	252.9
28	S4	0.16666669	0.190	0.145	11.7	125.4	113.7	137.1
29	2MK5	0.202S0355	0.244	-0.030	16.2	50.6	34.4	66.8
30	2SK5	0.20844740	0.082	-0.037	94.3	9s.7	1.4	189.9
31	2MN6	0.24002206	0.333	-0.027	118.6	133.4	14.8	252.0
32	M6	0.24153417	0.271	0.195	85.0	107.0	22.0	192.0
33	2MS6	0.24435616	0.296	-0.037	72.0	163.2	91.2	235.2
34	2SM6	0.24717808	0. 058	0.033	96.8	292.4	195.5	29.2
35	3MK7	0.28331494	0.110	0.031	85.2	197.0	111.8	282.2
36	M8	0.32204562	0.118	-0. 031	110.3	272.9	162.6	23.2

ANALYSIS RESULTS IN CURRENT ELLIPSE FORM
AMPLITUDES HAVE BEEN SCALED ACCORDING TO APPLIED FILTERS

STN: SHELIKOF STRAIT — LAT: 57 39 0.0 N
DEPTH: 46 M — LONG: 155 3 19.8 W
START: 2300Z 14/ 6/84 — END: 1200Z 10/ 8/84

	NAME	FREQUENCY (CY/HR)	MAJOR (CM/S)	MINOR (CM/S)	INC	G	G+	G-
1	Z0	0.00000000	3.839	0.000	59.8	180.0	120.2	239.8
2	MM	0.00151215	12.868	5.271	116.3	261.9	145.7	18.2
3	MSF	0.002S2193	5.479	-0.565	20.5	223.2	194.7	251.6
4	ALP1	0.03439657	0.531	0.356	45.6	161.5	115.9	207. 1
5	2Q1	0.03s7063s	0.741	0.473	5.2	39.0	33.s	44.1
6	Q1	0.03721850	0.97$	0.273	104.6	299.5	195.0	44.1
7	O1	0.03s73065	1 .754	-0.126	38.9	227. 1	188.2	266.0
8	NO1	0.04026860	0.429	-0.014	119.5	25.3	265.8	144.7
9	K1	0.0417s075	3.449	0.076	41.3	243.6	202.4	284.9
10	J1	0.04329290	0.616	-0.240	99.4	330.9	231.5	70.3
11	OO1	0.044s3084	0 .252	0.044	44.6	135.1	90.4	179.7
12	UPS1	0.04634299	0.199	0.106	145.$	174.8	29.0	320.6
13	EPS2	0.0?617730	0.073	0. 833	5.7	331.7	326.1	337.4
14	MU2	0.07?6a947	0.979	-0. 165	31.1	[illegible]	197.6	[illegible]
15	N2	0.07s99922	2.529	0.692	38.5	230.2	191 .7	268. 7
16	M2	0.08051139	13.766	-0.023	39.9	250.7	210.9	290.6
17	L2	0.09202356	2.234	0.772	119.5	156.9	37.4	276.5
18	S2	0.08333331	4.516	-0.032	41.2	297.1	255.9	338. 3
19	ETA2	0.08507365	1.105	0.417	85.5	221.8	136.3	307.2
20	MO3	0.11924207	0.292	0.249	125.3	137.4	12.1	262.7
21	M3	0.12076712	0.478	0.048	143.8	269.2	125.4	53.1
22	MK3	0.12229216	0.306	-0.031	11.5	126.0	114.6	137.5
23	SK3	0.1251140S	0.191	0.064	25.4	155.0	129.6	180.5
24	MN4	0.15951067	0.289	0.019	171.3	2S3. 5	82.2	64.9
25	M4	0.16102278	0.527	0.118	13.3	348.0	334.7	1.3
26	SN4	0.16233259	0.374	-0.117	110.8	289. 1	178.3	40.0
27	MS4	0.16384470	0.351	0.032	7.5	0.5	353.0	8.0
28	S4	0.16666669	0.347	0.257	157.4	171.8	14.4	329.2
29	2MK5	0.20290355	0. 386	0.136	170.2	315.9	145.6	126.1
30	2SK5	0.20844740	0.%06	0.035	95.1	223.7	128.6	318.8
31	2MN6	0.24002206	0.141	0.073	123.6	196.4	72.8	320.0
32	M6	0.24353417	0.132	-0.060	104.5	293.9	189.4	3s.5
33	2MS6	0.244356%6	0.212	0.115	177.4	157.8	340.4	335.1
34	2SM6	0.24717S0S	0.239	0.158	57.7	252.9	195.2	310.5
35	3MK7	0.28331494	0.307	-0.007	73.6	337.3	263.5	50.7
36	M8	0.32204562	0.170	0.087	109.3	33.1	283.9	142.4

ANALYSIS RESULTS IN CURRENT ELLIPSE FORM
AMPLITUDES HAVE BEEN SCALED ACCORDING TO APPLIED FILTERS

STN: SHELIKOF STRAIT — LAT: 57 39 0.0 N
DEPTH: 157 M — LONG: 155 3 19.8 W
START: 2300Z 14/ 6/84 — END: 1200Z 10/ 8/84

	NAME	FREQUENCY (CY/HR)	MAJOR (CM/S)	MINOR (CM/S)	INC	G	G+	G-
1	ZO	0.00000000	1.343	0.000	52.6	360.0	307.4	52.6
2	MM	0.00151215	5.314	2.274	123.6	263.7	140.1	27.3
3	MSF	0.00282193	4.241	-1.419	4$.3	205.2	157.0	253.5
4	ALP1	0.03439657	0.245	0.011	151.7	104.5	312.8	256 .2
5	2Q1	0.0357063s	0.241	0.080	80.6	18.9	298.2	99.5
6	Q1	0.03721850	0.514	0.277	103.9	299.9	196.1	43.s
7	O1	0.03S73065	1.496	-0.061	49.4	205. 1	155.7	254.5
8	NO1	0.04"026860	0.241	0. 121	161.5	80.5	279.0	242.0
9	K1	0.04178075	2.956	-o. 148	47.9	226.4	178.5	274.3
10	J1	0.04329290	0.396	-0.006	132. 1	342.2	210. 1	114.3
11	001	0.044s3084	o* 285	-0.013	94.%	239.6	144.8	334.4
12	UPS1	0.04634299	0.301	0.090	155.2	209. 8	54.5	5.0
13	EPS2	0.07617730	0.591	0. 268	141.3	317.0	175.7	98.3
14	MU2	0.07768947	0.482	0.349	53.2	147.0	?33.9	200,2
15	N2	0.07633922	3.111	1 .006	45.8	233 .4	***c	279.2
16	M2	0.08051139	14.870	0.598	43,0	248. 2	205.2	291.3
17	L2	0.0S202356	i . 725	0.210	119.2	138.4	19.2	257.6
18	S2	0.08333331	4.333	0.141	46.8	296.0	249.2	342. 8
19	ETA2	0.08507365	0.602	-0.114	49.3	269.9	220.5	319.2
20	MO3	0.11924207	0 .308	0.068	45.0	136.3	91.3	181.3
21	M3	0.12076712	0.251	0.008	87.5	259.9	172.4	347.4
22	MK3	0.22229216	0.496	-0.073	30. 1	164.3	134.2	194.4
23	SK3	0.12511408	0.246	-0.144	170.0	66.2	256.2	236. 1
24	MN4	0.15951067	0.208	0.150	33.1	204.0	170.9	237.2
25	M4	0.16102278	0.307	0.014	114.4	299.6	185.2	54.0
26	SN4	0.16233259	0.169	-0.019	175.4	7.5	192.1	183.0
27	MS4	0.16384470	0.239	0.043	108.3	6.3	258 .0	114.6
28	S4	0.16666669	0.205	0.100	46.1	220.3	174.2	266.3
29	2MK5	0.202S0355	0.187	0. 038	42.5	114.6	72.1	157. 1
30	2SK5	0.20844740	0.125	0.057	90.7	96.5	5.8	187. 1
31	2MN6	0.24002206	0.141	0.054	12.0	10.4	358 .5	22.4
32	M6	0.24$53417	0. 103	-0.060	53.4	313.5	260. 2	6.9
33	2MS6	0.244356%6	0.111	-0.010	163.9	246.3	82.4	50.3
34	2SM6	0.24717808	0.111	0.071	18.5	306. 2	287.7	324.7
35	3MK7	0.20331494	0. 156	0. 050	27.5	359.7	332.2	27.3
36	M8	0.32204562	0.098	-0.009	68.3	31.0	322.7	99.3

Appendix 2

Time Series of Filtered Velocity, Geostrophic Wind, Surface Wind Stress

TIME SERIES OF U, V AND LONGSHORE, OFFSHORE COMPONENTS
SHELIKOF STRAIT METER 3127 DEPTH(m) 46 TYPE FILTERED
57 39' 00"N 155 03' 19.8"W AANDERAA RCM DT(min) 360

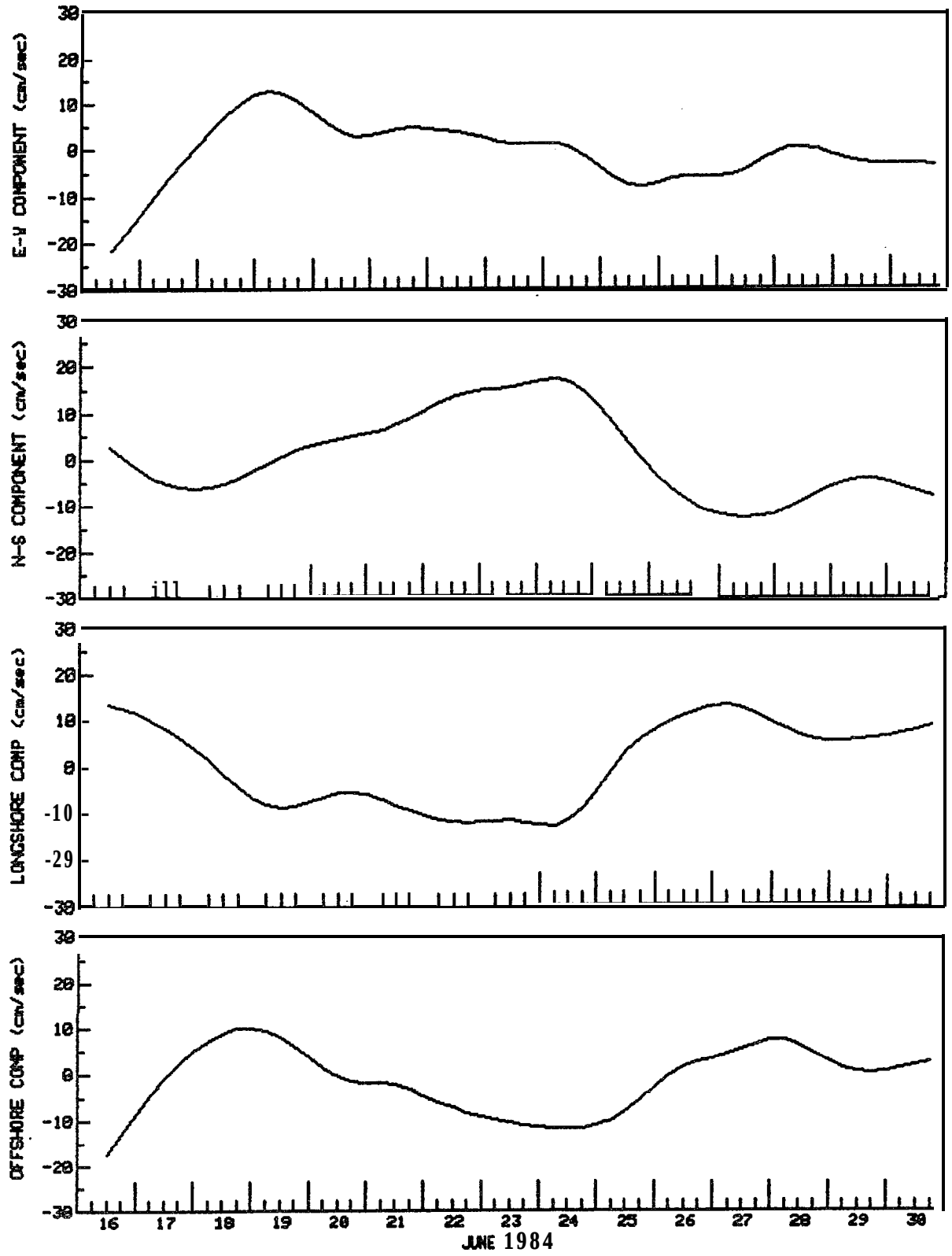

TIME SERIES OF U, V AND LONGSHORE, OFFSHORE COMPONENTS
SHELIKOF STRAIT METER 3127 DEPTH(m) 46 TYPE FILTERED
57 39' 00"N 155 03' 19.8"W AANDERAA RCM DT(min) 360

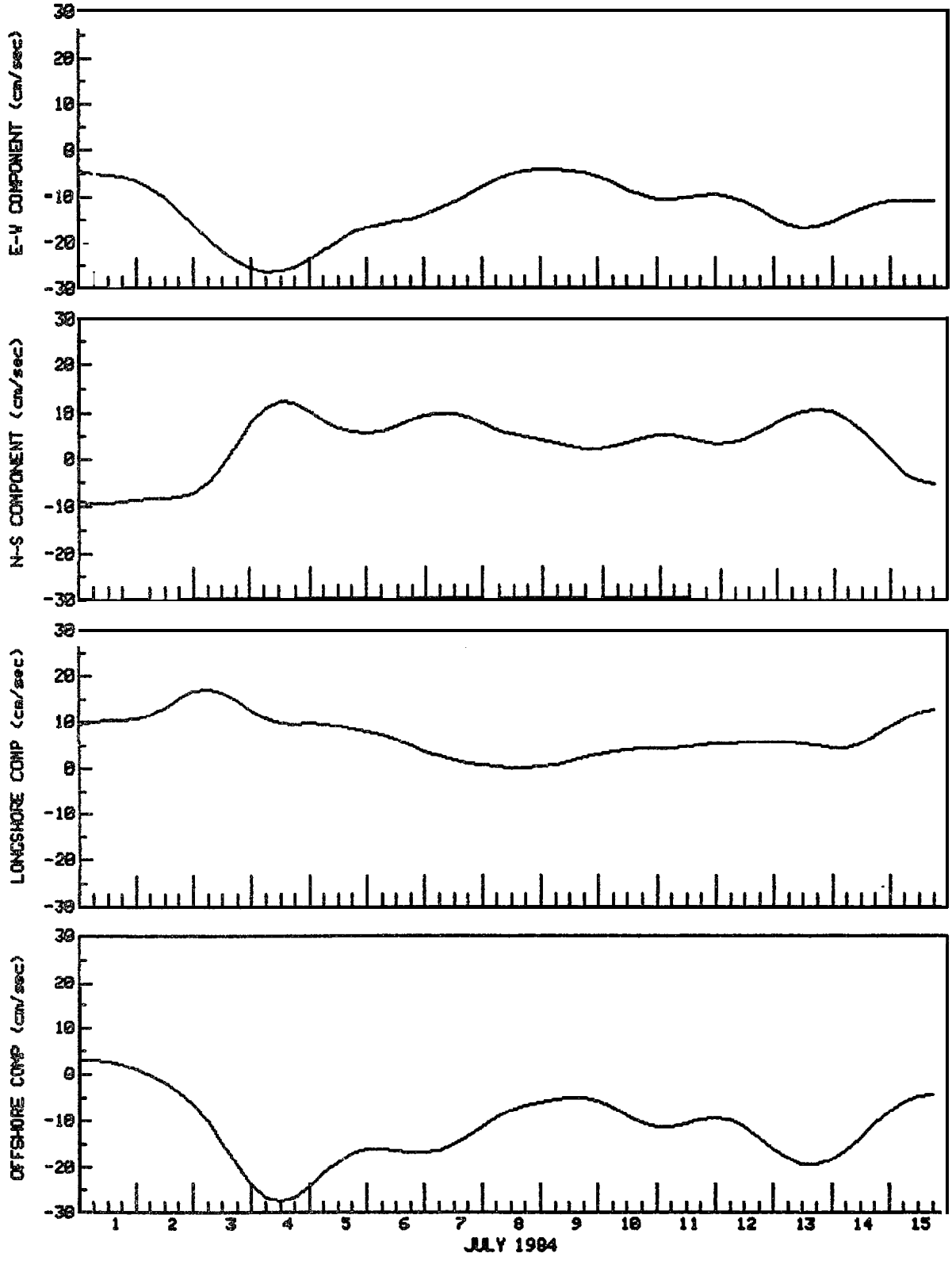

TIME SERIES OF (.J,V AND LONGSHORE, OFFSHORE COMPONENTS
SHELIKOF STRAIT METER 3127′ DEPTH(m) 46 TYPE FILTERED
57 39′ 00"N 155 03′ 19.8"W AANDERAA RCM DT(min) 360

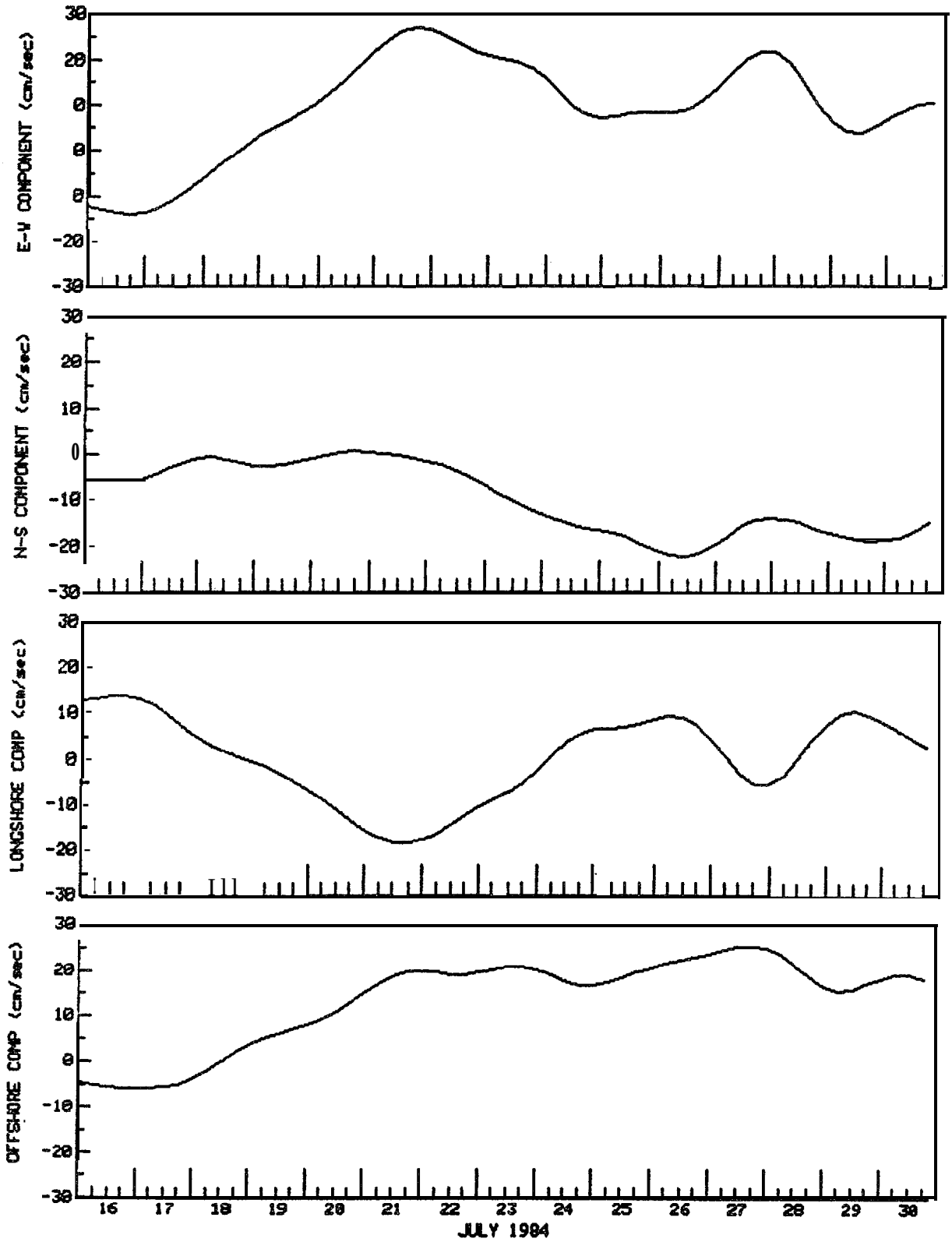

TIME SERIES OF U, V AND LONGSHORE, OFFSHORE CONPONENTS

SHELIKOF STRAIT METER 3127 DEPTH(m) 46 TYPE FILTERED

57 39' 00"N 155 03' 19.8"W AANDERAA RCM DT(min) 360

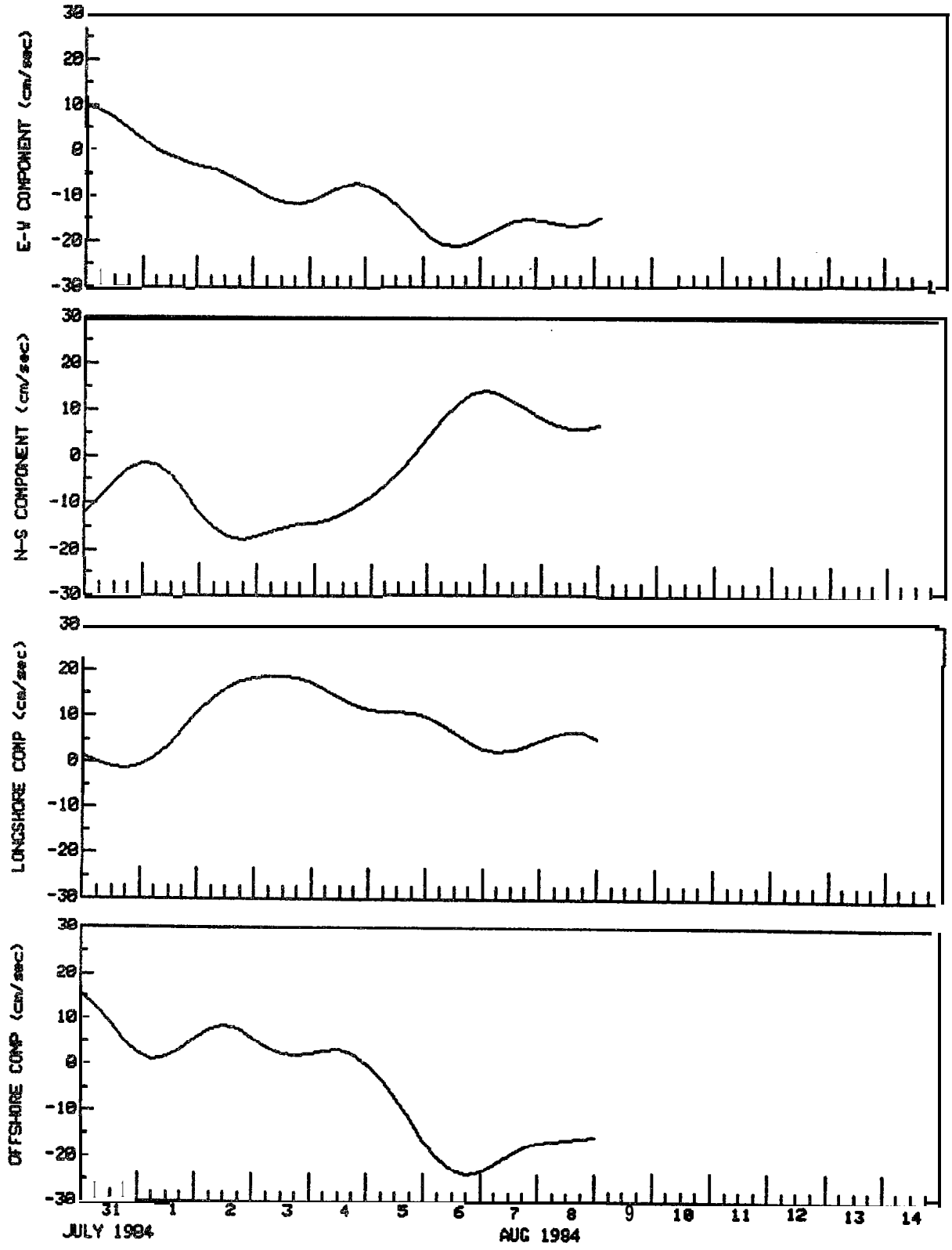

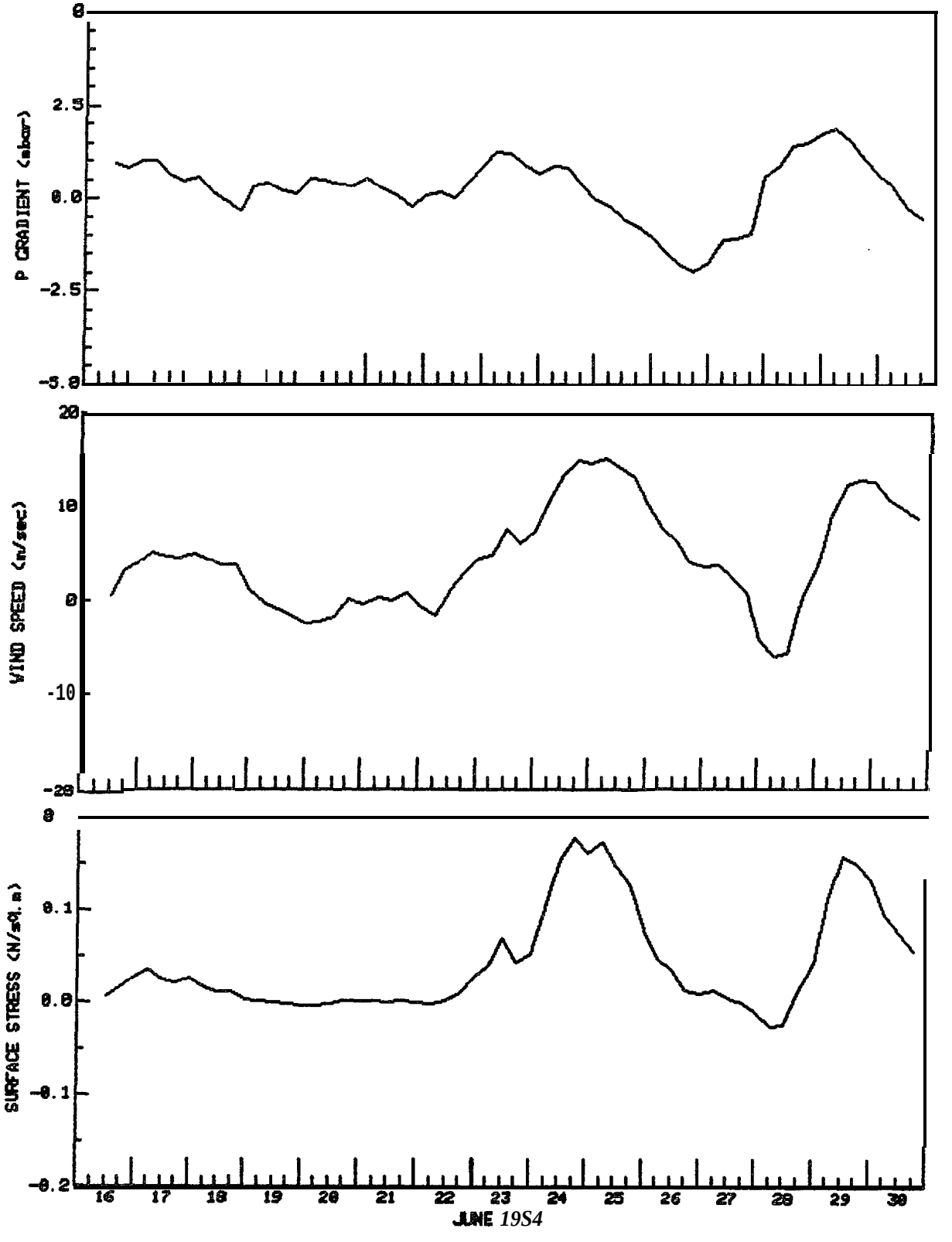
TIME SERIES OF OFFSHORE COMPONENT OF
PRESSURE GRADIENT, GEOSTROPHIC WIND AND SURFACE WIND STRESS
SHELIKOF STRAIT
DT(min) 360
P GRADIENT (mbar)
WIND SPEED (m/sec)
SURFACE STRESS (N/sq.m)
JUNE 1984

TIME SERIES OF OFFSHORE COMPONENT OF
PRESSURE GRADIENT, GEOSTROPHIC WIND AND SURFACE WIND STRESS
SHELIKOF STRAIT DT(min) 360

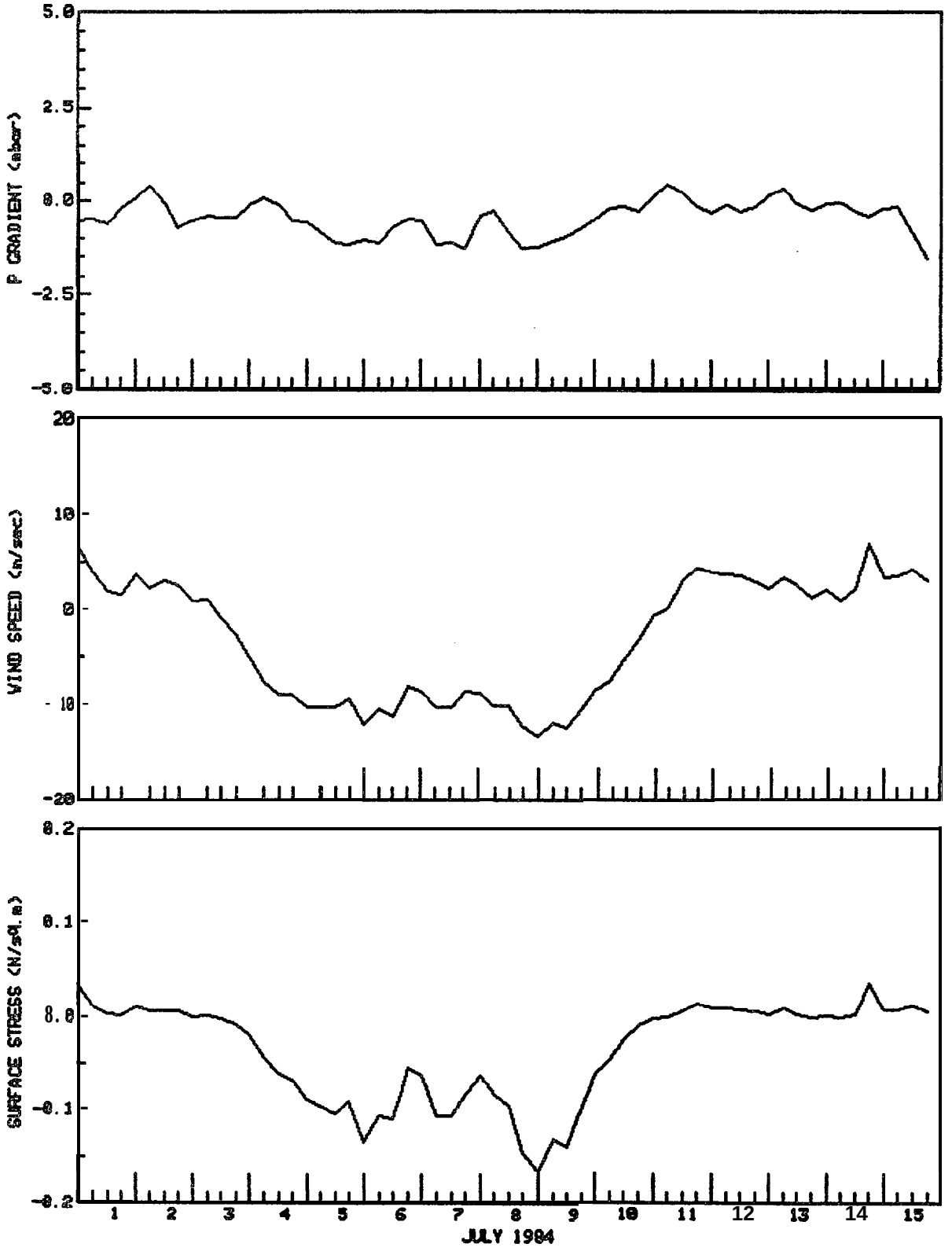

TIME SERIES OF OFFSHORE COMPONENT OF
PRESSURE GRADIENT, GEOSTROPHIC WIND AND SURFACE WIND STRESS
SHELIKOF STRAIT DT(min) 3613

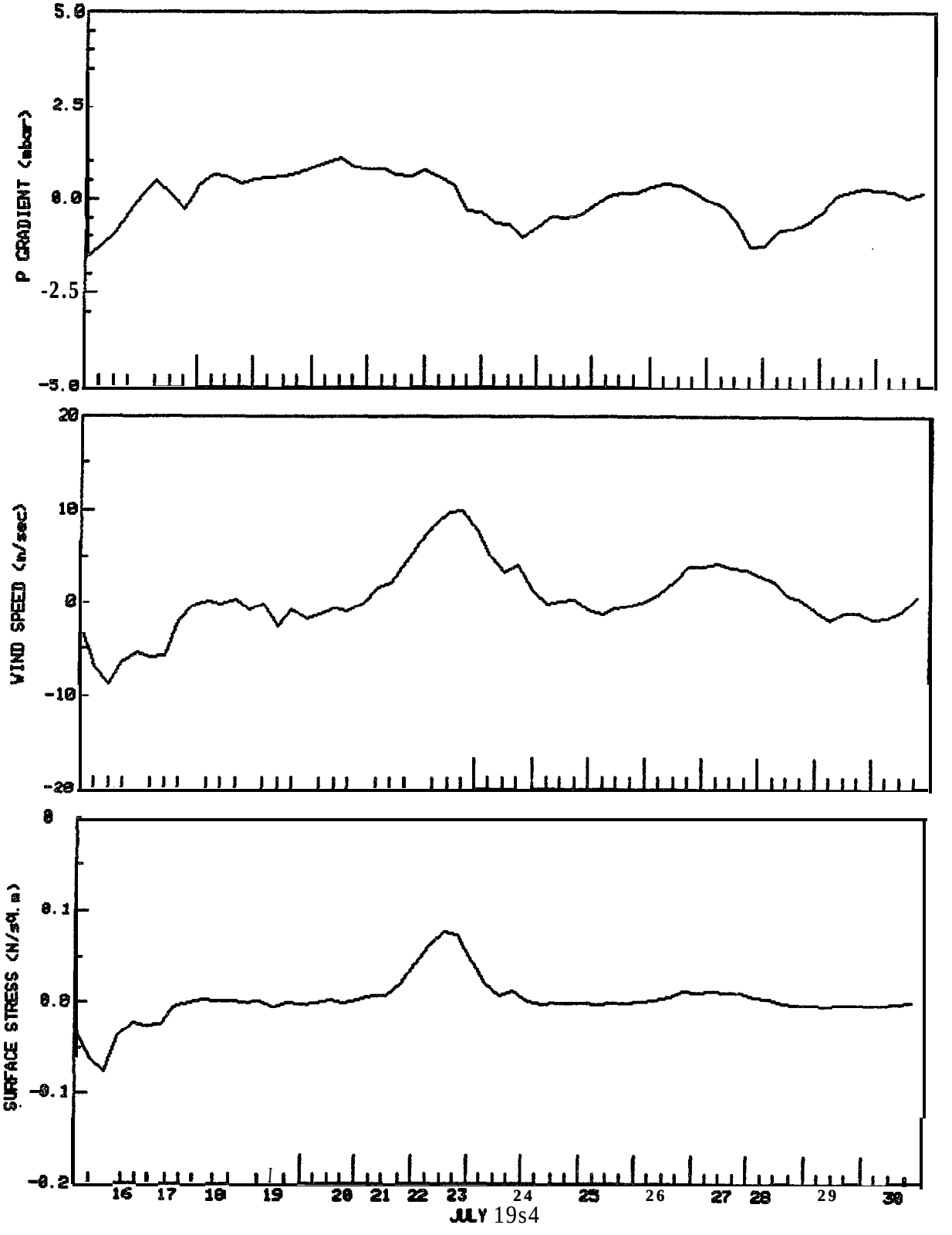

TIME SERIES OF OFFSHORE COMPONENT OF
PRESSURE GRADIENT, GEOSTROPHIC WIND AND SURFACE WIND STRESS
SHELIKOF STRAIT DT(min) 360

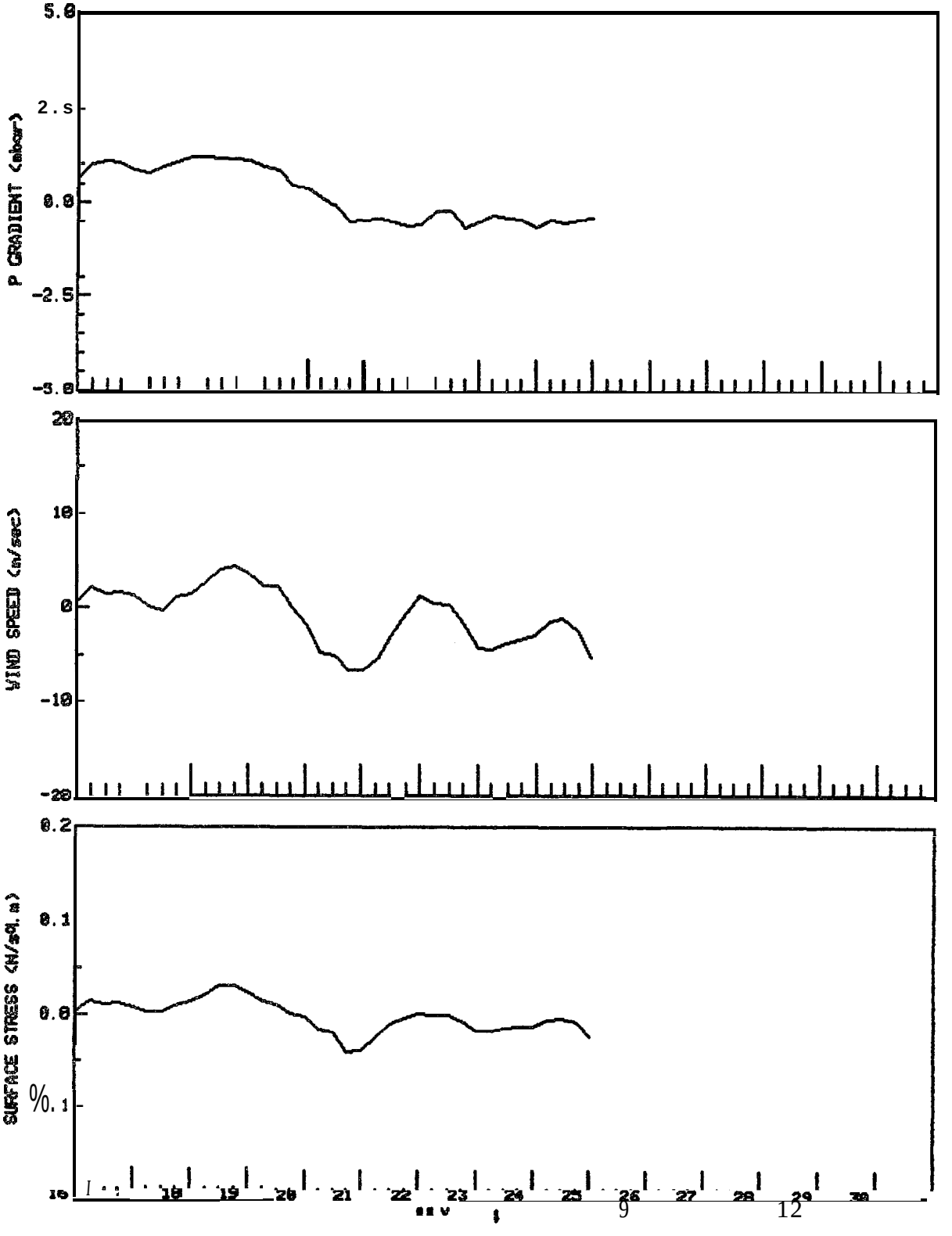

TIME SERIES OF LONGSHORE COMPONENT OF
PRESSURE GRADIENT, GEOSTROPHIC WIND AND SURFACE WIND STRESS
SHELIKOF STRAIT DT(min) 360

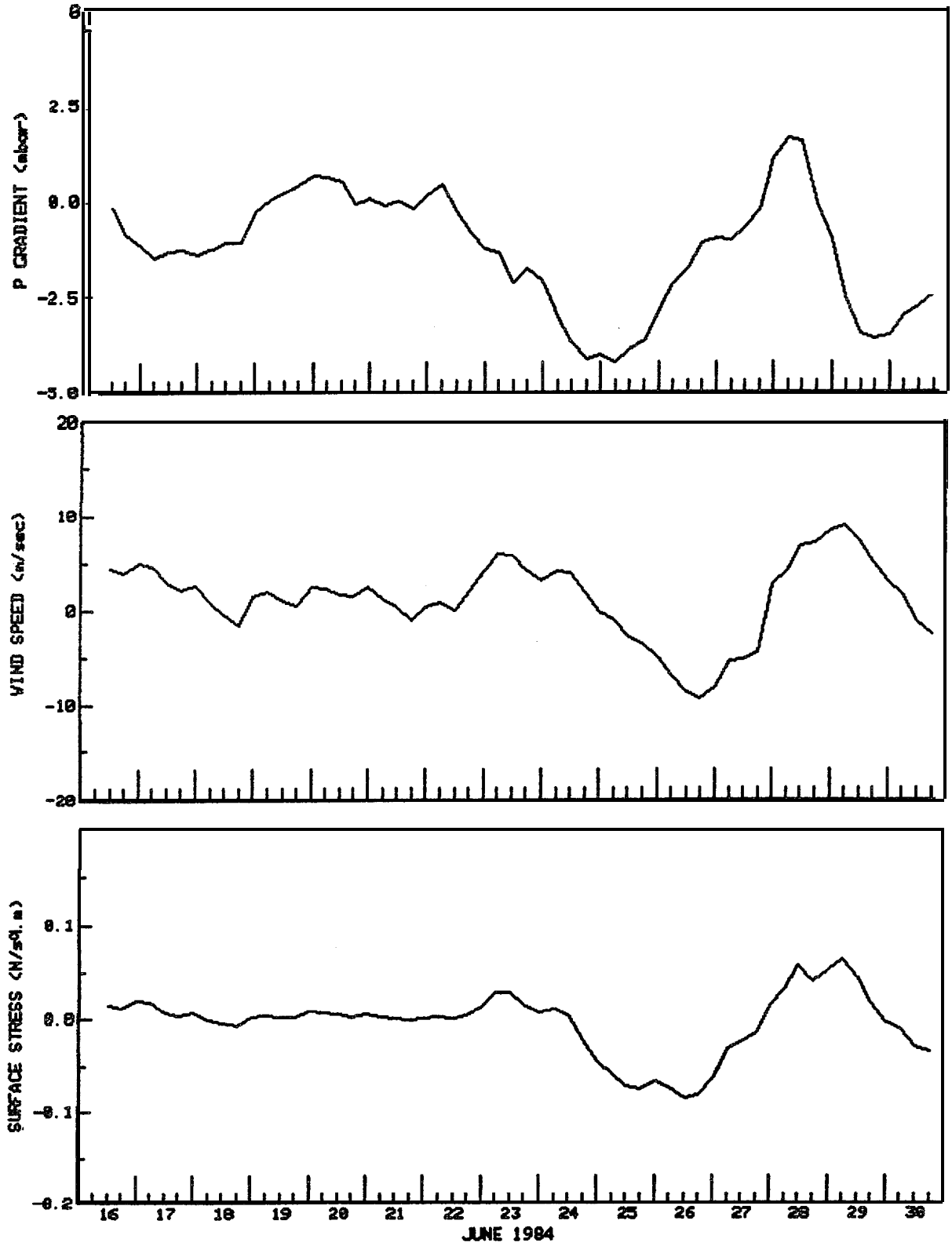

TIME SERIES OF LONGSHORE COMPONENT OF
PRESSURE GRADIENT, GEOSTROPHIC WIND AND SURFACE WIND STRESS
SHELIKOF STRAIT DT(min) 360

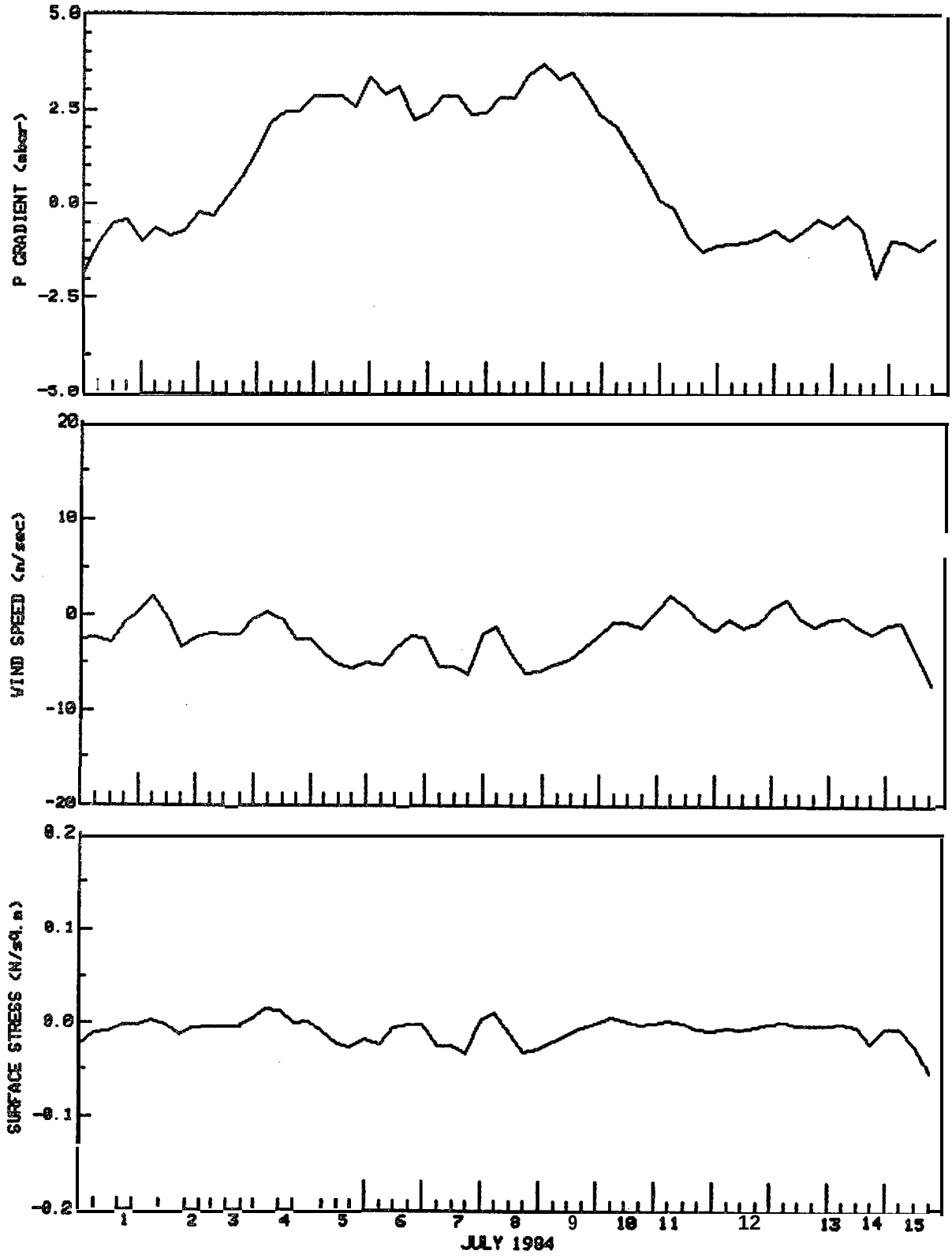

TIME SERIES OF LONGSHORE COMPONENT OF
PRESSURE GRADIENT, GEOSTROPHIC WIND AND SURFACE WIND STRESS
SHELIKOF STRAIT
DT(min) 360

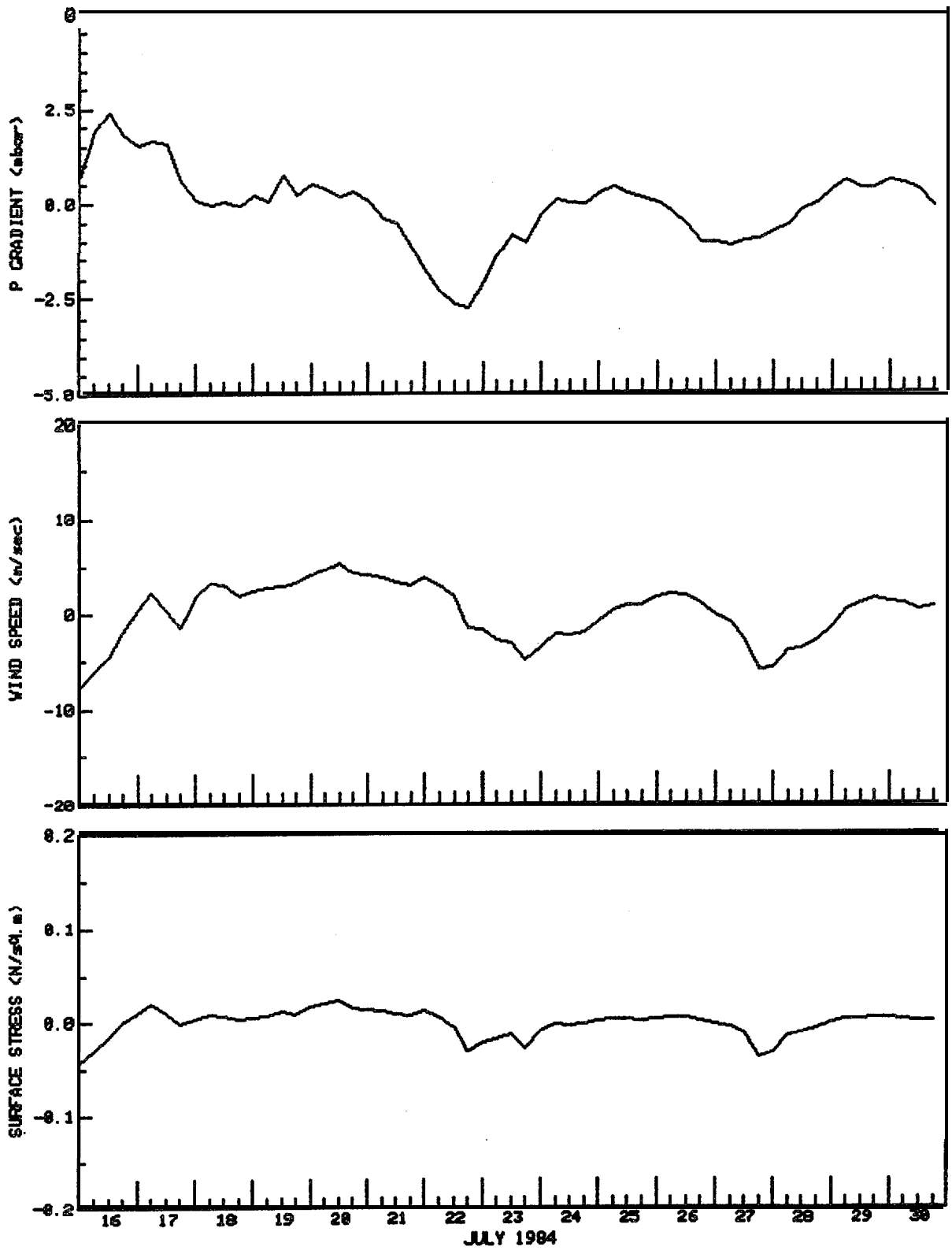

TIME SERIES OF LONGSHORE COMPONENT OF
PRESSURE GRADIENT, GEOSTROPHIC WIND AND SURFACE WIND STRESS
SHELIKOF STRAIT DT(min) 360